Discovery and Optimization of Novel Small-molecular Inhibitors Suppressing Stat3-dependent Tumor Process

2011

Xiaolei Zhang
University of Central Florida

DISCOVERY AND OPTIMIZATION OF NOVEL SMALL-MOLECULAR INHIBITORS SUPPRESSING STAT3-DEPENDENT TUMOR PROCESS

by

XIAOLEI ZHANG

M.S. University of Central Florida, 2010
M.S. Jilin University, China, 2006
B.S. Jilin University, China, 2003

A dissertation submitted in partial fulfillment of the requirements
for the degree of Doctor of Philosophy
in the Burnett School of Biomedical Sciences
in the College of Medicine
at the University of Central Florida
Orlando, Florida

Summer Term
2011

Major Professor: James Turkson, Ph.D.

ABSTRACT

With the critical role of aberrantly active Signal Transducer and Activator of Transcription (Stat) 3 protein in many human cancers, selective small-molecule inhibitors targeting the dimerization event which is required for stat3 activation, would be valuable as therapeutic agents. And the inhibitors will be useful chemical probes to clarify the complex biological functions of Stat3. By computational and structural analyses of the interaction between Stat3 and the lead dimerization disruptor, S3I-201, we have designed a diverse set of analogs.

One of the most active analogs, S3I-201.1066 is derived to contain a cyclo-hexyl benzyl moiety on the amide nitrogen, which increases the binding to the Stat3 SH2 domain. Evidence is presented from in vitro biochemical and biophysical studies that S3I-201.1066 directly interacts with Stat3 or the SH2 domain, with an affinity (K_D) of 2.74 μM, and disrupts the binding of Stat3 to the cognate pTyr-peptide, GpYLPQTV–NH2, with an IC_{50} of 23 μM. Moreover, S3I-201.1066 selectively blocks the association of Stat3 with the epidermal growth factor receptor (EGFR), and inhibits Stat3 tyrosine phosphorylation and nuclear translocation in EGF-stimulated mouse fibroblasts. In cancer cells that harbor aberrant Stat3 activity, S3I-201.1066 inhibits constitutive Stat3 DNA-binding and transcriptional activities. By contrast, S3I-201.1066 has no effect on

Src activation or the EGFR-mediated activation of the Erk1/2MAPK pathway. S3I-201.1066 selectively suppresses the viability, survival, and malignant transformation of the human breast and pancreatic cancer lines and the v-Src-transformed mouse fibroblasts harboring persistently active Stat3. Treatment with S3I-201.1066 on malignant cells harboring aberrantly active Stat3 down regulated the expression of c-Myc, Bcl-xL, Survivin, matrix metalloproteinase 9, and VEGF, which are known Stat3-regulated genes important in diverse tumor processes. The in vivo administration of S3I-201.1066 induced significant anti-tumor response in mouse models of human breast cancer, which correlates with the inhibition of constitutively active Stat3 and the suppression of known Stat3-regulated genes.

Further computer-aided lead optimization derives higher-affinity (K_D, 504 nM), orally bioavailable Stat3 SH2 domain-binding ligand, BP-1-102 as a structural analog of S3I-201.1066. The most significant modification is the pentafluorobenzene sulfonamide component of BP-1-102, which permits accessibility of a third sub-pocket of the Stat3 SH2 domain surface. BP-1-102-mediated inhibition of aberrantly-active Stat3 in human pancreatic cancer, Panc-1, breast cancer, MDA-MB-231, and prostate (DU145) cancer cells and in the mouse transformed fibroblasts harboring aberrantly-active Stat3. It also disrupts Stat3-NFκB cross-talk and suppresses the release of granulocyte

colony-stimulating factor, soluble intercellular adhesion molecule-1, macrophage-migration-inhibitory factor/glycosylation-inhibiting factor, interleukin-1 receptor antagonist and the serine protease inhibitor (serpin) protein 1, and the expression of c-Myc, Cyclin D1, Bcl-xL, Survivin, and vascular endothelial growth factor expression *in vitro* and *in vivo*. Inhibition of tumor cell-associated constitutively-active Stat3 further suppresses focal adhesion kinase and paxillin induction, enhances E-cadherin expression, and down-regulates Krüppel-like factor 8 expression. Consequently, BP-1-102 selectively suppresses anchorage-dependent and independent growth, survival, migration and invasion of Stat3-dependent tumor cells *in vitro*. Intravenous or oral gavage delivery of BP-1-102 furnishes micromolar or microgram levels in tumor tissues and inhibits growth of mouse xenografts of human breast and lung tumors.

Computer-aided lead optimization has therefore derived a more suitable small-molecule inhibitor as a drug candidate. Our studies of the Stat3 SH2 protein surface and of the interactions between lead agents and the SH2 domain provided significant data to facilitate the structural optimization. From S2I-201 to S3I-201.1066 and to BP-1-102, we note the substantial gain in potency and efficacy, and the pharmacokinetic improvements. The oral bioavailability of BP-1-102 represents a substantial advancement in the

discovery of small-molecule Stat3 inhibitors as novel anticancer agents.

ACKNOWLEDGMENTS

I am deeply indebted to my mentor, Dr. James Turkson, who gave me the chance to work in his laboratory, and for his help, kind suggestions and encouragement that helped me through my research work and the writing of this thesis. I am glad to have worked in the Turkson Lab, and indeed, I have learned so much from Dr. Turkson, not only how to do the innovative work, but also the dedication to science and the pursuit of knowledge. It has been an amazing learning experience under his guidance. I also express my sincere gratitude to my committee members, Dr. Annette Khaled, Dr. Otto Phanstiel, and Dr. William T. Self for all their valuable help and feedback on my project and their role in helping me to complete my graduate program.

I also wish to extend my heartfelt gratitude to all the lab members, Dr. Peibin Yue, Dr. Wei Zhao, Dr. Soumya Jaganathan, Bhaswati Sengupta, Melissa Wason, David Paladino and Jennifer Turkson for their kind help and suggestions. I would like to express my special thanks to Dr. Peibin Yue, who is knowledgeable and who gave me so many suggestions and was available to help when I needed him. I also would like to thank my friends Liang Li, Botao Yu, Baichuan Li, Wenjun Song, Mingpei Wang, Binbin Yan, and others not listed here for their encouragement, and finally my parents for their generous support and encouragement.

TABLE OF CONTENTS

LIST OF FIGURES

LIST OF ACRONYMS AND ABBREVIATIONS

Bcl-2 : B-cell Lymphoma 2

Bcl-xl : B-Cell Lymphoma-Extra Large

BSA : Bovine serum albumin

Con : Control

DMEM: Dulbecco's modified Eagle's medium

DTT : Dithiothreitol

DU145: Human prostate carcinoma, epithelial-like cell line

EDTA : Ethylenediaminetetraaceticacid

EGFR : Epidermal growth factor receptor

EGTA : Ethylene glycol tetraacetic acid

EMSA: Electrophoretic Mobility Shift Assay

EPSTi1: epithelial–stromal interaction 1

Erk: Extracellular signal-regulated kinases

FAK : Focal Adhesion Kinase

FP: Fluorescence polarization

G-CSF: Granulocyte colony-stimulating factor

GOLD: Genetic optimization for ligand docking

hSIE: high affinity sis-inducible element

HPDEC: Human pancreatic duct epithelial cell.

IgG : Immunoglobulin

IL : Interleukin

IL-1RA : Interleukin 1 receptor antagonist

IP : Immunoprecipitation

i.v. : Intravenous

JAK : Janus kinase

K8ikd : KLF8 inducible knockdown

K_D : Kinetic dissociation constant

*K*i : Kinetic inhibition constant

KLF8: Kruppel-like factor 8

MIF/GIF : Macrophage migration inhibitory factor (glycosylation-inhibiting factor)

MGF3 : Mammary gland factor element

NaCl : Sodium Chloride

NaF : Sodium Fluoride

$NaHCO_3$: Sodium bicarbonate

$Na_4P_2O_7$: Sodium Diphosphate

Na_3VO_4 : Sodium vanadate

NF-κB: Nuclear factor kappa-light-chain-enhancer of activated B cells

NP-40: Nonidet P-40

PBS: phosphate Buffer

pY : Phosphotyrosine

S3I: Stat3 inhibitor

SAR: Structure and relationship

SDS-PAGE: Sodium dodecyl Sulfate- Polyacrylamide gel electrophoresis

Serpin E1: Serpin peptidase inhibitor, clade E (nexin, plasminogen activator inhibitor type 1)

sICAM: Soluble Intracellular Adhension Molecule-1

SH2: Src Homology domain 2

SPR: Surface plasmon resonance

siRNA : Small Interfering Ribonucleic Acid

SRE: Serum response element

Stat3: Signal transducer and activator of transcription 3

TE-71: Thymus epithelial stromal cell

VEGF: Vascular endothelial growth factor

INTRODUCTION

The signal transducer and activator of transcription (Stat) family of proteins was originally discovered as latent cytoplasmic transcription factors that mediate growth and differentiation, survival, development, and inflammation [1,2]. Normal Stat signaling in response to cytokines and growth factors are rapid and transient [2]. However, many human solid and hematological tumors harbor aberrant Stat3 activity which is persistently activated [3]. Evidence shows constitutively active Stat3 is a critical molecular mediator of carcinogenesis and tumor progression [4-6]. Several studies testing the proof-of-concept show that the inhibition of Stat3 activation or disruption of dimerization induces cancer cell death and tumor regression [7-12].

For the activation of Stats, upon the binding of cytokines or growth factors to their receptors, Stats are recruited to the receptor via their SH2 domains and are phosphorylated on a key tyrosine residue (Tyr705 for Stat3) by receptor-associated tyrosine kinases [2]. Two phosphorylated Stat monomers dimerize through reciprocal pTyr-SH2 domain interactions, and the dimers translocate to the nucleus, where they bind to specific DNA-response elements of target genes and regulate gene expression [1]. All steps towards the activation of functional Stat3 [1, 2] offer opportunities to inhibit aberrant Stat3 activity. Since the SH2 domain is required for both the binding to

phospho-Tyr peptide motifs of receptors and the dimerization of Stats, inhibiting the function of the SH2 domain would represent an effective approach to inhibit Stat3 function [4-6]. This should not only inhibit Stat activation, but also prevent dimerization of single Stat molecules. Fig. 1 shows the classical approaches to inhibit Stat activity [13].

In this project, I focused on disrupting the dimerization of Stat molecules for the reasons provided above. Molecular modeling was used to identify candidate compounds as leads that bind to the Stat3 SH2 domain and to study in silico the interactions with the SH2 domain for the purposes of structural optimization, potency and efficacy enhancement, and pharmacological improvements. Computational modeling together with integrative biochemical experiments were employed to identify specific Stat3 inhibitors that block the dimerization of Stat3. Compounds were subsequently tested in biological assays *in vitro*, and in *in vivo* tumor models, and *in vivo* pharmacokinetic experiments in order to identify suitable molecules that can be used for therapeutic purposes and also as tools for investigating the regulation of Stat3 protein in cancer cells.

The emergence of computational modeling has paved the way to study the molecular events of which structural information is available and develop approaches to rationally design compounds that can interfere with biochemical and biological systems.

Computational modeling was applied together with *in silico* screening and structure-based approach to design novel compounds that can disrupt the dimerization of Stat3. The biochemical activity and anti-tumor cell effects, and the in vivo antitumor efficacy and pharmacokinetic properties of select compounds were investigated to assess their suitability as potential novel anticancer agents.

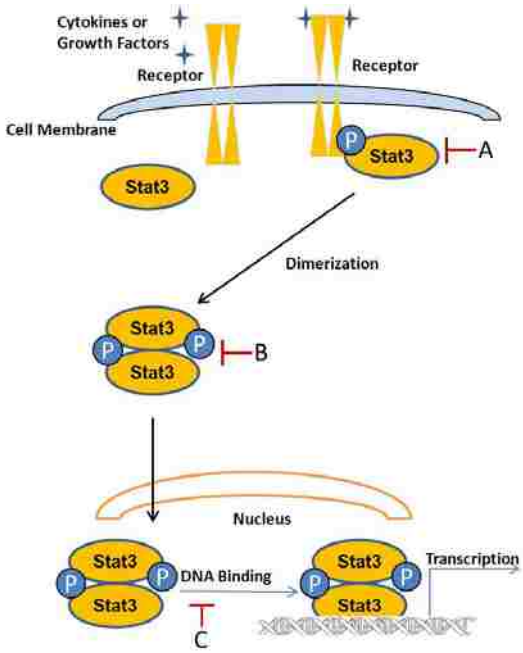

Figure 1. Approaches to inhibit Stat3 pathway

A: inhibition of tyrosine phosphorylation

B: inhibition of Stat3 dimerization.

C: inhibition of Stat3 DNA binding

Inhibition is indicated by the symbol "|—". This dissertation is focusing on approach B.

DISCOVERY OF S3I-201.1066, A NOVEL SMALL MOLECULE DISRUPTS STAT3 SH2 DOMAIN-PHOSPHOTYROSINE INTERACTIONS AND STAT3 -DEPENDENT TUMOR PROCESSES

The targeting of aberrant Stat3 signaling provides a novel strategy for treating the wide variety of human tumors that harbor abnormal Stat3 activity. The critical step of dimerization between two monomers within the context of STAT activation presents an attractive strategy to interfere with Stat3 signaling and functions and this approach has been exploited in prior work. In the present study, key structural information from the computational modeling of S3I-201 bound to the Stat3 SH2 domain facilitated the design of novel analogs of which S3I-201.1066 shows an improved Stat3-inhibitory activity.

Introduction

Signal transduction proteins have increased importance in carcinogenesis and tumor formation and represent attractive targets for the development of novel anticancer therapeutics. The signal transducer and activator of transcription (Stat) family of proteins are cytoplasmic transcription factors with important roles in the responses to cytokines and growth factors, including promoting cell growth and differentiation, and inflammation and immune responses [14,15]. Normal Stat's activation is initiated by the phosphorylation of a critical tyrosine residue upon the binding of cytokines or growth factors to cognate receptors. Stat's phosphorylation is induced by growth factor receptor tyrosine kinases, or cytoplasmic tyrosine kinases, such as Janus kinases (Jaks) and Src family kinases. While pre-existing Stat dimers have been detected [16, 17], studies show that phosphorylation induces dimerization between two Stat monomers through a phosphotyrosine interaction with the SH2 domain. In the nucleus, active Stat dimers bind to specific DNA-response elements in the promoters of target genes and regulate gene expression. Normal Stat activation is transient in accordance with physiological responses. However, the persistent activation of certain Stat family members, including Stat3 is frequently observed in many human tumors. It is now well established that aberrant activation of Stat3 contributes to malignant transformation and tumorigenesis. Evidence shows that persistently active Stat3 mediates oncogenesis and tumor

formation in part by the upregulation of the expression of critical genes, the dysregulation of cell growth and survival, the promotion of angiogenesis [15,18–24], and the induction of tumor immune-tolerance [25,26]. Thus, the targeting of aberrant Stat3 signaling provides a novel strategy for treating the wide variety of human tumors that harbor abnormal Stat3 activity.

The critical step of dimerization [27] between two monomers within the context of Stat3 activation presents an attractive strategy to interfere with Stat3 signaling and functions and this approach has been exploited in prior work [7, 12, 13, 28-35]. Leading agents from those earlier studies have been explored in the rational design of optimized molecules, in conjunction with molecular modeling of their binding to the Stat3 SH2 domain [12, 30], per the X-ray crystal structure of the Stat3b homodimer [36]. One of those leads, S3I-201 [12] had previously been shown to exert antitumor effects against human breast cancer xenografts via mechanisms that involve the inhibition of aberrant Stat3 activity.

In the present study, key structural information from the computational modeling of S3I-201 bound to the Stat3 SH2 domain facilitated the design of novel analogs of which S3I-201.1066 shows an improved Stat3-inhibitory activity. S3I-210.1066 inhibits Stat3 DNA-binding activity with an IC_{50} value of 35 μM *in vitro*, and shows the similar effect in

cell model. In this project, we provided evidence that S3I-201.1066 directly interacts with the Stat3 protein SH2 domain *in vitro*, thereby disrupting Stat3 binding to cognate pTyr peptide motifs of receptors and inhibiting Stat3 phosphorylation and activation, and Stat3 nuclear localization. Furthermore, evidence is provided that S3I-201.1066 selectively induces antitumor cell effects in human breast and pancreatic cancer cells, and mouse transformed fibroblasts harboring aberrant Stat3 activity, and inhibits growth of human breast tumors in xenografts.

Materials and Methods

Cells and reagents

Normal mouse fibroblasts (NIH3T3) and counterparts transformed by v-Src (NIH3T3/v-Src), v-Ras (NIH3T3/v-Ras) or overexpressing the human epidermal growth factor (EGF) receptor (NIH3T3/hEGFR), and the human breast cancer (MDA-MB-231) and pancreatic cancer (Panc-1) cells have all been previously reported [28, 37–39]. The normal human pancreatic duct epithelial cells (HPDEC) were a kind gift from Dr. Tsao (OCI, UHN-PMH, Toronto) [40], the Stat3 knockout mouse embryonic fibroblasts line was generously provided by Dr. Valerie Poli (University of Turin) [41], and the ovarian cancer line, A2780S was a kind gift from Dr. Jin Q. Cheng (Moffitt Cancer Center and Research Institute). The Stat3-dependent reporter, pLucTKS3 and the Stat3-independent reporter,

pLucSRE, and the v-Src transformed mouse fibroblasts that stably express pLucTKS3 (NIH3T3/v-Src/ pLucTKS3) have all been previously reported [38, 42, 43]. Cells were grown in Dulbecco's modified Eagle's medium (DMEM) containing 10% heat-inactivated fetal bovine serum, or in the case of HPDEC, they were grown in keratinocyte-SFM (GIBCO, Invitrogen Corp., Carlsbad, CA) supplemented with 0.2 ng EGF and 30 mg/ml bovine pituitary extract, and containing antimycol. Antibodies used are against Stat3, pY705Stat3, Src, pY416Src, Jak1, pJak1, Shc, pShc, Erk1/2, pErk1/2, and Survivin from Cell Signaling Technology (Danvers, MA), and anti-EGFR and anti-VEGF from Santa Cruz Biotech (Santa Cruz, CA).

Cloning and protein expression

The coding regions for the murine Stat3 protein and the Stat3 SH2 domain were amplified by PCR and cloned into vectors pET-44 Ek/LIC (Novagen, EMD Chemicals, Gibbstown, NJ) and pET SUMO (Invitrogen), respectively. The primers used for amplification were: Stat3 Forward: GACGACGACAAGATGGCTCAGTGGAACC AGCTGC; Stat3 Reverse: GAGGAGAAGCCCGGTTATCACATGGGGGAGGTAG CACACT; Stat3 SH2 Forward: ATGGGTTT CATCAGCAAGGA; Stat3 SH2 Reverse: TCACCTACAGTACTTTCCAAATGC. Clones were sequenced to verify the correct sequences and orientation. His-tagged recombinant proteins were expressed in BL21

(DE3) cells and purified on Ni-ion sepharose column.

Nuclear extract preparation, gel shift assays, and densitometric analysis

Nuclear extract preparations and electrophoretic mobility shift assay (EMSA) were carried out as previously described [38, 43]. The ^{32}P-labeled oligo-nucleotide probes used were hSIE (high affinity sis-inducible element from the c-fos gene, m67 variant, 5'-AGCTTCATTTCCCGTAAATCCCTA) that binds Stat1 and Stat3 [44] and MGFe (mammary gland factor element from the bovine β-casein gene promoter, 5'-AGATTTCTAGGAATTCAA) for Stat1 and Stat5 binding [45,46]. Except where indicated, nuclear extracts were pre-incubated with compound for 30 min at room temperature prior to incubation with the radiolabeled probe for 30 min at 30°C before subjecting to EMSA analysis. Bands corresponding to DNA-binding activities were scanned and quantified for each concentration of compound using ImageQuant and plotted as percent of control (vehicle) against concentration of compound, from which the IC_{50} values were derived, as previously reported [47].

Immunoprecipitation, immunoblotting and densitometric analyses

Immunoprecipitation from whole-cell lysates, and tumor tissue lysate preparation, and immunoblotting analysis were performed as previously described [7, 12, 43, 48]. Primary antibodies used were anti-Stat3, pY705Stat3, pY416Src, Src, pErk1/2, Erk1/2, pJak1,

Jak1, pShc, Shc, Grb 2, c-Myc, Bcl-xL, Survivin, MMP-9, and β-actin (Cell Signaling), and VEGF (Santa Cruz Biotech.).

Cell viability and proliferation assay

Cells in culture in 96-well plates were treated with or without S3I-201.1066 for 24h and subjected to CyQuant cell vaibility assay (Invitrogen Corp./Life Technologies Corp.). Or cells in culture in 6-well plates were treated with or without S3I-201.1066 for 96h, and harvested, and the viable cells counted by trypan blue exclusion with phase-contrast microscopy.

Immunofluorescence imaging/confocal microscopy

NIH3T3/hEGFR cells were grown in multi-cell plates, serum starved for 8 h and treated with or without S3I-201.1066 for 30 min prior to stimulation by rhEGF (1 μg/mL) for 10 min. Cells were fixed with ice-cold methanol for 15 min, washed 3 times in phosphate buffered saline (PBS), permeabilized with 0.2% Triton X-100 for 10 min, and further washed 3–4 times with PBS. Specimens were then blocked in 1% bovine serum albumin (BSA) for 30 min and incubated with anti-EGFR (Santa Cruz) or anti-Stat3 (Cell Signaling) antibody at 1:50 dilution at 4°C overnight. Subsequently, cells were rinsed 4–5 times in PBS, incubated with Alexa fluor 546 rat antibody for EGFR detection and Alexa

fluor 488 rabbit antibody for Stat3 detection (Invitrogen) for 1 h at room temperature in the dark. Specimens were then washed 5 times with PBS, covered with cover slides with VECTASHIELD mounting medium containing DAPI (Vector Lab, Inc., Burlingame, CA), and examined immediately under a Leica TCS SP5 confocal microscope (Germany) at the appropriate wavelengths. Images were captured and processed using the Leica TCS SP 5 software.

Soft-agar colony formation assay

Colony formation assays were carried out in 6-well dishes, as described previously [29, 47]. Briefly, each well contained 1.5 ml of 1% agarose in Dulbeco's modified Eagle's medium as the bottom layer and 1.5 ml of 0.5% agarose in Dulbeco's modified Eagle's medium containing 4–6 $X10^3$ NIH3T3/v-Src, NIH3T3/v-Ras, A2780S, MDA-MB-231 or Panc-1 cells, as the top layer. Treatment with S3I-201.1066 was initiated 1 day after seeding cells by adding 80 µl of medium with or without S3I-201.1066, and repeating every 2 or 3 days, until large colonies were evident. Colonies were quantified by staining with 20 µl of 1 mg/ml crystal violet (Thermo- Fisher, Waltham, MA), incubating at 37°C overnight, and counting the next day under phase-contrast microscope.

Fluorescence polarization assay

Fluorescence polarization (FP) assay was conducted as previously reported [33], with some modification using the phosphopeptide, 5-carboxyfluorescein -GpYLPQTV– NH2 (where pY represents phospho-Tyr) as probe and Stat3. A fixed concentration of the fluorescently labeled peptide probe (10 nM) was incubated with an increasing concentration of the Stat3 protein for 30 min at room temperature in the buffer, 50mM NaCl, 10mM HEPES, 1 mM EDTA, 0.1% Nonidet P-40, and the fluorescent polarization measurements were determined using the POLARstar Omega (BMG LABTECH, Durham, NC), with the set gain adjustment at 35 mP. The Z' value was derived per the equation $Z' = 1-(3SD_{bound} + 3SD_{free})/ (mP_{bound} - mP_{free})$, where SD is the standard deviation and mP is the average of fluorescence polarization. In the ''bound'' state, 10 nM 5-carboxyfluorescein- GpYLPQTV–NH2 was incubated with 150 nM purified Stat3 protein, while the ''free'' (unbound) state represents the same mixture, but incubated with an additional 10 μM unlabeled Ac-GpYLPQTV–NH2. For evaluating agents, Stat3 protein (150 nM) was incubated with serial concentrations of S3I-201.1066 at 30 ℃ for 60 min in the indicated assay buffer conditions. Prior to the addition of the fluorescent probe, the protein:S3I-201.1066 mixtures were allowed to equilibrate at room temperature for 15 min. Probe was added at a final concentration of 10 nM and incubated for 30 min at room temperature. And then the FP measurements were taken

using the POLARstar Omega, with the set gain adjustment at 35 mP.

Surface plasmon resonance analysis

SensiQ and its analysis software Qdat (ICX Technologies, Oklahoma City, OK) were used to analyze the interaction between the agent and the Stat3 protein and to determine the binding affinity. Purified Stat3 was immobilized on a HisCap Sensor Chip by injecting 50 mg/ml of Stat3 onto the chip. Various concentrations of S3I-201.1066 in running buffer (1×PBS, 0.5% DMSO) were passed over the sensor chip to produce response signals. The association and dissociation rate constants were calculated using the Qdat software. The ratio of the association and dissociation rate constants was determined as the affinity (K_D).

Colony survival assay

This was performed as previously reported [49]. Briefly, cells were seeded as single-cell in 6-cm dishes (500 cells per well), treated once the next day with S3I-201.1066 for 48 h, and allowed to culture until large colonies were visible. Colonies were stained with crystal violet (ThermoFisher) for 4 h and counted under a phase-contrast microscope.

Wound healing assay for migration

Wounds were made using pipette tips in monolayer cultures of cells in 6-well plates. Cells were treated with or without increasing concentrations of S3I-201.1066 and allowed to migrate into the denuded area for 12–24 h. The migration of cells was visualized at a 10× magnification using an Axiovert 200 Inverted Fluorescence Microscope (Zeiss, Göttingen, Germany), with pictures taken using a mounted Canon Powershot A640 digital camera (Canon USA, Lake Success, NY). Cells that migrated into the denuded area were quantified.

Mice and in vivo tumor studies

Six-week-old female athymic nude mice were purchased from Harlan and maintained in the institutional animal facilities approved by the American Association for Accreditation of Laboratory Animal Care. Athymic nude mice were injected subcutaneously in the left flank area with 5×10^6 human breast cancer MDA-MB-231 cells in 100 µL of PBS. After 5–10 days, tumors of a diameter of 3 mm were established. Animals were grouped so that the mean tumor sizes in all groups were nearly identical, then given S3I-201.1066, i.v. at 3 mg kg^{-1} every 2 or every 3 days for 17 days and monitored every 2 or 3 days, and tumor sizes were measured with calipers. Tumor volume, V, was calculated according to the formula $V = 0.52 \times a^2 \times b$, where a, smallest superficial diameter, b, largest superficial

diameter. For each treatment group, the tumor volumes for each set of measurements were statistically analyzed in comparison to the control (non-treated) group. Upon completion of the study, tumors were extracted and tumor tissue lysates were prepared for immunoblotting and gel shift analyses.

Statistical analysis

Statistical analysis was performed on mean values using Prism GraphPad Software, Inc. (La Jolla, CA). The significance of differences between groups was determined by the paired t-test at $*p < 0.05$, $**p < 0.01$, and $***p < 0.001$.

Results

Computer-aided design of S3I-201 analogs as Stat3 inhibitors

Structural analysis of the lowest genetic optimization for ligand docking (GOLD) [50] conformation of the lead Stat3 inhibitor, S3I-201 (green) (IC_{50} = 86 μM for inhibition of Stat3:Stat3 [12]) (Fig. 2A and C) bound within the Stat3 SH2 domain (Fig. 2C), per the X-ray crystal structure of DNA-bound Stat3b homodimer [36] showed significant complementary interactions between the protein surface and the compound and identified key structural requirements for tight binding. Docking studies permitted in silico

structural design of analogs of differing Stat3 SH2 domain-binding characteristics in order to derive Stat3 inhibitors of improved potency and selectivity. GOLD studies showed limited structural occupation of the Stat3 SH2 domain, identifying a potential means for improving inhibitor potency. The SH2 domain is broadly composed of three sub-pockets, only two of which are accessed by S3I-201 (Fig. 2C). Lead agent, S3I-201 (Fig. 2A) has a glycolic acid scaffold with its carboxylic acid condensed with a 4-amino-salicylic acid to furnish an amide bond, and its hydroxyl moiety O-tosylated. The ortho- hydroxybenzoic acid component is a known pTyr mimetic, and low energy GOLD studies consistently placed this unit in the pTyr-binding site, making hydrogen bonds and electrostatic interactions with Lys591, Ser611, Ser613 and Arg609. Due to the strength of such ionic interactions between oppositely charged ions, it is likely that a considerable portion of the binding between the SH2 domain and S3I-201 arises from the pTyr mimetic. The O-tosyl group binds in the mostly hydrophobic pocket that is derived from the tetramethylene portion of the side chain of Lys592 and the trimethylene portion of the side chain of Arg595, along with Ile597 and Ile634. Given the potency of S3I-201 towards Stat3 inhibition, a rational synthetic program was undertaken to modify and optimize the core scaffold to furnish more potent analogs. We additionally exploited key hydrophobic interactions with Phe716, Ile659, Val637 and Trp623 (Fig. 2C, see the yellow arrow) in generating compounds made of N-substituted (para-cyclohexyl)benzyl analogs [51],

including S3I- 201.1066 (Fig. 2B). The present study of the analog S3I-201.1066 (Fig. 2B and D) was undertaken to derive biochemical and biophysical evidence of binding to Stat3 and to define the mechanisms of inhibition of Stat3 and its functions in the context of Stat3-dependent malignant transformation and tumorigenesis.

Fig. 2

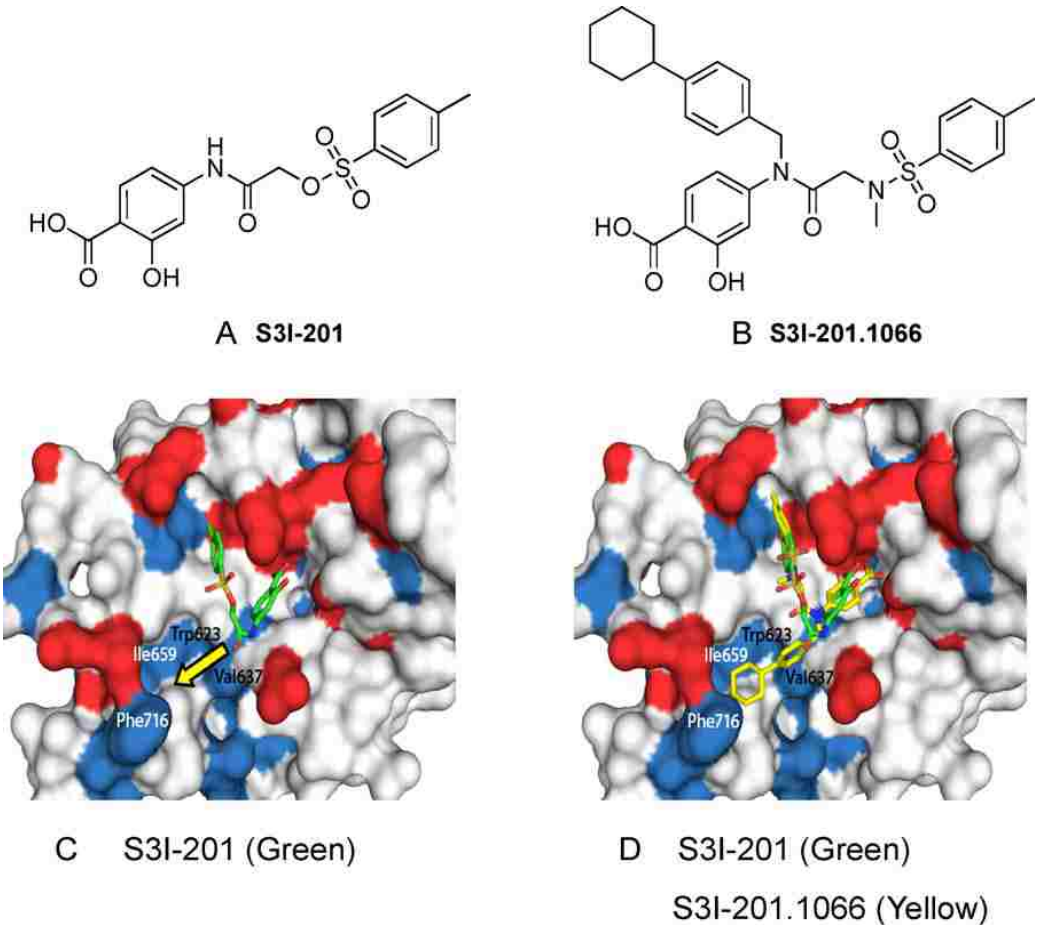

Figure 2. Structure and computer modeling of S3I-201 and S3I-201.1066 to Stat3 SH2 domain

(A and B) Structures of (A) S3I-201, (B) S3I-201.1066; (C and D) GOLD of (C) S3I-201 (green), and (D) S3I-201 (green) and S3I-201.1066 (yellow) to the SH2 domain of Stat3; arrow denotes potential binding sub-pocket accessed by S3I-201.1066, but not S3I-201.

Inhibition of Stat3 DNA-binding activity

S3I-201 analogs derived per in silico structural optimization and molecular modeling of the binding to the Stat3 SH2 domain were synthesized and evaluated in Stat3 DNA-binding assay in vitro, as previously done [12]. Nuclear extracts containing activated Stat3 prepared from v-Src-transformed mouse fibroblasts (NIH3T3/v-Src) that harbor aberrantly active Stat3 were incubated for 30 minutes at room temperature with or without increasing concentrations of the analog, S3I-201.1066, prior to incubation with the radiolabeled hSIE probe that binds to Stat3 and Stat1 and subjected to electrophoretic mobility shift assay (EMSA) analysis [12]. Stat3 DNA-binding activity was inhibited in a dose-dependent manner by S3I- 201.1066 (Fig. 3A(i)), with average IC_{50} value of 35 ±9 μM. This value represents 3 fold improvement over the activity of the lead agent, S3I-201 (IC_{50} of 86 μM) [12]. For selectivity, nuclear extracts containing activated Stat1, Stat3 and Stat5 prepared from EGF stimulated NIH3T3/hEGFR (mouse fibroblasts over-expressing the human epidermal growth factor receptor) were pre-incubated at room temperature with or without increasing concentrations of

S3I-201.1066 for 30 min, prior to incubation with the radiolabeled oligonucleotide probes and subjecting to EMSA analyses, as previously done [12]. EMSA results of the binding studies using the hSIE probe show the strongest complex of Stat3:Stat3 with the probe (Fig. 3A (ii) upper band, lanes 1 and 2), which is significantly disrupted at 50 μM S3I-201.1066 and completely disrupted at 100 μM S3I-201.1066 (Fig. 3A (ii), upper band, lanes 2 and 3). EMSA analysis further shows a less intense Stat1:Stat3 complex (intermediate band), which is similarly repressed at 50 μM and completely disrupted at 100 μM S3I- 201.1066 (Fig. 3A (ii), lanes 2 and 3). By contrast, we observe no significant inhibition of the Stat1:Stat1 complex that is of the lowest intensity (lower band) at 50 μM S3I-201.1066 a moderate inhibition at 100 μM S3I-201.1066, but a complete inhibition at 200 μM S3I- 201.1066 (Fig. 3A (ii), lower band). Of importance, at the 100 μM S3I-201.1066 concentration at which only a moderate inhibition of Stat1:Stat1 complex occurred, the larger Stat3:Stat3 complex is completely dissociated (Fig. 3A (ii), lane 3). Moreover, EMSA analysis showed no effect on Stat5:Stat5 complex with the MGFe probe, up to 300 μM S3I-201.1066 (Fig. 3A (iii)). Thus, S3I-201.1066 preferentially inhibits DNA-binding activity of Stat3 over that of Stat1 or Stat5.

Fig. 3

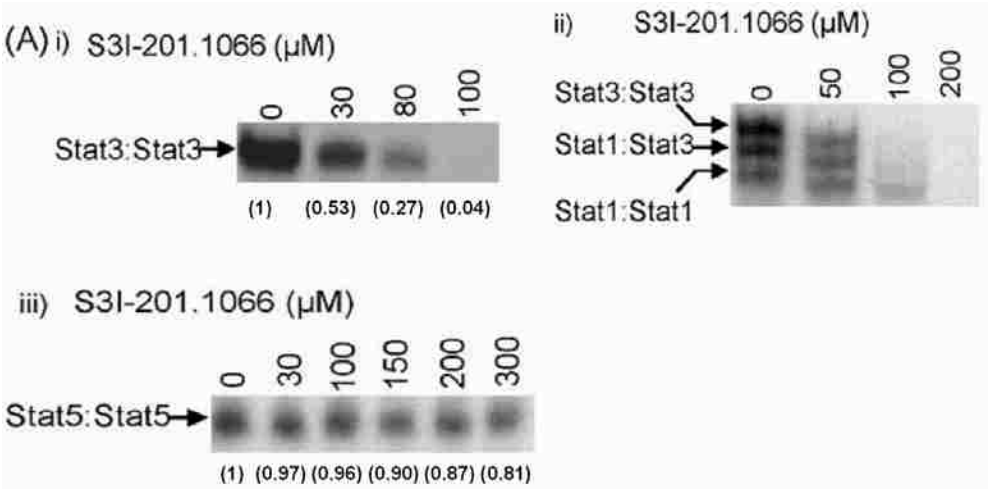
(A) i) S3I-201.1066 (μM)
0
30
80
100
Stat3:Stat3
(1)
(0.53)
(0.27)
(0.04)
ii) S3I-201.1066 (μM)
Stat3:Stat3
Stat1:Stat3
Stat1:Stat1
0
50
100
200
iii) S3I-201.1066 (μM)
0
30
100
150
200
300
Stat5:Stat5
(1) (0.97) (0.96) (0.90) (0.87) (0.81)

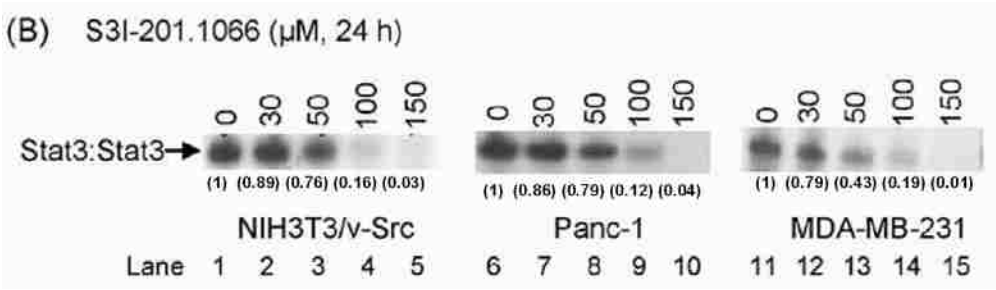
(B) S3I-201.1066 (μM, 24 h)
0
30
50
100
150
Stat3:Stat3
(1) (0.89) (0.76) (0.16) (0.03)
(1) (0.86) (0.79) (0.12) (0.04)
(1) (0.79) (0.43) (0.19) (0.01)
NIH3T3/v-Src
Panc-1
MDA-MB-231
Lane 1 2 3 4 5 6 7 8 9 10 11 12 13 14 15

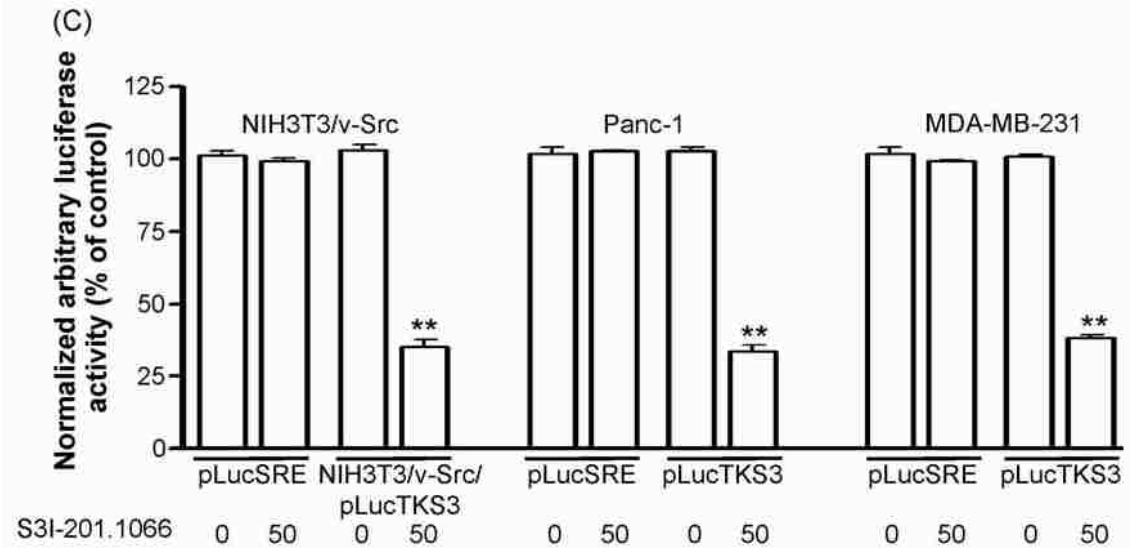
(C)
Normalized arbitrary luciferase activity (% of control)
125
100
75
50
25
0
NIH3T3/v-Src
Panc-1
MDA-MB-231
**
pLucSRE
NIH3T3/v-Src/ pLucTKS3
pLucTKS3
S3I-201.1066
0
50

(D)

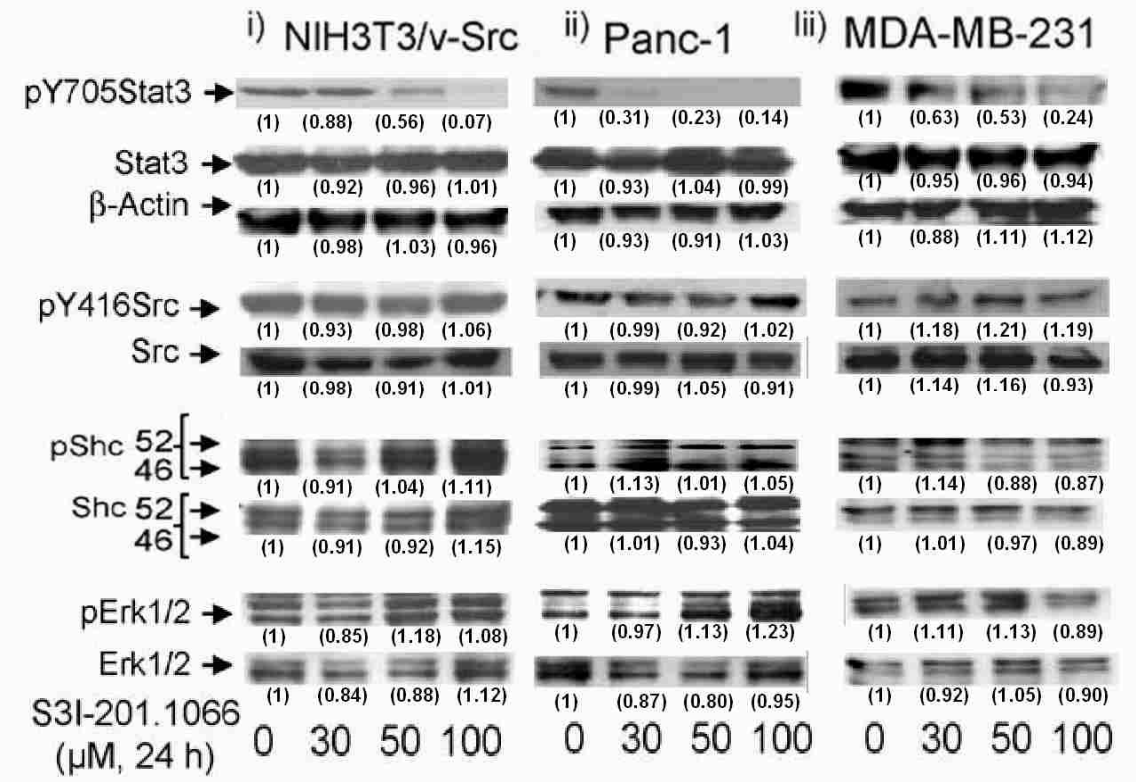

Figure 3. Effects of S3I-201.1066 on the activities of STATs, Src, Shc, and Erks.

(A) Nuclear extracts of equal total protein containing activated Stat1, Stat3, and/or Stat5 were pre-incubated with or without S3I-201.1066 for 30 min at room temperature prior to the incubation with the radiolabeled (i) and (ii) hSIE probe that binds Stat1 and Stat3 or the (iii) MGFe probe that binds Stat5 and subjected to EMSA analysis;

(B) nuclear extracts of equal total protein prepared from the designated malignant cells following 24h treatment with or without S3I-201.1066 were subjected to in vitro DNA-binding assay using the radiolabeled hSIE probe and analyzed by EMSA;

(C) cytosolic extracts of equal total protein were prepared from 24 h, S3I-201.1066- treated or untreated NIH3T3/v-Src fibroblasts that stably express the Stat3- dependent luciferase reporter (pLucTKS3) or from treated or untreated NIH3T3/v-Src fibroblasts, the human pancreatic (Panc-1) and breast (MDA-MB-231) carcinoma lines that are transiently transfected with pLucSRE or pLucTKS3 and analyzed for luciferase activity using a luminometer;

(D) SDS-PAGE and Western blotting analysis of whole-cell lysates of equal total protein prepared from S3I-201.1066- treated or untreated NIH3T3/v-Src, Panc-1 and MDA-MB-231 cells probing for pY705Stat3, Stat3, pY416Src, Src, pShc, Shc, pErk1/2 and Erk1/2. Positions of STATs:DNA complexes or proteins in gel are labeled; control lanes (0) represent nuclear extracts treated with 0.05% DMSO, or nuclear extracts or whole-cell lysates prepared from 0.05% DMSO-treated cells; luciferase activities were normalized to β-galactosidase activity. Data are representative of 3–4 independent determinations: **$p < 0.05$.

Inhibition of intracellular Stat3 activation

Stat3 is constitutively activated in a variety of malignant cells, including human breast and pancreatic cancer cells [13, 22, 23,]. Given the effect against Stat3 DNA-binding activity in vitro, we evaluated S3I-201.1066 in v-Src transformed mouse fibroblasts (NIH3T3/v-Src), human breast cancer (MDA-MB-231) and human pancreatic cancer (Panc-1) lines that harbor aberrant Stat3 activity. Twenty-four hours after treatment,

nuclear extracts were prepared from cells and subjected to Stat3 DNA-binding assay in vitro using the radio-labeled hSIE probe and analyzed by EMSA. Compared to the control (0.05% DMSO-treated cells, lane 1), nuclear extracts from S3I-201.1066-treated NIH3T3/v-Src, Panc-1 and MDA-MB- 231 cells showed dose-dependent decreases of constitutive Stat3 activation, with significant inhibition at 50 μM S3I-201.1066. (Fig. 3B, compare lanes 2–5, 8–10, and 12–15 to their respective controls (0)). Luciferase reporter studies were performed to further determine the effect of S3I-201.1066 on Stat3 transcriptional activity. Results show that the treatment with S3I-201.1066 of the v-Src transformed mouse fibroblasts (NIH3T3/v-Src) that stably express the Stat3-dependent luciferase reporter (NIH3T3/v-Src/pLucTKS3) [28,42,43] significantly (**$p < 0.01$) repressed the induction of the Stat3-dependent reporter (Fig. 3C, left panel, NIH3T3/v-Src /pLucTKS3). Similar results were obtained when the human pancreatic cancer, Panc-1 and breast cancer, MDA-MB-231 cells harboring aberrant Stat3 activity were transiently transfected with the Stat3-dependent reporter, pLucTKS3 and treated with S3I-201.1066 (Fig. 3C, middle and right panels, pLucTKS3). By contrast, a similar treatment of malignant cells that are transiently transfected with the Stat3-independent luciferase reporter, pLucSRE, which is driven by the serum response element (SRE) of the c-fos promoter, had no observable effect on the reporter induction (Fig. 3C, pLucSRE). Moreover, immunoblotting analysis showed a concentration dependent reduction of

pTyr705Stat3 levels in NIH3T3/v-Src (Fig. 3D (i), top panel), Panc-1 cells (Fig. 3D (ii), top panel), and MDA-MB-231 (Fig. 3D (iii), top panel). Cells upon treatment with S3I-201.1066 for 24 h, presumably through the blockade of Stat3 binding to pTyr motifs of receptors and the prevention of de novo phosphorylation by tyrosine kinases. By contrast, immunoblotting analysis showed no significant effects of S3I-201.1066 on the phosphorylation of Src (pY416Src), Shc (pShc), and Erk1/2 (pErk1/2) under the same treatment conditions (Fig. 3D(i)–(iii), panels 2–4 from the top). In spite of the inhibition of aberrant Stat3 activity, no observable change in total Stat3 protein was made, consistent with previous reports [12, 30]. Also, total Src, Shc and Erk1/2 protein levels remained unchanged. We infer that at the concentrations that inhibit Stat3 activity, S3I-201.1066 has minimal effect on Src, Shc and Erk1/2 activation.

In vitro evidence that S3I-201.1066 interacts with Stat3 (or SH2 domain) and selectively disrupts Stat3 binding to cognate pTyr peptide motif of receptor

Given the computational modeling prediction that S3I-201.1066 interacts with the Stat3 SH2 domain, we deduce that S3I-201.1066 blocks Stat3 DNA-binding activity by binding to the Stat3 SH2 domain, thereby disrupting Stat3:Stat3 dimerization. To determine therefore if the Stat3 SH2 domain could interact with S3I-201.1066, we tested whether the addition of purified recombinant Stat3 SH2 domain into the DNA-binding assay mixture could intercept the inhibitory effect of the agent on Stat3 activity, as observed in

Fig. 3A(i). The purified histidine-tagged Stat3 SH2 domain was added at increasing concentrations (1–500 ng) to the nuclear extracts containing activated Stat3 and the mixed extracts were pre-incubated with 100 μM S3I-201.1066 for 30 min at room temperature and subjected to DNA-binding assay in vitro for the study of the effect of S3I-201.1066, as was done in Fig. 3A(i). EMSA analysis shows a strong inhibition by S3I-201.1066 of Stat3 DNA-binding activity, as shown in Fig. 3A (i), when no purified Stat3 SH2 domain was added to the nuclear extracts (Fig. 4A, lanes 2, 7, and 9, compared to lane 1). By contrast, the observed S3I-201.0166- mediated inhibition of Stat3 DNA-binding activity was progressively eliminated by the presence of an increasing concentration of the purified Stat3 SH2 domain (Stat3SH2), leading to the full recovery of Stat3 activity when the recombinant SH2 domain protein was present at 125–500 ng (Fig. 4A, lanes 3–6, 8 and 10). The preceding studies suggest that S3I-201.1066 interacts with the Stat3 SH2 domain. However, the studies do not demonstrate a direct binding to the Stat3 SH2 domain. To provide definitive evidence of direct binding to Stat3, biophysical studies were performed. His-tagged Stat3 protein (or SH2 domain; 50 ng) was immobilized on a Ni-NTA sensor chip surface for surface plasmon resonance (SPR) analysis of the binding of S3I-201.1066 as the analyte.

Fig. 4

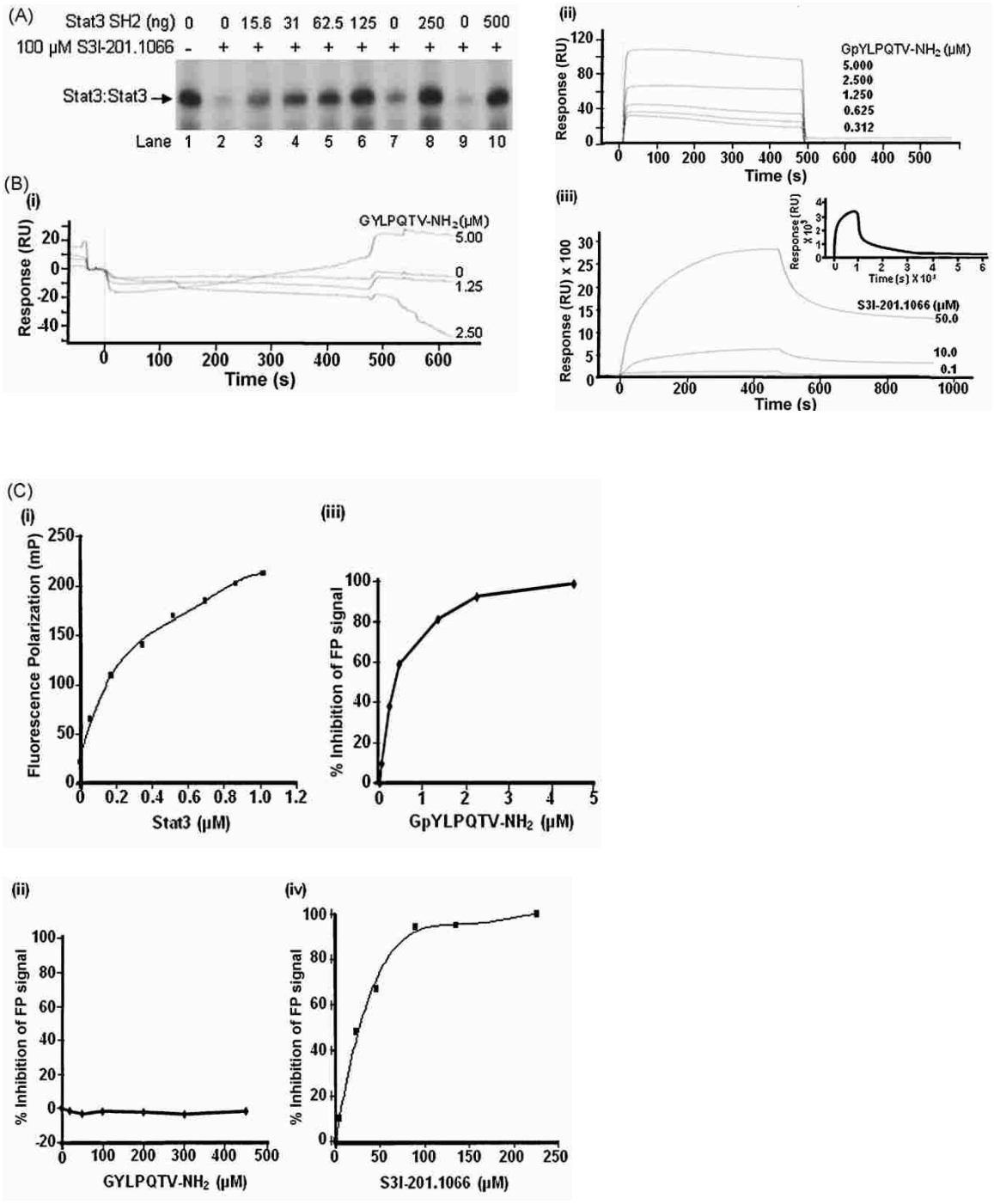

Figure 4. Studies of the interaction of S3I-201.1066 with Stat3 or the Stat3 SH2 domain.

(A) EMSA analysis of in vitro binding activity of Stat3 to the radiolabeled hSIE probe using nuclear extracts containing activated Stat3 pre-incubated with 0 or 100 μM S3I-201.1066 in the presence or absence of 0–500 ng of purified His-tagged Stat3 SH2 domain;

(B) surface plasmon resonance analysis of the binding of (i) 0–5 mM GYLPQTV–NH2 (unphosphorylated, gp-130 peptide), (ii) 0–5 mM GpYLTQTV–NH2 (phosphorylated, high affinity gp-130 peptide), or (iii) 0–50 mM S3I-201.1066 (or 50 mM S3I-201.1066, inset) as the analyte to the purified His-tagged Stat3 protein immobilized on HisCap sensor chip; and (C) fluorescence polarization assay of the binding to the 5-carboxy- fluorescein-GpYLPQTV–NH2 probe of (i) an increasing concentration of purified His-Stat3, or (ii)–(iv) a fixed amount of purified His-Stat3 (150 nM) in the presence of increasing concentrations of (ii) GpYLPQTV–NH2, (iii) GYLPQTV–NH2 or (iv) S3I-201.1066. Stat3: DNA complexes in gel are shown, control (-) lane or zero (0) represent 0.05% DMSO. Data are representative of 2–4 independent determinations.

Association and dissociation measurements were taken and the binding affinity of S3I-201.1066 for Stat3 was determined using Qdat software. Results showed gradual increase and decrease with time in the signals (response unit, RU) for the association and dissociation, respectively, of the agent upon its addition to the immobilized His-Stat3 (Fig. 4B(iii)), indicative of the binding of S3I-201.1066 to and dissociation from the Stat3 protein, with a binding affinity, K_D of 2.74 μM. These data provide the first definitive

evidence of the direct binding of Stat3 to derivatives of S3I-201. This SPR analysis of the conformational changes in His-Stat3 was validated by using the high affinity Stat3 binding phosphoTyr (pY) peptide, GpYLPQTV–NH2, derived from the interleukin-6 receptor (IL-6R) subunit, gp-130 [32,33] (with a K_D of 24 nM) (Fig. 4B(ii)), and its non-phosphorylated counterpart, GYLPQTV–NH2, which showed no significant binding to Stat3 (Fig. 4B(i)). Interestingly, the dissociation curve for S3I-201.1066 showed a large residual binding of S3I-201.1066 to Stat3 at 500–1000 s (Fig. 4B(iii), 10–50 μM, 500–1000 s), which gradually dissipated over a period longer than 6000 s (Fig. 4B(iii), inset). The natural dissociation time of S3I-201.1066 from Stat3 was determined to be 103 min. This contrasts with the rapid dissociation of the high affinity phosphopeptide, GpYLPQTV–NH2 from Stat3 (Fig. 4B(ii)). The slower “off” rate for S3I-201.1066 could impact its overall functional effects, with implications for its in vivo therapeutic application. Differences in the physicochemical properties would account for the different behaviors of the interactions with the Stat3 protein.

The studies so far demonstrate that S3I-201.1066 interacts with Stat3 or the Stat3 SH2 domain (data not shown). The interaction with the Stat3 SH2 domain could block the binding of Stat3 to cognate pTyr peptide motifs of receptors. To verify that S3I-201.1066 disrupts pTyr–Stat3 SH2 domain interactions, hence Stat3:Stat3 dimerization, we set up

a fluorescence polarization (FP) study based on the binding of Stat3 to the high affinity phosphopeptide, GpYLPQTV–NH2 [32, 33]. It has previously been reported that Stat3 binds to GpYLPQTV–NH2 with a higher affinity than to the Stat3-derived pTyr peptide, PpYLKTK. It is also reported that this high affinity peptide disrupted Stat3 DNA-binding activity in vitro with an IC_{50} value of 0.15 μM [32]. The FP assay utilizing the 5-carboxyfluorescein-GpYLPQTV–NH2 as a probe showed increasing fluorescence polarization signal (mP) with increasing concentration (in μM) of purified His-Stat3 for a robust Z' value of 0.84 (Fig. 4C(i)), which closely matches the previously reported value of 0.87 [33]. The test of the non-phosphorylated, unlabeled GYLPQTV–NH2 in the FP assay showed no evidence of inhibition (Fig. 4C(iii)), while as expected, the phosphorylated, unlabeled counterpart, GpYLPQTV– NH2 induced a complete inhibition with an IC_{50} value of 0.3 μM(Fig. 4C(iii)), consistent with the previously reported value of 0.25 ± 0.03 μM [33]. The FP assay was used to further test the ability of S3I-201.1066 to disrupt the Stat3 interaction with cognate pTyr peptide (GpYLPQTV–NH2), which showed a concentration -dependent inhibition of the fluorescent polarization signal (Fig. 4C(iv)). Inhibitory constant (IC_{50} value) was derived to be 20 ± 7.3 μM, which is within the range for the IC_{50} value (35 ± 9 μM) determined for the inhibition of Stat3 DNA-binding activity (Fig. 3A(i)). These findings together demonstrate that S3I-201.1066 binds to Stat3 or the Stat3 SH2 domain and disrupts the interaction of Stat3 with cognate pTyr

peptide motifs. This mode of action underlies the blocking Stat3 DNA-binding activity by S3I-201.1066.

To extend the studies to verify that S3I-201.1066 could disrupt the binding of Stat3 to receptors, mouse fibroblasts over-expressing the EGF receptor (NIH3T3/hEGFR) were treated with or without the compound prior to stimulation with EGF for 10 min. Cells were then subjected to immuno-fluorescence staining for EGFR (red) and Stat3 (green) and confocal microscopy for the EGF induced colocalization of Stat3 and EGFR and the Stat3 nuclear translocation. In the resting NIH3T3/hEGFR fibroblasts, EGFR (red) is widely localized at the plasma membrane, Stat3 (green) is localized at both the plasma membrane and in the cytoplasm, with no visible presence in the nucleus (stained blue for DAPI), while the colocalization of Stat3 with EGFR is minimal at the plasma membrane (Fig. 5A, upper panels). The stimulation by EGF of untreated cells induced a strong nuclear presence of Stat3 (cyan for merged Stat3 (green) and DAPI (blue)), as well as the colocalizations of EGFR and Stat3 (yellow for merged EGFR (red) and Stat3 (green)) at the plasma membrane, cytoplasm, and peri-nuclear space, and in the nucleus (Fig. 5A, bottom left).

Fig. 5

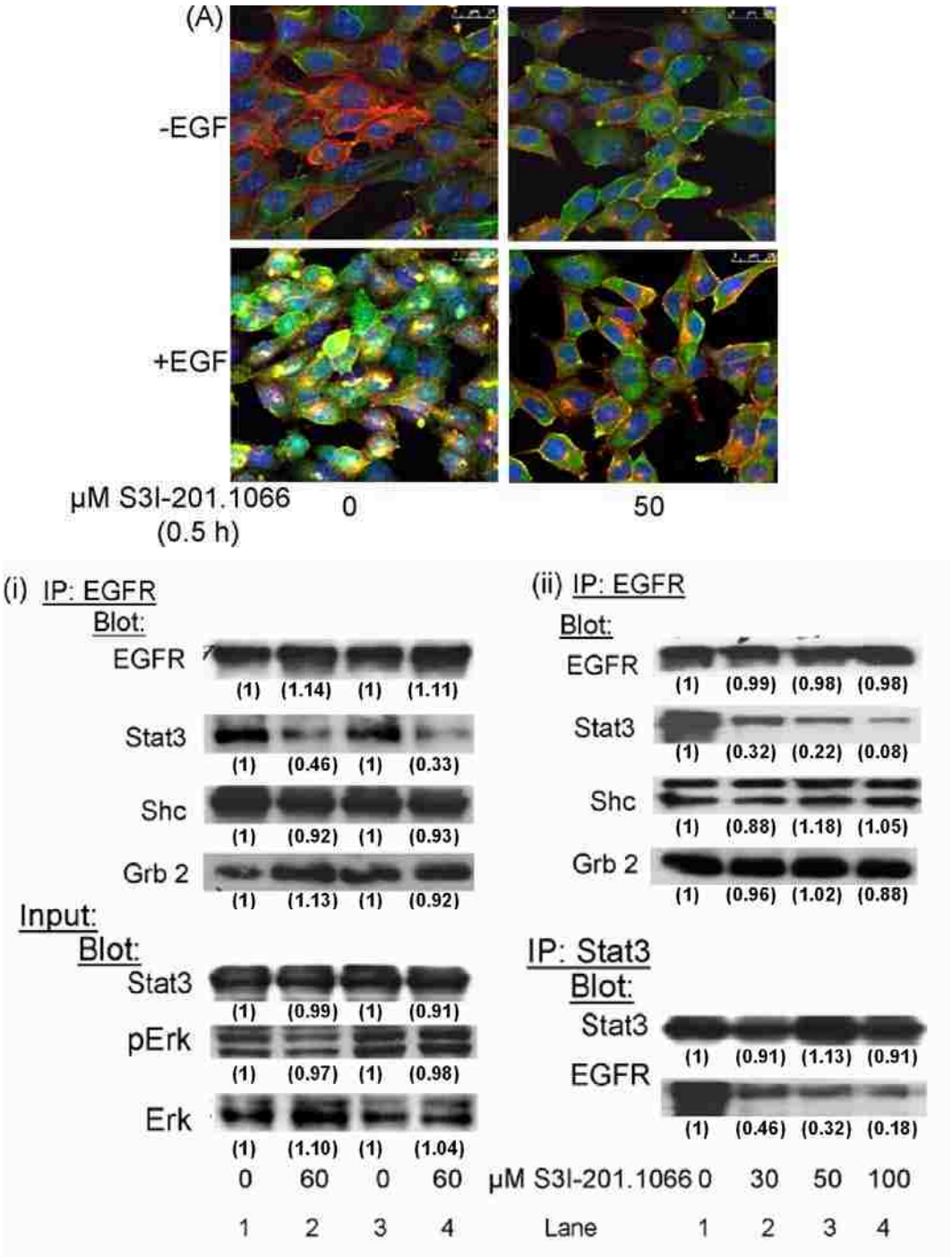

Figure 5. Effect of S3I-201.1066 on the colocalization or association of Stat3 with EGF receptor and on Stat3 nuclear translocation.

(A) Immunofluorescence imaging/confocal microscopy of Stat3 colocalization with EGFR and Stat3 nuclear localization in EGF-stimulated (100ng/ml; 10 min) NIH3T3/hEGFR pre-treated with or without 50 mM S3I- 201.1066 for 30 min;

(B) (i) immunoblotting analysis of EGFR immunecomplex (upper panel) or whole-cell lysates (lower panel) from S3I-201.1066-treated Panc-1 and MDA-MB-231 cells, or (ii) immunecomplexes of EGFR (upper panel) or Stat3 (lower panel) were treated with the indicated concentrations of S3I-201.1066, and subsequent immunecomplexes of EGFR or Stat3 were probed for EGFR, Stat3, Shc, Grb 2, or Erk1/2^{MAPK}. Data are representative of 3 independent studies.

Both of the EGF stimulated colocalization between EGFR and Stat3 and the Stat3 nuclear localization events were strongly blocked when cells were pre-treated with S3I-201.1066 before stimulating with EGF (Fig. 5A, bottom right compared to non-treated, bottom left), indicating that the compound disrupts Stat3 binding to EGFR. We infer that by blocking Stat3 binding to the receptor, S3I-201.1066 attenuates Stat3 phosphorylation/activation and thereby prevents Stat3 nuclear translocation. To investigate further the Stat3 interaction with the EGFR receptor and the effect of S3I-201.1066, co-immunoprecipitation with immunoblotting studies were performed in which EGFR immune-complex prepared from whole-cell lysates of treated and untreated

cancer cells were blotted for Stat3, and for Shc and Grb 2 as negative control. Results showed that the EGFR immune-complex from the untreated Panc-1 and MDA-MB-231 cells contained Stat3, Shc and Grb 2 (Fig. 5B(i), lanes 1 and 3, i.p. EGFR, blot Stat3, Shc, and Grb 2). By contrast, treatment of both cell lines with S3I-201.1066 significantly diminished the level of Stat3 that associated with EGFR immune-complex of equal total protein, without affecting the levels of Shc or Grb 2 (Fig. 5B (i), lanes 2 and 4, i.p. EGFR, blot Stat3, Shc and Grb 2). Western blotting of whole-cell lysates of equal total protein shows that the activated and total Erk1/2 levels are unaffected by the treatment of cells with S3I-201.1066 (Fig. 5B (i), input, blot pErk and Erk), and that the levels of Stat3 protein were the same (Fig. 5B (i), input, blot Stat3). To further analyze the effect of S3I-201.1066 on Stat3 binding to EGFR, a sequential immune-complex precipitation study was performed in which EGFR and Stat3 immune-complexes were independently prepared from whole-cell lysates of untreated Panc-1 cells. Immune-complexes of equal total protein were directly treated with 0, 30, 50, and 100 μM S3I-201.1066 for 3 h, and then subjected to a second EGFR or Stat3 immune- complex precipitation and immunoblotting analysis. Compared to untreated samples (Fig. 5B (ii), lane 1),results show that the direct treatment with S3I-201.1066 of the EGFR immune-complex dramatically diminished the level of Stat3 protein that remained associated with EGFR in the complex (Fig. 5B(ii), i.p. EGFR, blot Stat3, lanes 2–4), but had no visible effect on the

levels of Shc or Grb 2 (Fig. 5B(ii), i.p. EGFR, blot Shc or Grb 2). The EGFR levels in the immune-complexes are the same (Fig. 5B(ii), upper band). Similarly, the Stat3 immune-complex that is directly treated with S3I-201.1066 and blotted for EGFR showed strongly reduced EGFR levels, compared to the untreated Stat3 immune-complex of equal total protein (Fig. 5B(ii), i.p. Stat3, blot EGFR, compare lanes 2–4 to lanes 1). The Stat3 levels in the immunocomplexes are the same (Fig. 5B(ii), i.p. Stat3, blot Stat3). Altogether, these findings strongly demonstrate that S3I-201.1066 selectively disrupts the binding of Stat3 to cognate receptor motifs. By this mode of activity, it could block Stat3 phosphorylation and nuclear translocation.

S3I-201.1066 blocks growth, viability, malignant transformation, and the migration of malignant cells harboring constitutively active Stat3

Constitutively active Stat3 promotes malignant cell proliferation, survival and malignant transformation [13, 23, and 52]. We asked the question whether S3I-201.1066 is able to selectively decrease the viability and growth of malignant cells that harbor aberrant Stat3 activity. The human breast (MDA-MB-231) and pancreatic (Panc-1) cancer lines and the v-Src- transformed mouse fibroblasts (NIH3T3/v-Src) that harbor constitutively active Stat3, and cells that do not harbor aberrant Stat3 activity (Stat3 knockout mouse embryonic fibroblasts (MEFs) ($Stat3^{-/-}$) [41], normal human pancreatic duct epithelial cells (HPDEC) [40], and the ovarian cancer line, A2780S) in culture were treated with or

without an increasing concentration of S3I-201.1066 for up to 6 days and analyzed for viable cell numbers by CyQuant cell proliferation/viability kit or trypan blue exclusion/phase-contrast microscopy. Compared to the control (DMSO-treated) cells, the mouse fibroblasts transformed by v-Src (NIH3T3/v-Src), and the human breast cancer, MDA-MB-231 and pancreatic cancer, Panc-1 lines showed significantly reduced viable cell numbers (Fig. 6A) and were growth inhibited (data not shown) following treatment with increasing concentrations of S3I-201.1066 for 24–48 h.

By contrast, the viability and growth of the Stat3-null MEFs ($Stat3^{-/-}$), the ovarian cancer line, A2780S and the normal human pancreatic duct epithelial cells (HPDEC) that do not harbor aberrant Stat3 activity were not significantly altered by S3I-201.1066 treatment (Fig. 6A, and data not shown), with derived IC_{50} values that are beyond 100 μM, compared to values of 35, 48, and 37 μM for the inhibition of NIH3T3/v-Src, Panc-1, and MDA-MB-231, respectively (Fig. 6A, lower panel). These findings indicate that S3I-201.1066 exerts preferential biological effects on malignant cells that harbor constitutively active Stat3, with little effects on non-target cells at concentrations that inhibit Stat3 activity.

We extended these studies to examine the effect of S3I-201.1066 in colony survival

assay performed as previously reported [49]. Cultured single-cells were untreated or treated once with S3I-201.1066 and allowed to grow until large colonies were visible, which were stained and enumerated.

Results showed a dose-dependent suppression of the number of colonies for the v-Src transformed mouse fibroblasts (NIH3T3/v-Src), and the human pancreatic cancer, Panc-1 and breast cancer, MDA-MB-231 cells (Fig. 6B(iii)–(v)) (paired t-test was used to compare treated samples to their respective untreated controls). By contrast, minimal effect was observed on the colony numbers for mouse fibroblasts transformed by v-Ras (NIH3T3/v-Ras) and the ovarian cancer line, A2780S that do not harbor constitutively active Stat3 (Fig. 6B(i) and (ii)).

Furthermore, growth in soft-agar suspension of NIH3T3/v-Src, MDA-MB-231 and Panc-1 cells treated with S3I-201.1066 was significantly inhibited (Fig. 6C(iii)–(v)), compared to the minimal effect on the soft-agar growth of NIH3T3/v-Ras and the ovarian cancer line, A2780S at concentrations that inhibit Stat3 activity (Fig. 6C(i) and (ii)). Thus, it selectively blocks Stat3-dependent malignant transformation.

Fig.6

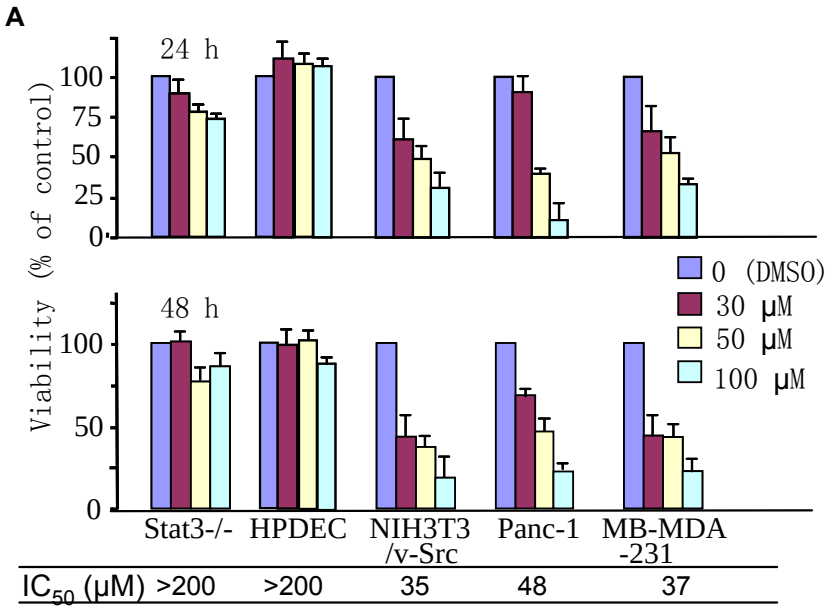
A
24 h
48 h
Viability (% of control)
100
75
50
25
0
0 (DMSO)
30 μM
50 μM
100 μM
Stat3-/-
HPDEC
NIH3T3 /v-Src
Panc-1
MB-MDA -231
IC50 (μM) >200 >200 35 48 37

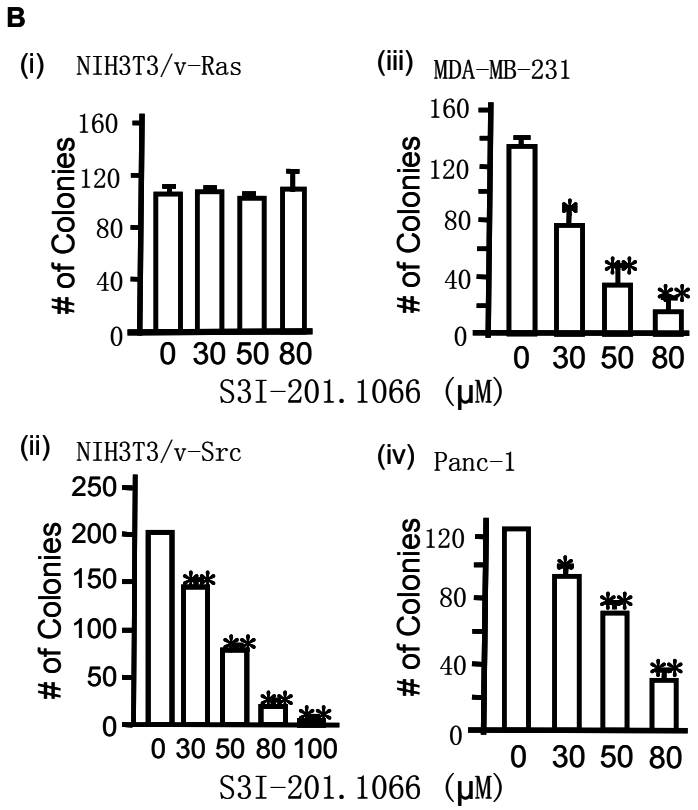
B
(i) NIH3T3/v-Ras
(iii) MDA-MB-231
# of Colonies
0 30 50 80
S3I-201.1066 (μM)
(ii) NIH3T3/v-Src
(iv) Panc-1
0 30 50 80 100

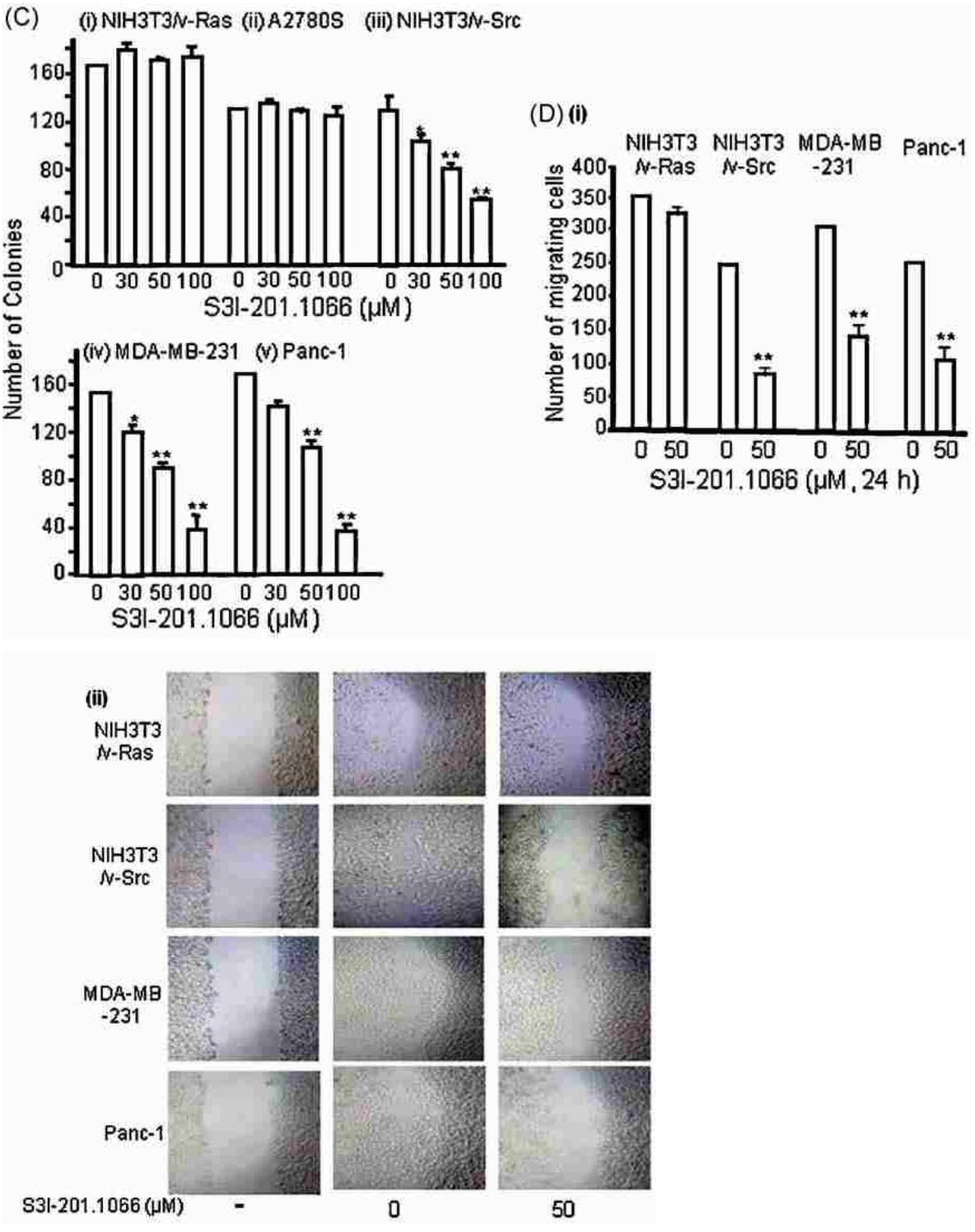

Figure 6. S3I-201.1066 suppresses viability, survival, malignant transformation and

migration of malignant cells that harbor persistently active Stat3.

(A and B) Human breast (MDA-MB-231), pancreatic (Panc-1), and ovarian (A2780S) cancer cells, the v-Src transformed mouse fibroblasts (NIH3T3/v-Src) and their v-Ras-transformed counterparts (NIH3T3/v-Ras), the Stat3-null mouse embryonic fibroblasts (Stat3-/-), and the normal human pancreatic duct epithelial cells (HPDEC) were treated once or untreated with 30–100 μM S3I-201.1066 for 24–48 h.

(A and B) cells were (A) assayed for viability using CyQuant cell proliferation kit; IC_{50} values (bottom panel) were derived from graphical representation, or (B) allowed to culture until large colonies were visible, which were stained with crystal violet and enumerated;

(C) cells (NIH3T3/v-Src, NIH3T3/v-Ras, A2780S, MDA-MB-231, and Panc-1) growing in soft-agar suspension were treated with or without 30–100 mM S3I-201.1066 every 2–3 days until large colonies were visible, which were stained with crystal violet and enumerated; and

(D) cells (MDA-MB-231, Panc-1, NIH3T3/v-Src and NIH3T3/v-Ras) in culture were wounded and treated with or without 50mM S3I-201.1066 for 12 or 24 h and allowed to migrate into the denuded area in a wound healing assay. Cultures were visualized at 10 × magnification by light microscopy and (i) cells that migrated into the denuded area counted and plotted against the concentration of S3I-201.1066 or (ii) cultures were photographed. Values are the mean and SD of 3–4 independent determinations, data are representative of 4 independent studies. p-Values: *$p < 0.05$, and **$p < 0.01$.

Studies also demonstrate that Stat3 is important for tumor progression [53, 54]. To further investigate the biological effects of S3I-201.1066 and to assess the ability to block Stat3-dependent tumor progression processes, a wound healing study was performed as a measure of the migration of malignant cells. Significantly reduced numbers of MDA-MB-231, Panc-1 and NIH3T3/v-Src cells migrating into the denuded area were observed following 12–24 h treatment with S3I-201.1066 (Fig. 6D and data not shown), with statistically significant lower numbers observed at 30 μM S3I-201.1066 treatment (data not shown). By contrast, the migration of NIH3T3/v-Ras fibroblasts was minimally affected by the same treatment conditions (Fig. 6D). In the 12–24 h treatment duration, there was no evidence of apoptosis of the treated cells (data not shown). These findings demonstrate that S3I-201.1066 selectively suppresses the migration of malignant cells that harbor aberrant Stat3 activity.

S3I-201.1066 represses the expression of c-Myc, Bcl-xL, VEGF, Survivin, and MMP-9

Known Stat3 target genes are critical to the dysregulated biological processes promoted by aberrantly active Stat3 [13, 22, 52]. We sought to validate the inhibitory effect of S3I-201.1066 on aberrant Stat3 signaling and to define the underlying molecular mechanisms for the anti-tumor cell effects of the agent by investigating the changes in the induction of known Stat3-regulated genes. In the human breast carcinoma,

MDA-MB-231 and pancreatic cancer, Panc-1 lines, and the mouse fibroblasts transformed by v-Src, which harbor constitutively active Stat3, immunoblotting analysis of whole-cell lysates shows that treatment with 50 μM S3I-201.1066 for 24 h down-regulated the expression of c-Myc, Bcl-xL, VEGF, Survivin, and MMP-9 proteins (Fig. 7A). Bands were quantified, normalized to β-actin, and the values corresponding to the band intensities for the samples from treated cells relative to the respective control (set at 1) are reported in parenthesis. These data indicate that S3I-201.1066 sufficiently represses the constitutive induction of Stat3-regulated genes. We infer that in doing so, S3I-201.1066 is able to thwart the ability of aberrant Stat3 to promote the dysregulation of growth and survival of malignant cells. These findings are in agreement with the results in Fig. 2C and together support the ability of S3I-201.1066 to block Stat3 transcriptional activity.

S3I-201.1066 inhibits growth of human breast tumor xenografts

Given Stat3's importance in tumor growth and tumor progression, we evaluated S3I-201.1066 in xenograft models of the human breast cancer (MDA-MB-231) cells that harbor aberrant Stat3 activity. Compared to control (vehicle-treated) tumor-bearing mice, treatment (i.v. injection) with S3I-201.1066 at 3 mg/kg every 2 or 3 days for 17 days induced significant decrease in tumor growth (Fig. 7B). At the dosing schedule used, the

drug was well tolerated and the animals showed no obvious signs of toxicity. The underlying premise of the antitumor effects is the ability of S3I-201.1066 to inhibit aberrant Stat3 activity.

To determine whether the treatment with S3I-201.1066 modulated the in vivo activity and function of aberrant Stat3 in the human breast tumor xenografts, we evaluated the status of Stat3 activity and the expression of known Stat3-regulated genes in vivo. Upon the completion of the study, control tumors and residual tumors from treated mice were harvested and tissue lysates were prepared and analyzed by electrophoretic mobility shift assay using the radiolabeled hSIE probe that binds Stat3 (Fig. 7C(i)) or immunoblotting (Fig. 7C(ii)). Representative data for one control, untreated tumor and three treated tumor tissues showed both decreased phosphorylation (pY705Stat3) (Fig. 7C(ii), upper band) and DNAbinding activity (Fig. 7C(i)) of Stat3 in tumors from treated mice(T1–T3, versus C). Furthermore, immunoblotting analysis showed diminished expression of c-Myc, Bcl-xL, VEGF, and Survivin in the tumor tissues from treated mice compared to control (Fig. 7C(ii)). These data indicate that the i.v. administration of S3I-201.1066 at the dosing schedule used achieved sufficient intra-tumoral levels of S3I-201.1066, which led to the suppression of Stat3 tyrosine phosphorylation, DNA-binding and transcriptional activities. These findings together demonstrate that

S3I-201.1066 inhibits constitutive Stat3 activation, leading to decreased expression of known Stat3-regulated genes, and hence inducing antitumor cell effects and tumor regression.

Fig. 7

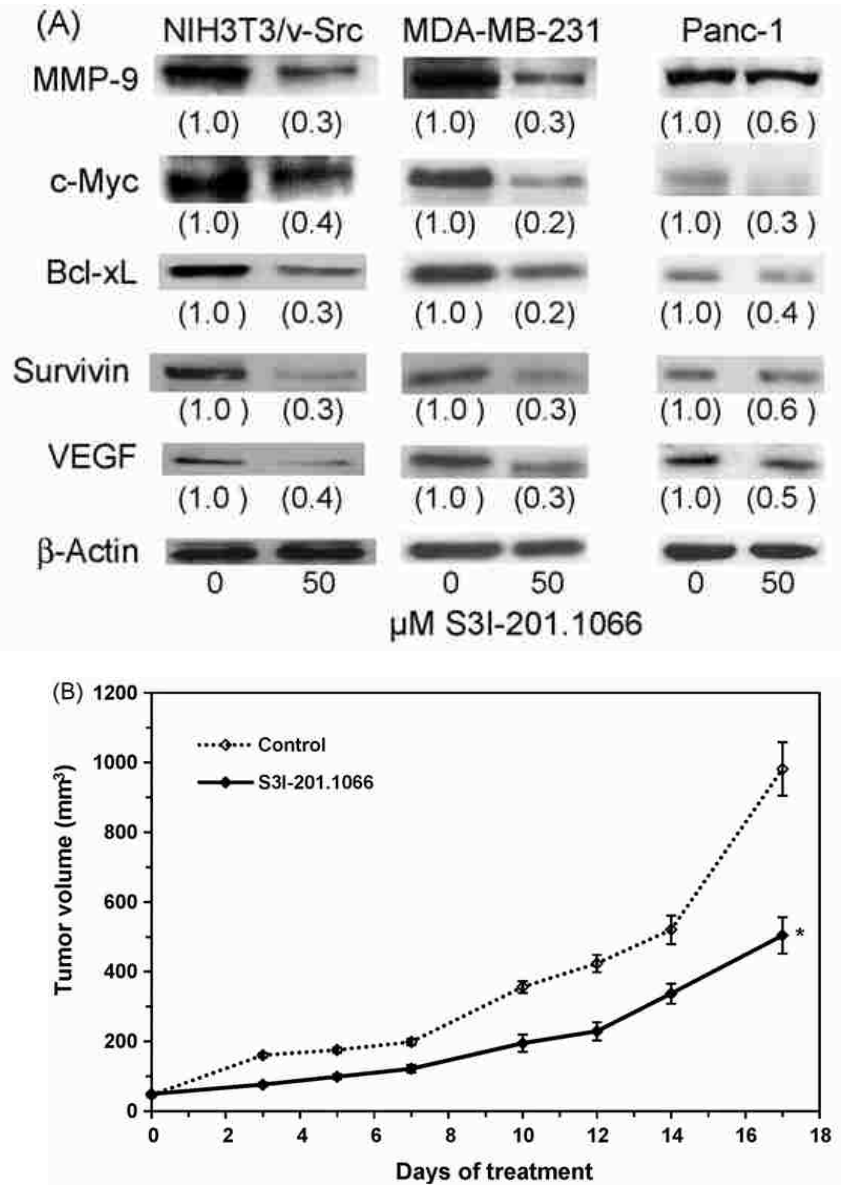

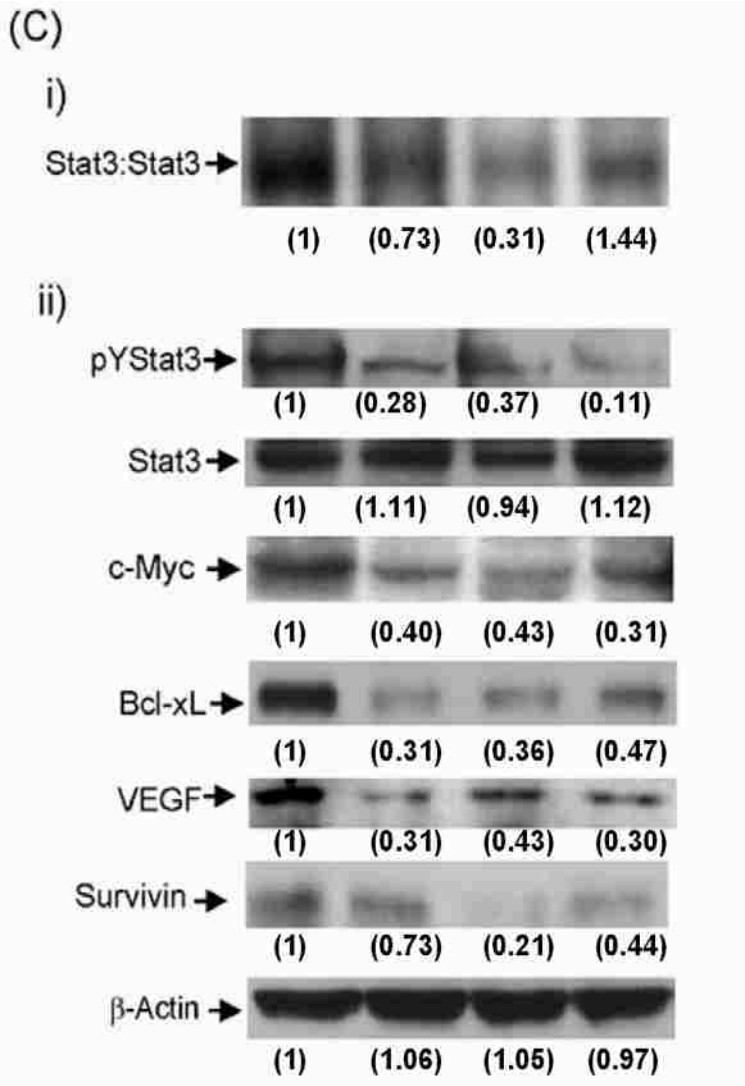

Figure 7. S3I-201.1066 suppresses c-Myc, Bcl-xL, Survivin, MMP-9 and VEGF expression in vitro and in vivo and inhibits growth of human breast tumor xenografts.

(A) SDS-PAGE and Western blotting analysis of whole-cell lysates prepared from the human breast cancer, MDA-MB-231 and pancreatic cancer, Panc-1 cells, and the v-Src-transformed mouse fibroblasts (NIH3T3/v-Src) untreated (DMSO, control) or treated with 50 mM

S3I-201.1066 for 24 h and probing with anti-Myc, Bcl-xL, MMP-9, Survivin, VEGF or β-actin antibodies;

(B) Human breast (MDA-MB-231) tumor-bearing mice were given S3I-201.1066 (3 mg/ kg) or vehicle (0.1% DMSO in PBS) i.v. every 2 or 3 days. Tumor sizes, measured every 2 or 3 days, were converted to tumor volumes and plotted against treatment days; (C) tumor tissue lysates prepared from extracted tumor tissues from one control;

(C) Three treated (T1–T3) mice were subjected to (i) Stat3 DNA-binding activity and EMSA analysis or (ii) immunoblotting analysis for pY705Stat3, Stat3, c-Myc, Bcl-xL, VEGF, Survivin, and b-actin. Positions of proteins in gel are shown. Data are representative of 2–3 independent determinations, values in parenthesis represent the band intensities for the samples from treated cells relative to the respective control (set at 1), data are the mean and SD from replicates of 12 tumor-bearing mice in each group. p-Values: *$p < 0.05$.

Discussion

Computational modeling of the interactions of the Stat3 SH2 domain with the previously reported Stat3 inhibitor lead, S3I-201 [12], derived key structural information for lead optimization and a rational synthetic program that furnished exciting new analogs. Analog, S3I-201.1066 shows improved Stat3-inhibitory potency and selectivity in vitro, with intracellular Stat3-inhibitory activity that is enhanced 2–3-fold. Moreover,

S3I-201.1066 exhibited improved target selectivity, with minimal inhibitory effect on the phosphorylation of Src, Erk1/2^{MAPK} and Shc proteins at concentrations (30–50 μM) that inhibit intracellular Stat3 activation, despite there being SH2 domains involved in the mechanisms leading to the activation of these other proteins. Per molecular modeling, the improved activity could in part be due to the enhanced interactions with the Stat3 protein, possibly by the (para-cyclohexyl) benzyl moiety that extends from the scaffold amide nitrogen and makes important contacts with the hydrophobic residues Trp623, Ile659, Val637 and Phe716 within the unexplored pocket.

The native Stat3 peptide inhibitor, PpYLKTK and its peptidomimetic analogs [28, 29] and several other Stat3 SH2 domain binding and dimerization disrupting peptides and derivatives have been reported [31, 32, and 35]. Previous studies have utilized the fluorescence polarization analysis to characterize the binding of the native, high affinity phosphopeptide, GpYLPQTV–NH2 (as 5-carboxyfluorescein-GpYLPQTV– NH2) to the Stat3 protein [32, 33]. Using this assay platform and SPR analysis, we provide definitive evidence for the physical interaction of S3I-201.1066 with Stat3 or the Stat3 SH2 domain, with an affinity (K_D) of 2.74 μM. The analysis of the interaction reveals a slower kinetics of the association and dissociation events, which contrasts the more rapid binding and dissociation of the native, high affinity peptide, GpYLPQTV–NH2 to and from Stat3, with

a corresponding affinity (K_D) of 24 nM. The second supporting evidence for the interaction of S3I-201.1066 with Stat3 comes by way of the disruption by S3I-201.1066 of the Stat3 binding to the pTyr peptide in a fluorescent polarization assay, with a derived IC_{50} of 20 μM. By comparison, the unlabeled, native phosphopeptide disrupts the Stat3 binding to the pTyr peptide probe, with an IC_{50} value of 0.3 μM, which is in line with the reported affinity of 0.15 ± 0.01 μM [33] or the IC_{50} value of 0.290 ± 0.063 μM [31]. The higher affinity of the native peptide for the protein should be expected, given the more favorable physicochemical properties that will facilitate a stronger binding to the Stat3 protein. Nonetheless, data showing a slower dissociation of S3I-201.1066 from Stat3 suggests this drug is likely to show a more prolonged effect on the target and its function per a given dose.

Current study provides support for the binding of S3I-201.1066 to Stat3 and for the disruption of the interaction between Stat3 and pTyr peptide. Given the disruption of the Stat3 binding to the cognate peptide, GpYLPQTV–NH2, we infer that inside cells, S3I-201.1066 could interfere with the ability of Stat3 (via SH2 domain) to bind to cognate pTyr motifs on receptors and thereby block *de novo* phosphorylation by tyrosine kinases, as well as disrupt preexisting Stat3:Stat3 dimers, particularly in malignant cells that harbor aberrantly active Stat3. Accordingly, we present evidence that both of the

association of Stat3 with EGFR and the Stat3 nuclear localization in ligand-stimulated cells are strongly blocked by the treatment of cells with S3I-201.1066. Although other Stat3 dimerization disruptors have been previously identified through molecular modeling [30, 55], the present study is the first to provide biophysical evidence for a direct interaction of a small-molecule, dimerization disruptor with the Stat3 protein.

Substantive evidence demonstrates that aberrant Stat3 activity promotes cancer cell growth and survival [28, 29, 39, 56, 57], and induces tumor angiogenesis [58, 59] and metastasis [53, 59]. Accordingly, inhibitors of Stat3 activation and signaling have been shown to induce antitumor cell effects consistent with the abrogation of Stat3 function [7, 12, 28-30, 47, 60–62]. The present study parallels those published reports in showing that a newly derived agent, S3I-201.1066 induces the growth inhibition and the loss of viability and survival of the human pancreatic cancer, Panc-1 and breast cancer, MDA-MB-231 cells, and transformed mouse fibroblasts (NIH3T3/v-Src) that harbor aberrant Stat3 activity, while having minimal effects on normal human pancreatic duct epithelial cells, the Stat3-null mouse embryonic fibroblasts [41], the ovarian cancer line, A2780S, and the viral Ras-transformed mouse fibroblasts that do not harbor aberrant Stat3 activity. Moreover, the S3I-201.1066-induced anti-tumor cell effects on malignant cells harboring aberrant Stat3 activity occurred at significantly lower concentrations, 30–50 μM than the 100 μM

cellular activity previously reported for the lead agent [12]. Mechanistic insight into the biological effects of S3I-201.1066 reveals the suppression of the constitutive expression of known Stat3-regulated genes, including c-Myc, Bcl-xL, VEGF, Survivin, and MMP-9, which control cell growth and apoptosis, promote tumor angiogenesis, or modulate tumor cell invasion [30, 53, 56, 59, 63, and 64]. Furthermore, the effect of S3I-201.1066 on Stat3 oncogenic function is shown by the significant antitumor response induced in human breast tumor xenografts following the in vivo administration of this agent. Data also suggest that at the dosing schedule used, the i.v. administration of S3I-201.1066 achieved intra-tumoral levels sufficient to modulate activated Stat3 and its function.

We report the application of computational modeling in conjunction with rational, structure-based virtual design approach for the optimization of S3I-201. The new agent, S3I-201.1066 binds to Stat3, disrupts Stat3 SH2 domain:pTyr interactions, and hence Stat3:Stat3 dimerization and Stat3 binding to receptor, thereby inhibiting Stat3 phosphorylation, nuclear translocation and oncogenic functions, and inducing antitumor cell effects in vitro and antitumor effects *in vivo*.

BP-1-102, AN ORALLY-BIOAVAILABLE SMALL-MOLECULE STAT3 INHIBITOR REGRESSES HUMAN BREAST AND LUNG CANCER XENOGRAFTS AND REVEALS NOVEL STAT3 FUNCTIONS

By computational and structural analyses of the interaction between Stat3 and the lead dimerization disruptor, S3I-201.1066, we have designed a diverse set of analogs. We found that BP-1-102, a structural analog of S3I-201.1066, directly interacts with Stat3, with an affinity (K_D) of 504 nM, and inhibits *in vitro* Stat3 DNA-binding activity, with IC_{50} of 6.8 μM, and selectively inhibits Stat3 activity in human and mouse tumor cell lines that harbor consecutively-active Stat3. The result together strongly suggest the anti-tumor cell effects of BP-1-102 is largely dependent on the inhibition of aberrant Stat3 activity. Significantly, BP-1-102 induced strong antitumor response in mouse xenografts of human breast cancer when administered via intravenous or oral gavage.

Introduction

The Signal Transducer and Activator of Transcription (STAT) family of proteins are cytoplasmic transcription factors that mediate responses to cytokines and growth factors, including promoting cell growth and differentiation, development, inflammation, and immune responses [65, 66]. Classically, during activation, STATs are recruited via the SH2 domain to the receptor phosphotyrosine (pTyr) peptide motifs, which facilitates STATs phosphorylation on a key tyrosyl residue by tyrosine kinases of growth factor receptors and cytoplasmic, non-receptor tyrosine kinases, such as Janus kinases (Jaks) and the Src family. Although pre-existing STAT dimers have been detected [17], phosphorylation induces STAT:STAT dimerization through a reciprocal pTyr-SH2 domain interaction. The active STAT:STAT proteins are predominantly in the nucleus where they induce gene transcription by binding to specific DNA-response elements in the promoters of target genes. Recent evidence has also revealed the transcriptional function for unphosphorylated STAT monomers [67].

The STAT proteins have importance in carcinogenesis and tumorigenesis. This is due to their aberrant activation, as is the case for the family member, Stat3, which occurs in many human cancers [13, 22] and promotes tumor progression. While the mechanisms of Stat3-mediated tumorigenesis continue to be elucidated, evidence strongly supports

de-regulation of gene expression leading to uncontrolled growth and survival of tumor cells, enhanced tumor angiogenesis and metastasis, and the development of resistance [4, 6, 20, 22, and 68]. More recent studies have also identified a non-traditional role of Stat3 as a regulator of mitochondrial function that potentially promotes malignant transformation [69]. Aberrant Stat3 signaling further regulates the tumor microenvironment to support the malignant phenotype [26]. Consecutively-active Stat3 in tumor cells controls the type and levels of inflammatory cytokines and chemokines that are released in the tumor microenvironment, thereby modulating the functioning of tumor-associated inflammatory and immune cells. While tumor cell-associated constitutively-active Stat3 suppresses the expression of pro-inflammatory cytokines, such as inteluekin-6 (IL-6), RANTES, and IP-10, it promotes the induction of vascular endothelial growth factor (VEGF), interleukin-10 (IL-10), and other soluble factors that activate Stat3 in dendritic cells and consequently inhibit dendritic cell maturation [70]. Stat3 further engages in signaling cross-talk with proteins important in inflammation, such as NFκB in a manner that supports the malignant phenotype [71]. Thus, Stat3 functions in many diverse contexts in directing cellular processes towards tumorigenesis.

Given its critical importance to cancer, there is increased focus on discovering and developing novel Stat3 inhibitors as anticancer drugs. The Stat3 SH2 domain:pTyr

peptide interaction has gained increased attention in these drug discovery efforts [7, 8, 9, 12, 13, 30, 34, 35, 72, 73] , due to its importance in Stat3:Stat3 dimerization. Although several dimerization-disrupting small-molecule Stat3 inhibitors have been reported, in some cases with cellular activities and evidence of *in vivo* efficacy [7, 12, 30, 72, 74], thus far none has reached the clinic for several reasons, including the suitability of the scaffolds and pharmacokinetic issues. The leading dimerization-disrupting agent, S3I-201.1066 [75] was subjected to computer-aided lead optimization. We describe the derivation and the characterization of the analog, BP-1-102, an orally-bioavailable, high-affinity Stat3 SH2 domain ligand that inhibits Stat3 activation, Stat3-mediated interactions, and known and novel Stat3-depedent functions *in vitro* and *in vivo*, and thereby inhibits growth of mouse xenografts of human breast and non-small cell lung cancers.

Materials and Methods

Cells and reagents

Normal mouse fibroblasts (NIH3T3) and counterparts transformed by v-Src (NIH3T3/v-Src) or v-Ras (NIH3T3/v-Ras), the human breast cancer line (MDA-MB-231) and counterpart expressing inducible KLF8 shRNA (231-K8ikd), and the human prostate

(DU145), non-small cell lung (A549), and pancreatic (Panc-1) cancer cells have all been previously reported [8, 43, 83, 100]. The Stat3-dependent (pLucTKS3) and Stat3-independent (pLucSRE), and the pLucKLF8 luciferase reporters, and the vectors expressing v-Src (pMv-Src) and β-galactosidase (β-gal) have been previously reported [42, 43, and 88]. The Human Cytokine Array Kit, ARY005 was purchased from R&D Systems (Minneapolis, MN). G-CSF was purchased from Sigma-Aldrich (St. Louis, MO) and was used at 100 ng/ml. Cells were grown in Dulbecco's modified Eagle's medium (DMEM) containing 10% heat-inactivated fetal bovine serum.

Cloning and protein expression

The molecular cloning, expression, and the purification of His-tagged Stat3 have previously been reported [75, 100].

Nuclear extract preparation, gel shift assays, and densitometric analysis

Nuclear extract preparations and electrophoretic mobility shift assay (EMSA) were carried out as previously described [43]. The ^{32}P-labeled oligonucleotide probe used was hSIE (high affinity sisinducible element from the c-fos gene, m67 variant, 5'-AGCTTCATTTCCCGTAAATCCCTA) that binds Stat3 [100]. For direct effect of BP-1-102 on Stat3 DNA-binding activity, nuclear extracts were pre-incubated with the

agent for 30 min at room temperature prior to incubation with the radiolabeled probe for 30 min at 30 ^{o}C before subjecting to EMSA analysis. Bands corresponding to DNA-binding activities were scanned, quantified for each concentration of BP-1-102 using ImageQuant and plotted as percent of control (vehicle) against concentration of compound, from which the IC_{50} values were derived, as previously reported [11].

SDS-PAGE/Western blotting analysis

Immunoblotting analysis of whole-cell lysates were performed as previously described [75, 100]. Primary antibodies used were anti- Stat3, pY705Stat3, pY416Src, Src, pErk1/2, Erk1/2, pJak1, Jak1, pShc, Shc, Cyclin D1, c-Myc, Bcl-xL, Survivin, FAK, paxillin, E-cadherin, HDAC1, and β-Actin (Cell Signaling Technology, Danvers, MA), KLF8 [82], and VEGF (Santa Cruz Biotechnolgy, Santa Cruz, CA), and EPSTI1 (Sigma Aldrich, St. Louis, MO).

Immunoprecipitation (IP) studies

These studies were performed as previously reported [7] using whole-cell lysates or nuclear extracts (500 μg total protein) and 2 μg of anti-Stat3, anti-NFκB/p65RelA, or anti-IκBpolyclonal antibody (Santa Cruz) or 5 μl of the monoclonal anti-Stat3 antibody (Cell SignalingTechnology).

Fluorescence polarization (FP) assay

Fluorescence polarization (FP) assay was conducted as previously reported [74] using the labeled phospho-peptide, 5-carboxyfluorescein-GpYLPQTV-NH2 (where pY represents phospho-Tyr) as probe and purified His-tagged Stat3, and the FP measurements were taken using POLARstar Omega (BMG LABTECH, Durham, NC) with the set gain adjustment at 35 mP.

Small-interfering RNA (siRNA) transfection

The Stat3 siRNA smart pool Stat3 (cat # M-003544) and the control, SiGENOME non-targeting siRNA pool were purchased from Dharmacon RNAi Technologies, Thermo Scientific (Lafayette, CO). Transfection into cells was performed following manufacturer's protocol and using 200 pmol siRNA with 10 µL of Lipofectamine RNAiMAX (Invitrogen Corporation, Carlsbad, CA) in serum-free OPTI-MEM culture medium (5 ml) (Invitrogen).

Cell viability and proliferation assay

Cells in culture in 6-well or 96-well plates were treated with or without increasing

concentrations of BP-1-102 for 24-96 h and subjected to CyQuant cell proliferation assay (Invitrogen), or harvested, and the viable cells counted by trypan blue exclusion with phase contrast microscopy.

Soft-agar colony formation assay

This was performed in 6-well plates, as previously reported [12]. BP-1-102 treatments were initiated 24 h following the seeding of cells and repeated every 2 days until large colonies were observed.

Transient transfection of cells

Eighteen hours following seeding, cells in 12-well plates were transiently co-transfected with 100 ng β-galactosidase (for normalizing), and 900 ng of pLucTKS3, pLucSRE, or pLucKLF8, and with or without 500 ng pMv-Src, where appropriate, for 3 h using Lipofectamine plus (Invitrogen) and following the manufacturer's protocol. Twelve hours after transfection, cells were treated or untreated with BP-1-102 (0-60 μM) for 16-24 h, after which they were harvested and cytosolic extracts prepared for luciferase assay, as previously reported [42,43].

Cytosolic extracts and cell lysates preparation and luciferase assay

Cytosolic extract preparation from mammalian cells and luciferase assay are as described previously [42, 43, and 75]. Luciferase activities were measured using a luminometer (Lumat LB 9507, EG&G Berthold, Germany) and normalized to β-galactosidase activity.

Immunostaining with laser-scanning confocal imaging

Cells were grown on glass cover slips in multi-well plates, fixed with ice-cold methanol for 15 min, washed 3 times with 1X phosphate buffered saline (PBS), permeabilized with 0.2% Triton X-100 for 10 min, and further washed 3-4 times with PBS. Specimens were then blocked in 1% bovine serum albumin (BSA) for 30 min and incubated with anti-pY705Stat3 (Cell Signaling) or anti-pS536 NFκB (Cell Signaling) antibody at 1:50 dilution (in 0.1% BSA) at 4 °C overnight. Subsequently, cells were rinsed 3 times with PBS and incubated with two AlexFluor secondary antibodies, AlexaFLuor546 (goat anti-mouse) and AlexaFluor488 (donkey anti-rabbit) (Molecular Probes, Invitrogen) for pY705Stat3 and pS536NFκB/p65 detection, respectively, for 1 h at room temperature in the dark. Specimens were then washed 3 times with PBS, mounted on slides with VECTASHIELD mounting medium containing DAPI (Vector Lab, Inc., Burlingame, CA), and examined immediately under a Leica TCS SP5 confocal microscope (Germany).

Images were captured and processed using the Leica TCS SP 5 software.

Surface plasmon resonance analysis (SPR)

SensiQ and its analysis software Qdat (ICX Technologies, Oklahoma City, OK) were used to analyze the interaction between agents and the purified His-tagged Stat3 protein and to determine the binding affinity, K_D, as previously reported [75, 100].

Colony survival assay

This was performed as previously reported [100]. Briefly, cells were seeded as single-cell in 6-cm dishes (500 cells per well), treated once the next day with different concentrations of BP-1-102 for 24 h, and allowed to culture until large colonies were visible., which were stained with crystal violet for 4 h and counted under phase-contrast microscope.

Wound-healing assay

Wounds were made using pipette tips in monolayer cultures of cells in six-well plates. Cells were treated with or without increasing concentrations of BP-1-102 and allowed to migrate into the denuded area for 16 h. Cells was visualized at a 10X magnification using

an Axiovert 200 Inverted Fluorescence Microscope (Zeiss, Göttingen, Germany) and pictures of cells were taken using a mounted Canon Powershot A640 digital camera (Canon USA, Lake Success, NY). Cells that migrated into the denuded area were quantified.

Cell migration/invasion assays

Cell migration/invasion experiments were carried out and quantified as previously reported [7, 12, 82] using Bio-Coat migration/invasion chambers (BD Biosciences, Bedford, MA) of 24-well companion plates with cell culture inserts containing 8 μm pore size filters and following the manufacturer's protocol, with some modifications. Briefly, for doxycycline (Dox) induction, cells were maintained un-induced, U (in the absence of Dox) or induced, I (in the presence of Dox) for three days. Cells were then resuspended in serum-free medium minus or plus Dox, transferred to the top chambers of the 24-well trans-well plates, and incubated for 16 h to allow the migration or invasion towards the serum-containing medium in the bottom chamber, and cells on the lower side were then counted. For treatment with BP-1-102 (15 μM), the drug was added to both the top and bottom chambers during the 16-h incubation. Where appropriate, the migration or invasion rates were normalized to the control, U cells in the absence of serum and in the bottom chambers.

Cytokine analysis

Cytokine analysis was performed using the human cytokine array kit and following the manufacturer's (R&D Systems, Minneapolis, MN) instructions. Briefly, following treatment of cells with 10 μM BP-1-102 for 48 h, 1 ml samples of conditioned culture medium or in the case of tumors, 500 μg of tumor tissues lysates in RIPA buffer (50 mM Tris-HCl, pH7.4, 1% NP-40, 150 mM NaCl, 2 mM EDTA, 0.1% SDS) were mixed with a cocktail of biotinylated detection antibodies. The mixture was incubated with the array membrane for antibody binding on the membrane. Membrane was processed for signal development using Streptavidin-HRP and chemiluminescent detection reagents, exposed to X-ray films, and then processed. The relative changes in cytokine levels between samples were analyzed by quantitation of pixel density in each spot of the array with ImageJ (National Institute of Health, Bethesda, MD).

Mice and in vivo tumor studies

Six-week-old female athymic nude mice were purchased from Harlan (Indianapolis, IN) and maintained in the institutional animal facilities approved by the American Association for Accreditation of Laboratory Animal Care. All mice studies were performed under an Institutional Animal Care and Use Committee (IACUC)-approved protocol. Athymic nude

mice were injected subcutaneously in the left flank area with 1 x 10^6 human breast cancer MDA-MB-231 or non-small cell lung cancer A549 cells in 100 µL of PBS. After 5 to 10 days, tumors of a 30-100 mm^3 volume were established. Animals with established tumors were grouped so that the mean tumor sizes in all groups were nearly identical and then given BP-1-102 (in 0.05% DMSO in water) at 1 or 3 mg/kg (i.v.) every 2 or every 3 days or 3 mg/kg (oral gavage, 100 µL) every day for 15 or 20 days. Animals were monitored every day, and tumor sizes were measured with calipers and body weights taken every 2 or 3 days. Tumor volumes were calculated according to the formula $V=0.52 \times a^2 \times b$, where a, smallest superficial diameter, b, largest superficial diameter. For each treatment group, the tumor volumes for each set of measurements were statistically analyzed in comparison to the control (non-treated) group using paired t-test.

Plasma and tumor tissue analysis

BP-1-102 concentrations in mouse plasma and tumor tissue lysates were assayed using validated analytical procedure via high-performance liquid chromatography (Shimadzu Prominence UHPLC,Shimadzu Scientific Instruments, Columbia, MD) and LC/MS/MS (API4000 Liner Ion Trap Mass Spectrometer, MDS Sciex, Ontario, Canada). The mass spectrometer was operated in a product ion scanning mode. BP-1-102 solution diluted in methanol was infused directly into the MS source at a flow of 10 µL/min. Tuning was

evaluated in both positive and negative MS modes using both turbo ion spray and atmospheric pressure chemical ionization sources. The chromatography used a Phenomenx Kinetex C18 2.1x50 mm, 1.7µ UHPLC column (Phenomenex, Torrance, CA) with a flow rate of 0.300 ml/min using a 5 mM ammonium acetate (in water) and 5 mM ammonium acetate (in acetonitrile) as mobile phase A and B, respectively.

Statistical analysis

Statistical analysis was performed on mean values using Prism GraphPad Software, Inc. (La Jolla, CA). The significance of differences between groups was determined by the paired t-test at $p < 0.05$*, < 0.01**, and < 0.005***.

Results

Computer-aided design of BP-1-102 as an analog of S3I-201.1066

The lead agent, S3I-201.1066 [75] is a moderately potent SH2 domain binding ligand [75]. Analysis of the structural composition and the topology of the Stat3 SH2 domain binding 'hotspot' show three solvent-accessible sub-pockets on the protein surface, including the key pTyr705-binding region, of which only two are accessed by S3I-201.1066 and all of the reported Stat3 inhibitors. We hypothesized that accessibility to the third pocket would

enhance Stat3-inhibitory activity. By extensive structure-activity relationship (SAR) analysis of the S3I-201.1066 and analogs structurally designed with appendages that promote interactions with all of the three sub-pockets, BP-1-102 (Fig. 8a) was identified. BP-1-102 retains the 4-aminosalicylic acid group as an effective pTyr mimetic [76, 77], which binds to the pTyr-binding portion of the SH2 domain, making interactions with Lys591, Glu594 and Arg609 (Fig. 8b), and contains the hydrophobic cyclohexyl-benzyl substituent, which forms van der Waals interactions with a series of predominantly hydrophobic residues, including, Val637, Ile659 and Trp623 (Fig. 8b) that comprise the pY+1 (Leu)- binding pocket. The most significant modification is the pentafluorobenzene sulfonamide component of the molecule, linked via a glycine unit to the salicylic acid. This interacts with the previously unexplored third sub-pocket composed of Lys591, Glu594, Ile634, and Arg595 (Fig. 8b). Critically, the pentafluorobenzene may better interact with the Stat3-SH2 domain surface by participating in more hydrogen bonds and also better interacting with the charged Lys side chain, as previously noted in a different context [78]. The more polar pentafluorobenzene unit also confers enhanced solubility.

Inhibition of Stat3 signaling and function

BP-1-102 (Fig. 8a) binds Stat3 with a higher affinity, K_D, 504 nM, as determined by Surface Plasmon Resonance (SPR) analysis (Fig. 9a), disrupts Stat3:pTyr peptide

interactions, with IC_{50} value of 4.1 μM, as assayed by Fluorescence Polarization (FP) (Fig. 9b), and inhibits Stat3 DNA-binding activity in vitro, with average IC_{50} value of 6.8 ± 0.8 μM (Fig. 10a), as measured by electrophoretic mobility shift assay (EMSA) [8, 12, 75]. These are substantial improvement over the lead, S3I-201.1066 (SPR, K_D of 2.7 μM, FP, IC_{50} of 23 μM, EMSA IC_{50} of 36 μM). [75]

Fig. 8

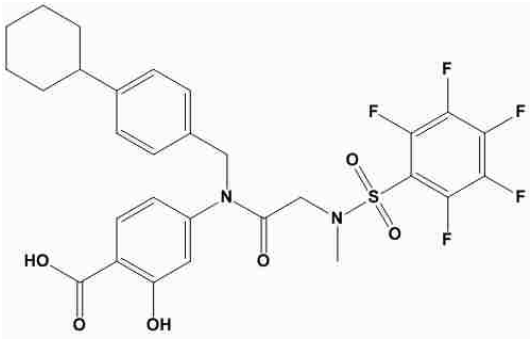

(a) Structure BP-1-102

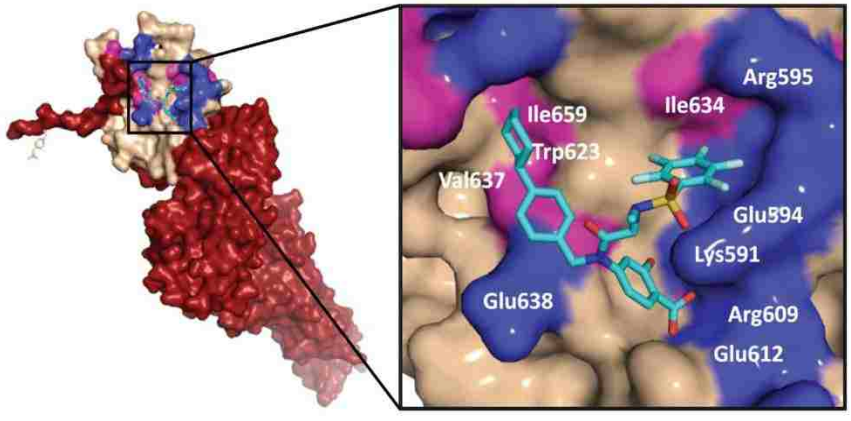

(b) Computational modeling of the binding of BP-1-102 to Stat3 SH2 domain

Figure 8. Structure of BP-1-102 and computational modeling

(a), Structure of BP-1-102. IC_{50} (EMSA), concentration of agent at which Stat3 DNA-binding activity *in vitro* is inhibited by 50%; K_D, binding affinity, as determined by surface plasmon resonance analysis; IC_{50} (FP assay), concentration of agent that inhibits by 50% the Stat3 binding to pTyr peptide motif in a fluorescent polarization assay; and

(b), Computational modeling of the binding of BP-1-102 to the Stat3 SH2 domain. Left, monomer Stat3 protein with the solvent-accessible surface of the SH2 domain (shown in off-white), color-coded, with hydrophilic residues (blue) and hydrophobic residues (pink) and overlaid with BP-1-102 (cyan). Right, the three solvent-accessible sub-pockets of the SH2 domain surface accessed by BP-1- 102, with the pentafluorobenzene sulfonamide component projecting into the third sub-pocket composed of Lys591, Gly594, Ile634, and Arg595.

Stat3 is consecutively-activated in many tumor cells [6, 13, and 22]. Twenty-four hours after treatment, BP-1-102 dose-dependently inhibited consecutively-active Stat3 in v-Src transformed mouse fibroblasts (NIH3T3/v-Src), and in the human cancer lines, MDA-MB-231 (breast), DU145 (prostate), Panc-1 (pancreatic), and A549 (non-small cell lung cancer), as evaluated by DNA-binding activity/EMSA analysis (Fig. 10b) or by pTyr705Stat3 immunoblots in whole-cell lysates (Fig. 10d and e).

Fig. 9

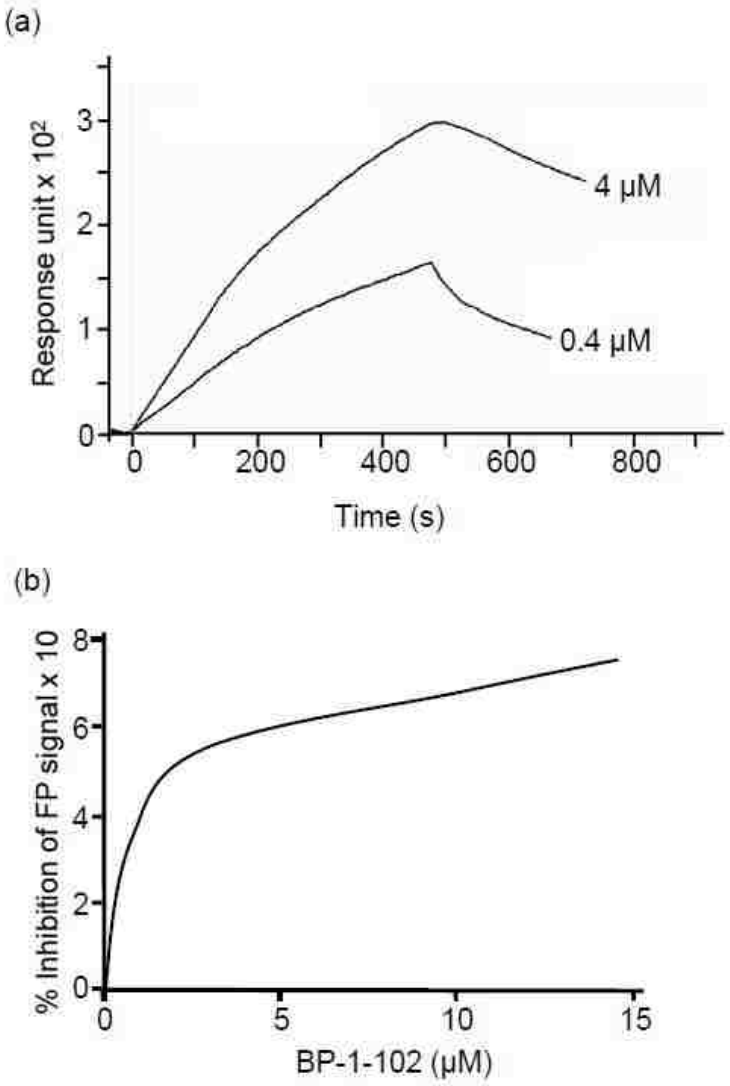

Figure 9. Surface Plasmon Resonance (SPR) Analysis and Fluorescence Polarization (FP) assay.

(a) SPR analysis of the binding of increasing concentration of BP-1-102 to the full-lengthStat3;

(b) FP assay of the binding to the 5-carboxyfluorescein-GpYLPQTV-NH2 probe of afixed amount of purified His-Stat3 (200 nM) in the presence of increasing concentrations of BP-1-102. Data are representative of 3 independent determinations.

Fig. 10

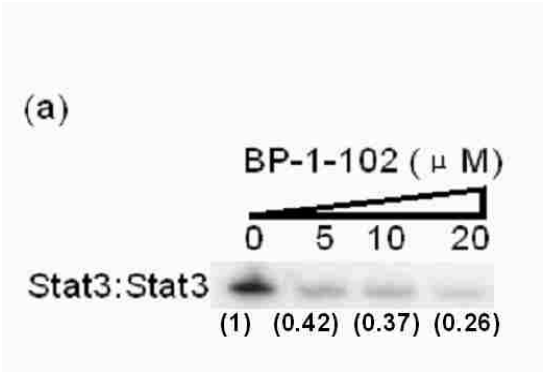
(a)
BP-1-102 (μ M)
0 5 10 20
Stat3:Stat3
(1) (0.42) (0.37) (0.26)

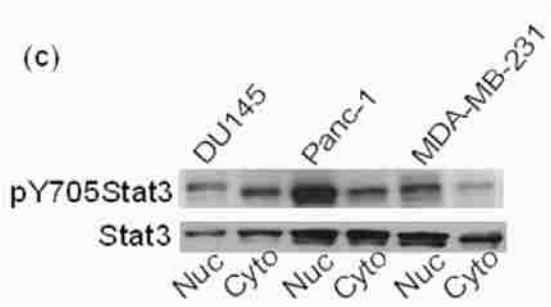
(c)
DU145
Panc-1
MDA-MB-231
pY705Stat3
Stat3
Nuc Cyto Nuc Cyto Nuc Cyto

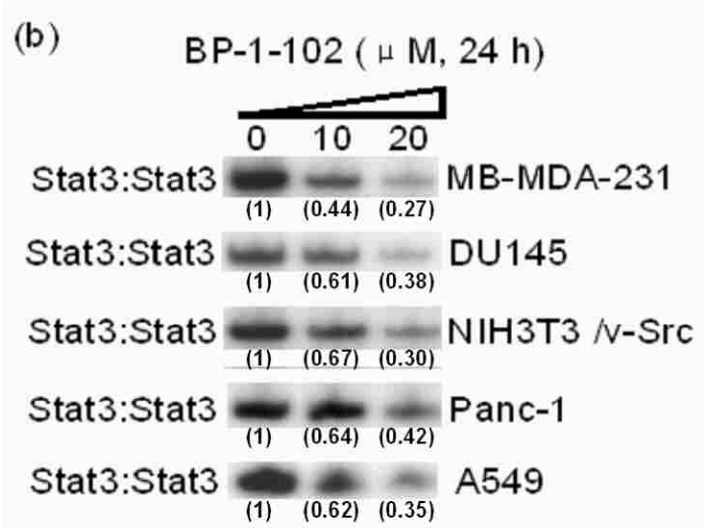
(b)
BP-1-102 (μ M, 24 h)
0 10 20
Stat3:Stat3 MB-MDA-231
(1) (0.44) (0.27)
Stat3:Stat3 DU145
(1) (0.61) (0.38)
Stat3:Stat3 NIH3T3 /v-Src
(1) (0.67) (0.30)
Stat3:Stat3 Panc-1
(1) (0.64) (0.42)
Stat3:Stat3 A549
(1) (0.62) (0.35)

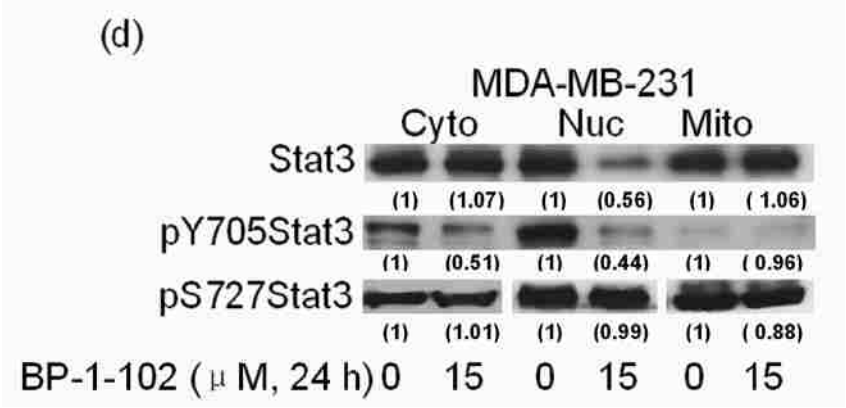
(d)
MDA-MB-231
Cyto Nuc Mito
Stat3
(1) (1.07) (1) (0.56) (1) (1.06)
pY705Stat3
(1) (0.51) (1) (0.44) (1) (0.96)
pS727Stat3
(1) (1.01) (1) (0.99) (1) (0.88)
BP-1-102 (μ M, 24 h) 0 15 0 15 0 15

(e)

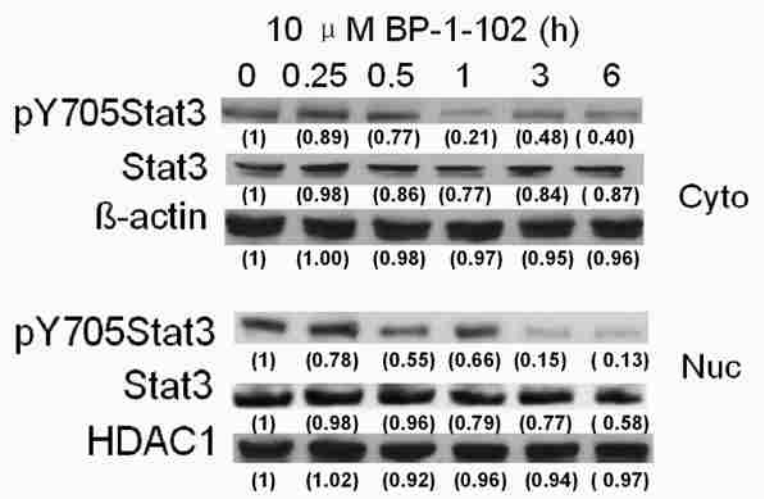

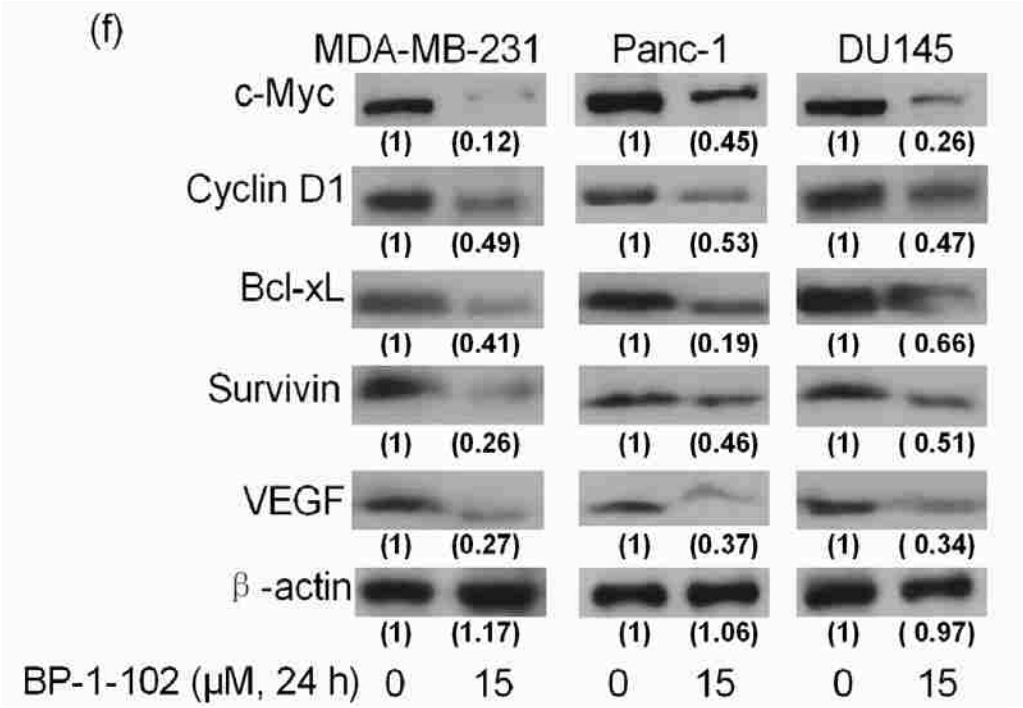

Figure 10. Effects of BP-1-102 on Stat3 activation and intracellular distribution and on the induction of Stat3 target genes.

(a) Nuclear extracts of equal total protein from NIH3T3/v-Src fibroblasts containing activated Stat3 were pre-incubated with 0-20 μM BP-1-102 for 30 min at room temperature prior to incubation with the radiolabeled hSIE probe that binds Stat3 and subjecting to EMSA analysis; (b) nuclear extracts of equal total protein prepared from the designated tumor cell lines (MDA-MB-231, DU145, NIH3T3/v-Src, Panc-1, and A549) treated with 0-20 μM BP-1-102 for 24 h were subjected to *in vitro* DNA-binding assay/EMSA analysis using the radiolabeled hSIE probe;

(c, d and e) immunoblotting analysis of cytosolic (Cyto), nuclear (Nuc) or mitochondrial (Mito) fractions of equal total protein prepared from the designated tumor cells untreated (c) or treated (d and e) with 0, 10 or 15 μM BP-1-102 for the 32 indicated times and probing for pY705Stat3, Stat3, pS727Stat3, histone deacetylase 1 (HDAC1) or β-actin; and

(f) immunoblotting analysis of whole-cell lysates prepared from tumor cell lines treated or untreated with BP-1-102 for 24 h and probing for c-Myc, Cyclin D1, Bcl-xL, Survivin, VEGF, and β-actin. Positions of Stat3: DNA complexes or proteins in gel are labeled; control lanes (0) represent nuclear extracts treated with 0.05% DMSO, or nuclear extracts, whole-cell lysates, or nuclear, cytosolic or membrane fractions prepared from 0.05% DMSO-treated cells. Data are representative of 4 independent determinations.

Fig. 11

(a)

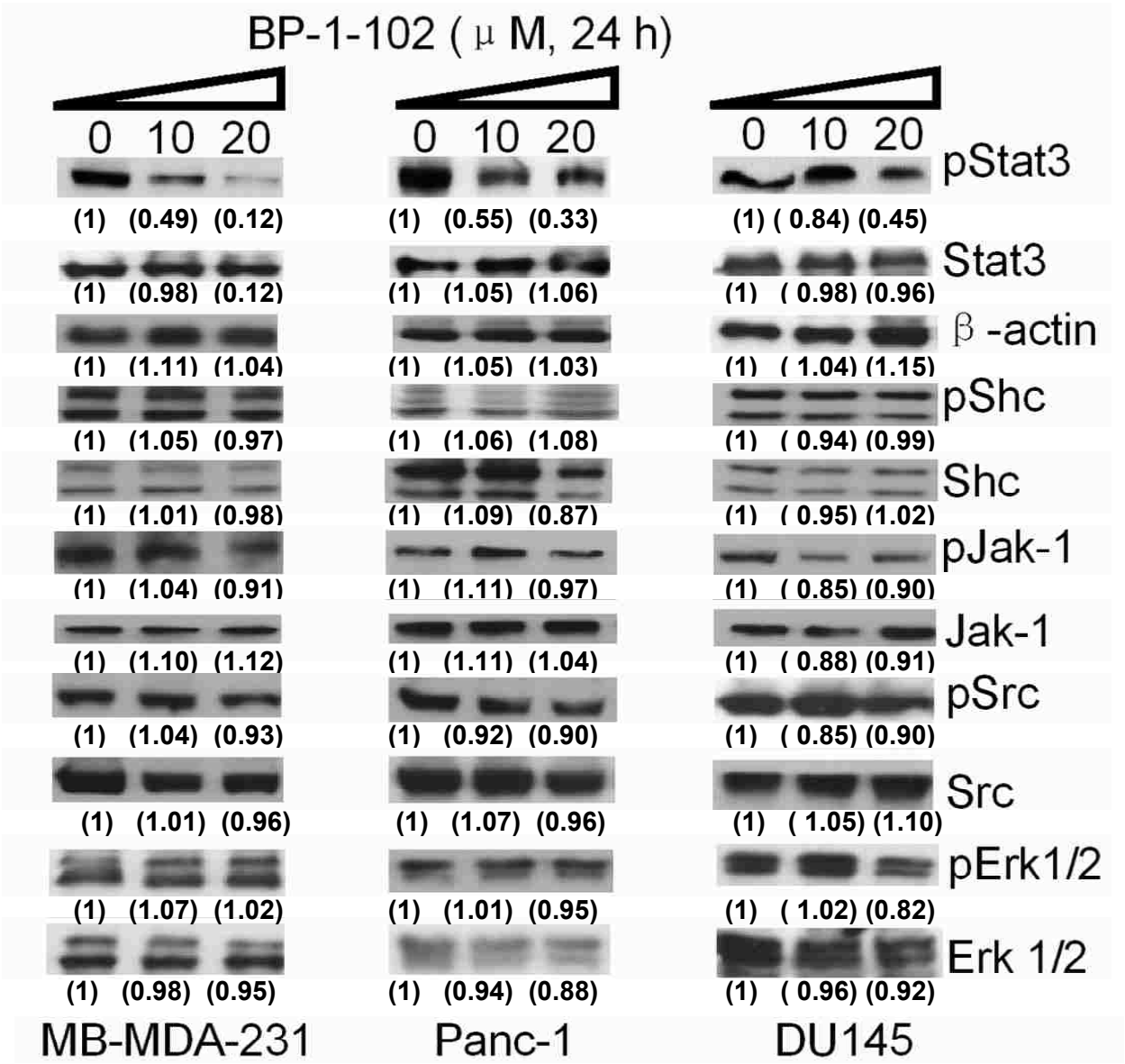
BP-1-102 (μ M, 24 h)
0 10 20
0 10 20
0 10 20
pStat3
(1) (0.49) (0.12)
(1) (0.55) (0.33)
(1) (0.84) (0.45)
Stat3
(1) (0.98) (0.12)
(1) (1.05) (1.06)
(1) (0.98) (0.96)
β -actin
(1) (1.11) (1.04)
(1) (1.05) (1.03)
(1) (1.04) (1.15)
pShc
(1) (1.05) (0.97)
(1) (1.06) (1.08)
(1) (0.94) (0.99)
Shc
(1) (1.01) (0.98)
(1) (1.09) (0.87)
(1) (0.95) (1.02)
pJak-1
(1) (1.04) (0.91)
(1) (1.11) (0.97)
(1) (0.85) (0.90)
Jak-1
(1) (1.10) (1.12)
(1) (1.11) (1.04)
(1) (0.88) (0.91)
pSrc
(1) (1.04) (0.93)
(1) (0.92) (0.90)
(1) (0.85) (0.90)
Src
(1) (1.01) (0.96)
(1) (1.07) (0.96)
(1) (1.05) (1.10)
pErk1/2
(1) (1.07) (1.02)
(1) (1.01) (0.95)
(1) (1.02) (0.82)
Erk 1/2
(1) (0.98) (0.95)
(1) (0.94) (0.88)
(1) (0.96) (0.92)
MB-MDA-231
Panc-1
DU145

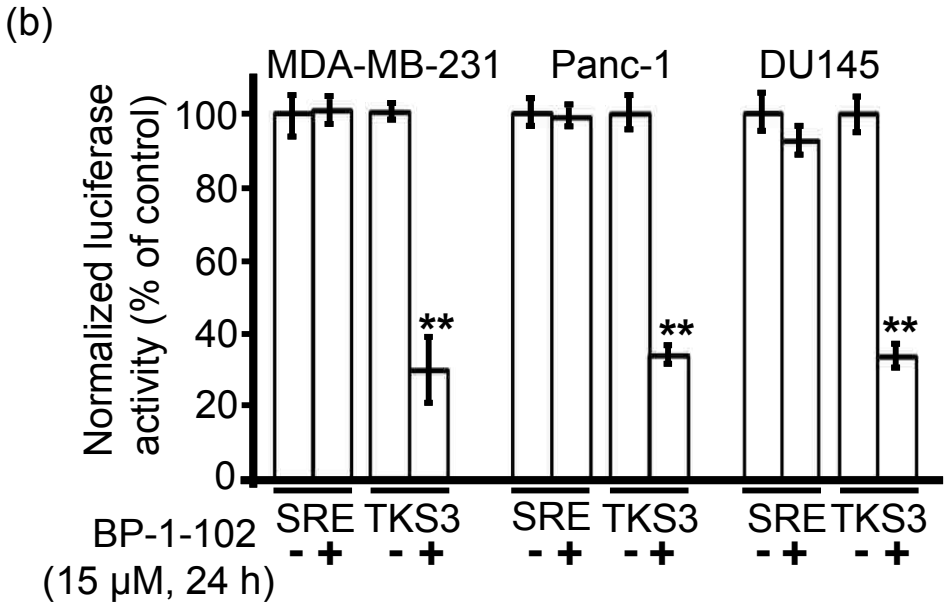

Figure 11. Effects of BP-1-102 on Stat3 activation and transcriptional activity and non-specific effects on other signaling proteins.

(a) Immunoblotting analysis of whole-cell lysates of equal total protein prepared from the designated tumor cells treated with 0, 10 or 15 μM BP-1-102 for 24 h and probing for pY705Stat3, Stat3, pS727Stat3, pShc, Shc, pJaks, Jak, pSrc, Src, pErk1/2, Erk1/2, or β-actin; (b) Cytosolic extracts of equal total protein were prepared from 24-h BP-1-102-treated or untreated MDA-MB-231, Panc-1, or DU145 cells transiently transfected with the Stat3-dependent (pLucTKS3, TKS3) or the Stat3-independent (pLucSRE, SRE) luciferase reporter and analyzed for luciferase activity using a luminometer. Positions of proteins in the gel are labeled; control (0) or (-) represents cytosolic or whole-cell lysates prepared from 0.05% DMSO-treated cells. Data

are representative of 3-4 independent determinations or mean and S.D of 3 independent determinations each performed in triplicate. *p - <0.05, **p -<0.01, and ***p - <0.005.

The inhibitory activities at 5-15 μM (Fig. 10a-f) compare more favorably to those of the lead, which were greater than 50 μM [25]. In malignant cells, Stat3 is distributed to the cytoplasm (cyto) and nucleus (nuc) (Fig. 10c and d), and to the mitochondria (mito) (Fig. 10d). Phospho-Y705Stat3 is higher in the nucleus than the cytoplasm (Fig. 10c and d), except in DU145 cells (Fig. 10c), and undetectable in the mitochondria (Fig. 10d), while pS727Stat3 is higher in the mitochondria and the nucleus, but low in the cytoplasm in MDA-MB-231 cells (Fig. 10d). Immunoblotting analysis of whole-cell lysates shows BP-1-102 treatment attenuated pY705Stat3 levels in a dose-dependent manner (Fig. 11a, pStat3), which was evident in both the nucleus and cytoplasm (Fig. 10d, pY705Stat3), and decreased nuclear Stat3 levels (Fig. 10d, Stat3), all in a time-dependent manner (Fig. 10e), with a corresponding down-regulation of Stat3-dependent luciferase reporter (pLucTKS3) [42, 43] induction (Fig. 11b, TKS3). By contrast, similar treatments had little effects on mitochondrial Stat3 levels (Fig. 10d), or on phospho- and total Shc, Src, Jak-1, and Erk1/2 levels (Fig. 11a), or on the induction of the Stat3-independent, serum response element (SRE)/c-fos promoter-driven luciferase reporter (pLucSRE) [42, 43] induction (Fig. 10B, SRE). Furthermore, BP-1-102 treatment of

malignant cells harboring aberrantly-active Stat3 suppressed c-Myc, Cyclin D1, Bcl-xL, Survivin, and VEGF expression (Fig. 10f), which occurred subsequent to the inhibition of persistently-active Stat3 (Fig. 10e). Therefore, BP-1-102-mediated inhibition of aberrantly-active Stat3 in tumor cells leads to re-localization of Stat3 outside of the nucleus, and hence the inhibition of Stat3-dependent gene regulation.

BP-1-102 suppresses growth, viability, malignant transformation, migration and invasion of malignant cells harboring constitutively-active Stat3

Consistent with the functions of aberrantly-active Stat3 [6, 13], BP-1-102 dose-dependently suppressed viability (Fig. 12a) and anchorage- dependent and independent growth (Fig. 13a and data not shown), decreased colony survival and numbers (Fig. 12b and l Fig. 13b), and decreased migration (Fig. 12c and Fig. 13c) and invasiveness (Fig.3d) of MDA-MB-231, Panc-1, DU145, and NIH3T3/v-Src that harbor aberrantly-active Stat3. At the 16-h treatment duration when migration and invasiveness were suppressed, no inhibitory effect on cell viability or growth is observed (data not shown). The antitumor cell effects are consistent with the downregulation of the known Stat3-inducible genes (Fig. 10f) [4, 6, 20, 22, 66, and 68]. By contrast, similar treatment of cells that do not harbor constitutively-active Stat3 (TE-71, NIH3T3, NIH3T3/v-Ras, A2780S, and $Stat3^{-/-}$MEFs) had minimal biological effects (Fig. 12a-c, and Fig. 13a and b).

Fig. 12

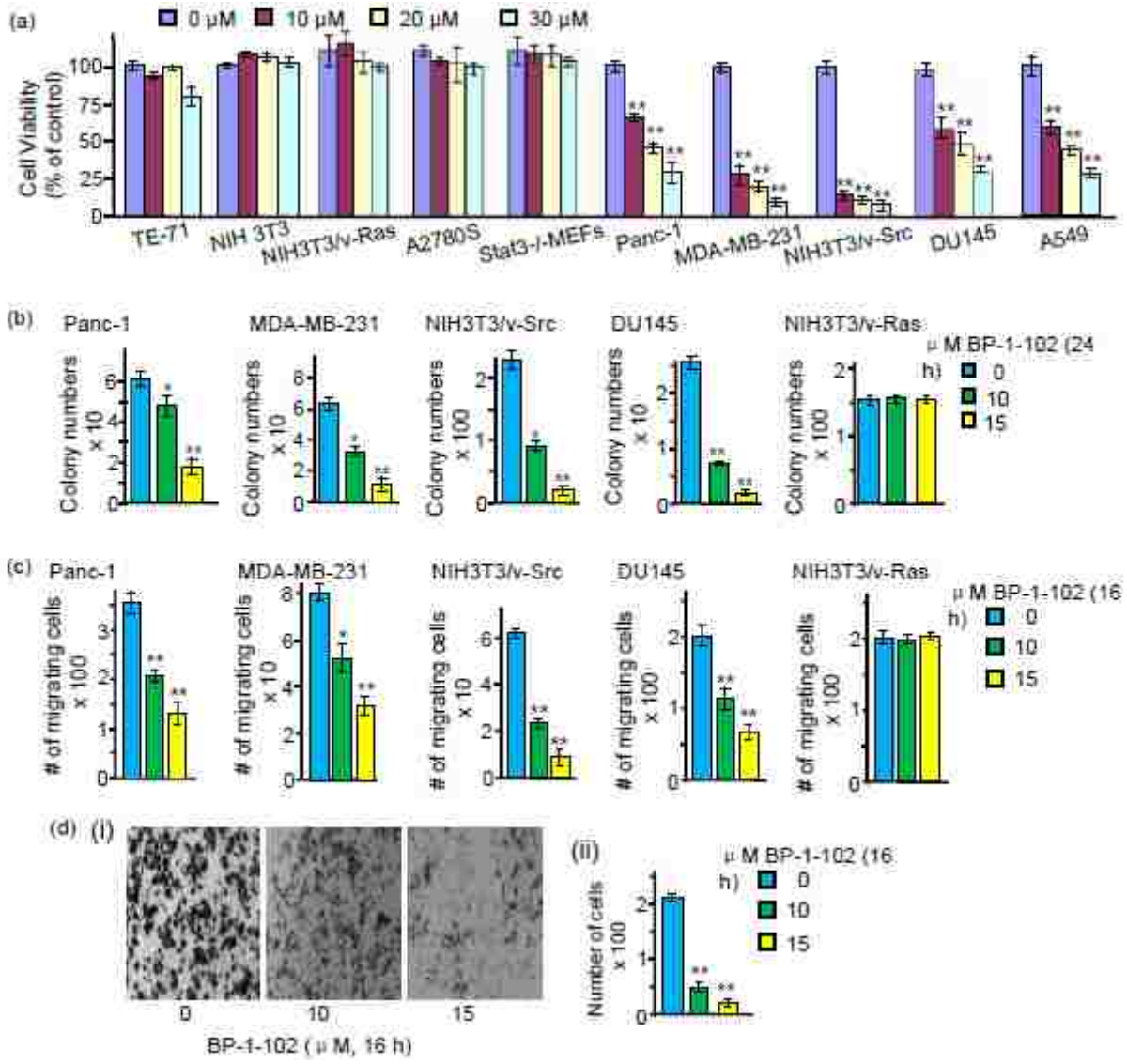

Figure 12. BP-1-102-mediated suppression of viability, survival, migration, and invasion in vitro of malignant and non-malignant cells.

(a and b) Tumor cells harboring aberrantly-activeStat3 (MDA-MB-231, DU145, Panc-1,

NIH3T3/v-Src, and A549) or cells that do not (normal NIH3T3, NIH3T3/v-Ras, mouse thymus stromal epithelial cells, TE-71, Cisplatin-sensitive ovarian cancer cells, A2780s, or the Stat3-null mouse embryonic fibroblasts, Stat3-/-MEFs) and

(a) growing in culture were treated once with 0-30 μM BP-1-102 for 24 h and subjected to CyQuant cell viability assay, or

(b) seeded as a single-cell culture were treated once with 15μM BP-1-102 for 24 h and allowed to culture until large colonies were visible, which were stained with crystal violet, enumerated and plotted;

(c) cultures of malignant cells harboringaberrant Stat3 activity (Panc-1, MDA-MB-231, NIH3T3/v-Src, DU145) or not (NIH3T3/v-Src) were wounded and treated once with 0-15 μM BP-1-102 for 16 h and allowed to migrate, and thecells in the denuded area were enumerated and plotted; and

(d) Bio-Coat migration/invasion chamber assay and the effects of 16-h-treatment with 0-15 μM BP-1-102 on the invasion of MDA-MB-231 cells represented as (i) photomicrographs or (ii) plots of number of cells invaded through membrane. Visualization was done at 10X magnification by light microscopy. Data are representative of 3-4 independent determinations. Values are the mean and S.D. of 3-4independent determinations each performed in triplicates of 3. *p - <0.05, **p - <0.01, and ***p- <0.005.

Fig. 13

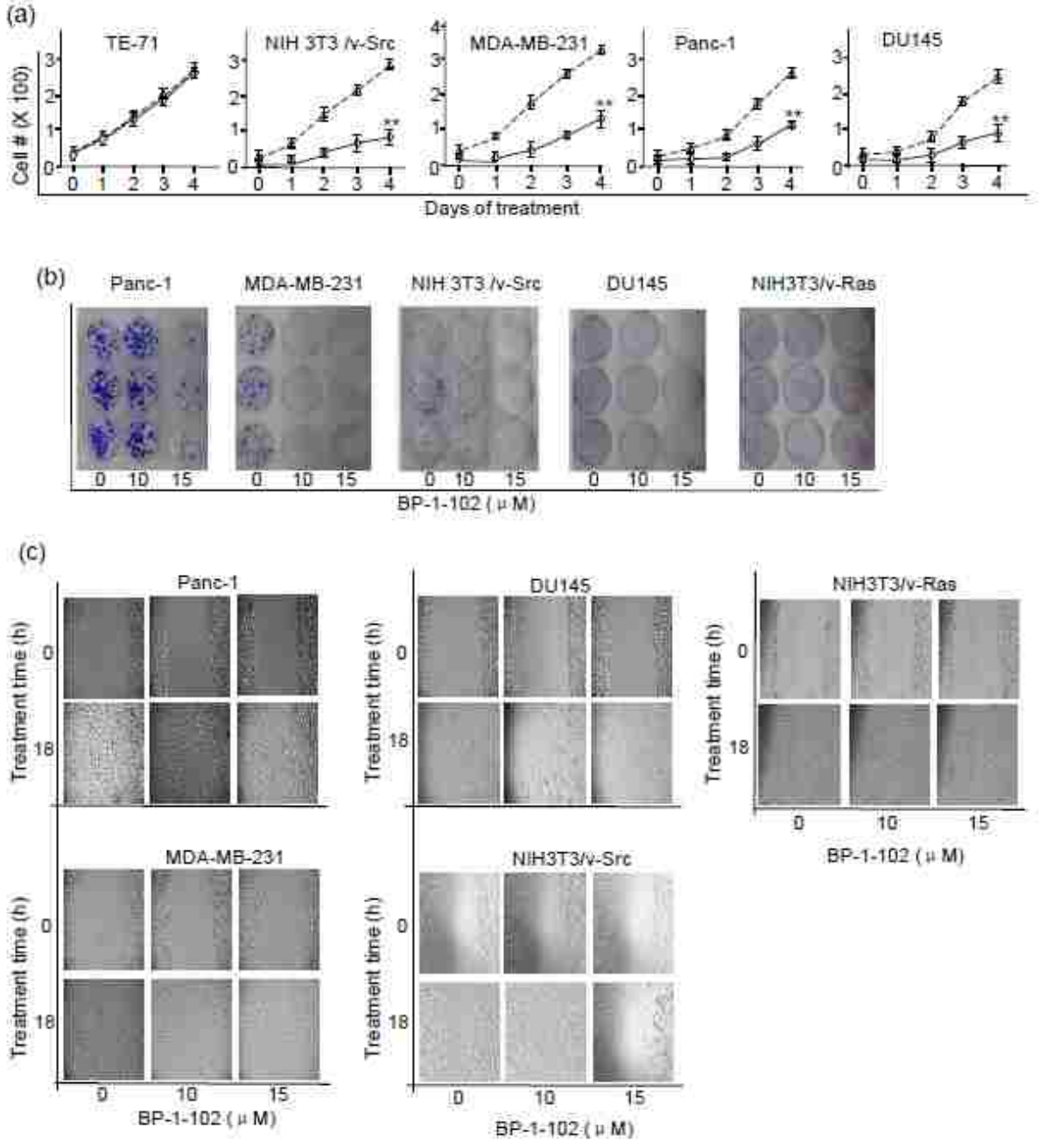

Figure 13. BP-1-102-mediated suppression of proliferation, colony survival, and wound healing of malignant cells harboring persistently-active Stat3.

(a and b) Tumor cells harboring aberrantly-active Stat3 (MDA-MB-231, DU145, Panc-1, and NIH3T3/v-Src) or cells that do not (NIH3T3/v-Ras and the mouse thymus stromal epithelial cells, TE-71) and (a) growing in culture were treated once with 0 or 15 μM BP-1-102 for 24-96 h cell viability assessed each day by trypan blue exclusion/phase contrast microscopy and plotted or (b) seeded as a single-cell culture were treated once with 0-15 μM BP-1-102 for 24 h and allowed to culture until large colonies were visible, which were stained with crystal violet and photographed, (c) photomicrographs of cultures of malignant cells harboring aberrant Stat3 activity (MDA-MB-221, DU145, Panc-1, NIH3T3/v-Src) or not (NIHT3T/v-Ras) wounded and treated once with 0-15 μM BP-1-102 for 16 h and allowed to migrate into the denuded area. Visualization was done at 10X magnification by light microscopy. Data are representative of 3-4 independent determinations. Values are the mean and S.D. of 4 independent determinations each performed in replicates of 3. *p - <0.05, **p - <0.01, and ***p - <0.005.

BP-1-102 modulates the induction or expression of focal adhesion kinase (FAK), paxillin, Ecadherin,Kruppel-like factor 8 (KLF8), and epithelial–stromal interaction 1 (EPSTI1) proteins

Although Stat3 promotes tumor cell metastasis, little is known about the Stat3-dependent molecular events that contribute to tumor progression. Reports show Stat3 associates with phospho-paxillin, FAK and Src in ovarian cancer cells, which is required for its localization to focal adhesions [79], and the induction of pS727Stat3 promoted FAK

expression [80]. Given the breadth of BP-1-102-induced antitumor cell effects, we were interested to probe further the underlying molecular changes relative to the functions of aberrantly-active Stat3 that contribute to its block of motility, migration, and invasion. In breast cancer cells harboring aberrantly-active Stat3 and treated with BP-1-102 for 16-24 h, immunoblotting analysis shows dose-dependent decreases in phospho-paxillin and pFAK levels, with little change in paxillin or FAK levels (Fig.14a), increased E-cadherin expression (Fig. 14a), and no change in pSrc or Src levels (data not shown). Thus aberrantly-active Stat3 may induce paxillin and FAK and repress E-cadherin expression. Reports further indicate that FAK promotes the induction of KLF8 transcription factor 33. KLF8 further induces the tumor-stroma interaction factor, EPSTI1 (Tianshu and Zhao, unpublished data), and both proteins promote tumor cell spread and invasiveness [82-84]. We were interested to explore further the action of BP-1-102 relative to Stat3 function. Treatment of breast cancer cells with BP-1-102 suppressed the expression of KLF8 and its downstream target, EPSTI1 in immunoblots (Fig 14b(i)). These changes were validated by the siRNA-knockdown of Stat3 (Fig. 14b (ii)). To determine whether Stat3 directly regulates KLF8 promoter, luciferase reporter studies were performed. In normal NIH3T3 fibroblasts transiently co-transfected with the KLF8 promoter-driven luciferase reporter and the vector expressing the viral Src oncoprotein, the activation of Stat3 by v-Src [43] led to the induction of KLF8 promoter-driven luciferase by 2-fold (Fig. 14b(iii)),

which was repressed by the treatment with BP-1-102 (Fig.14b(iii)). Therefore, aberrant Stat3 activity directly induces the KLF8 promoter.

To further test whether the expression of KLF8 in the MDA-MB-231 human invasive breast cancer cells plays a role in Stat3-mediated cell migration and invasion, we evaluated the ability of the Stat3 inhibitor to reduce the cell motility and invasiveness in a KLF8 knockdown background. The migration/matrigel invasion assays of the wild-type and our MDA-MB-231- K8ikd cell line that expresses the tetracycline- inducible KLF8 shRNA [83] show that the strong BP-1-102-induced inhibition of migration/motility of the wild-type (Fig. 12c) or un-induced (U) cells (Fig. 14c(i), compare bars 2 and 3) and invasiveness (Fig. 12 d and Fig. 13 c(ii), compare bars 2 and 3) are averted in the MDA-MB-231-k8id cells when KLF8 is knockdown by the induction (I) with doxycycline (Dox) (Fig. 14c(i) and d(i), compare bars 5 and 6). Accordingly, the BP-1- 102-mediated inhibition was substantially higher in the wild-type KLF8 background (U), compared to the knockdown cells (I) (Fig. 14c(ii) and d(ii)). Therefore, KLF8 has a critical role downstream from Stat3 in cell migration and invasion. We deduce that the induction of paxillin and FAK, together with the expression of KLF8 and EPSTI1 and the down-regulation of Ecadherin by Stat3 would facilitate enhanced tumor cell motility, migration, and invasive behaviors.

BP-1-102 represses Stat3 and Nuclear factor kappa B (NFκB) cross-talk and the extracellular production of cytokines and other soluble factors

Aberrantly-active Stat3 influences the tumor microenvironment to promote the malignant phenotype [26, 70, and 85]. Involved in this process is signaling cross-talks with factors, such as NFκB [71, 85] that redirects inflammation signal for oncogenic functions. We determined whether BP-1-102 treatment impacts pNFκB/p65RelA. In the breast cancer line, MDA-MB-231, immunoblotting analysis detect pY705Stat3, RelA, and their total proteins in whole-cell (WC), nuclear (nuc) and cytoplasmic (cyto) lysates (Fig. 14e, control, 0). The BP-1-102-mediated attenuation of pY705Stat3 (in nucleus and cytoplasm) and nuclear total Stat3 occurred in parallel with dramatically- decreased nuclear pRelA and total RelA levels, and moderately-decreased pRelA levels in whole-cell lysates (Fig. 14e, 15 μM BP-1-102), while cytoplasmic RelA levels, including pRelA appeared unchanged. Stat3 physically interacts with pRelA, and Stat3 knockdown suppressed nuclear pRelA [86]. To investigate the concurrent diminishing effect of BP-1-102 on nuclear RelA, we focused on the pStat3:pRelA complex. Interaction of Stat3 with RelA is detected in the nucleus (nuc), as determined by co-immunoprecipitation analysis (Fig. 14f, lane 1) and by nuclear colocalization in immunofluorescence/confocal microscopy (Fig. 15, control, merged). This interaction is disrupted in dose- and time-dependent manner by treatment of cells with increasing concentrations of BP-1-102 (Fig. 14f, lane 2, and Figure 15, compare bottom 16 h to control). These results were validated using siRNA knockdown

of Stat3, which attenuated nuclear pRel and moderately suppressed nuclear total RelA levels (Fig. 14g). By contrast, BP-1-102 treatment had no effect on IκB/RelA interactions (Fig. 14h). As previously reported [38], the nuclear Stat3:NFκB complex promotes nuclear NFκB retention. We propose that BP-1-102-mediated inhibition of Stat3 activation promotes Stat3 nuclear exit, which in turn down-regulates nuclear pNFκB levels.

In the tumor microenvironment, constitutively-active Stat3 also directly or indirectly suppresses the production of pro-inflammatory cytokines/ chemokines, while up-regulating other factors to not only support the tumor phenotype but also promote tumor immune tolerance [70]. To explore further the antitumor cell effects of BP-1-102, we examined the production of soluble factors by tumor cells. Culture medium from BP-1-102-treated MDA-MB-231 cells analyzed using a cytokine array kit showed decreased production of granulocyte colony-stimulating factor (GCSF), soluble intercellular adhesion molecule (sICAM)-1, and macrophage-migration-inhibitory factor (MIF)/ glycosylation-inhibiting factor (GIF) (Fig. 14i). We were interested to examine further the relevance of the soluble factors to tumor-cell associated Stat3 activation. Immunoblotting analysis showed the addition of exogenous G-CSF further induces Stat3 and RelA phosphorylation above the constitutive levels (Fig. 14j, compare lanes 1 and 3).

Consequently, the BP-1-102-mediated downregulation of pStat3 and pRelA in the nucleus was substantially impaired by G-CSF activity (Fig. 14j, compare lanes 2 and 4). Thus, the inhibition of Stat3-mediated induction of soluble factors contributes to BP-1-102's anti-tumor cell effects.

Fig. 14

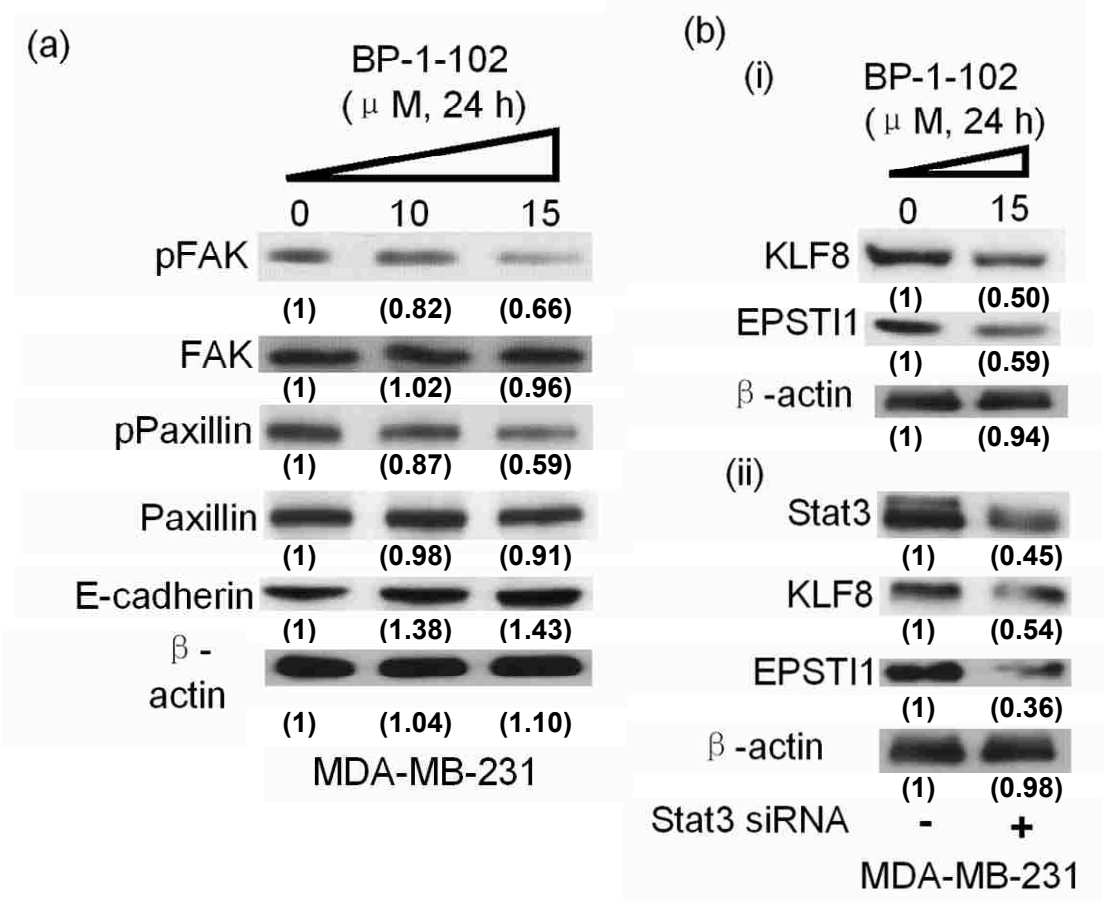

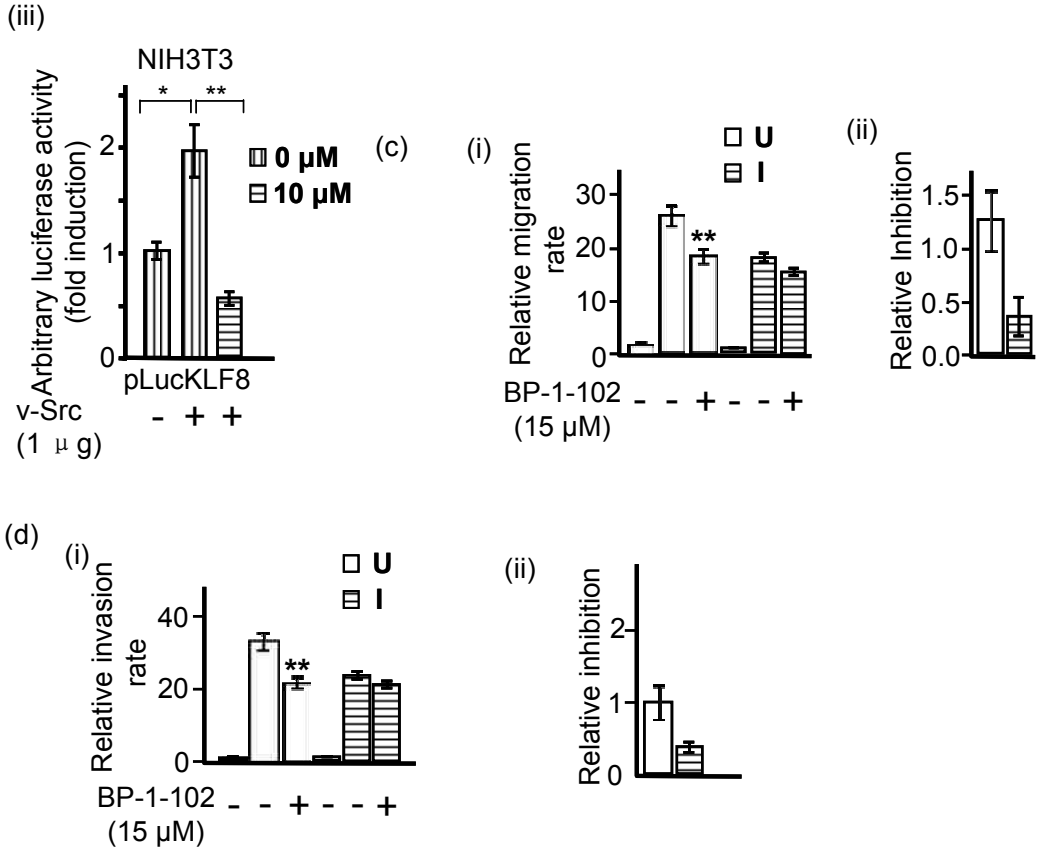
(iii)
NIH3T3
Arbitrary luciferase activity (fold induction)
0 μM
10 μM
pLucKLF8
v-Src (1 μg)
(c)
(i)
Relative migration rate
U
I
BP-1-102 (15 μM)
(ii)
Relative Inhibition
(d)
(i)
Relative invasion rate
(ii)
Relative inhibition
(e)
BP-1-102 (μ M, 24 h)
pY705Stat3
Stat3
pRelA
RelA
β -actin
HDAC1
WC
Cyto
Nuc

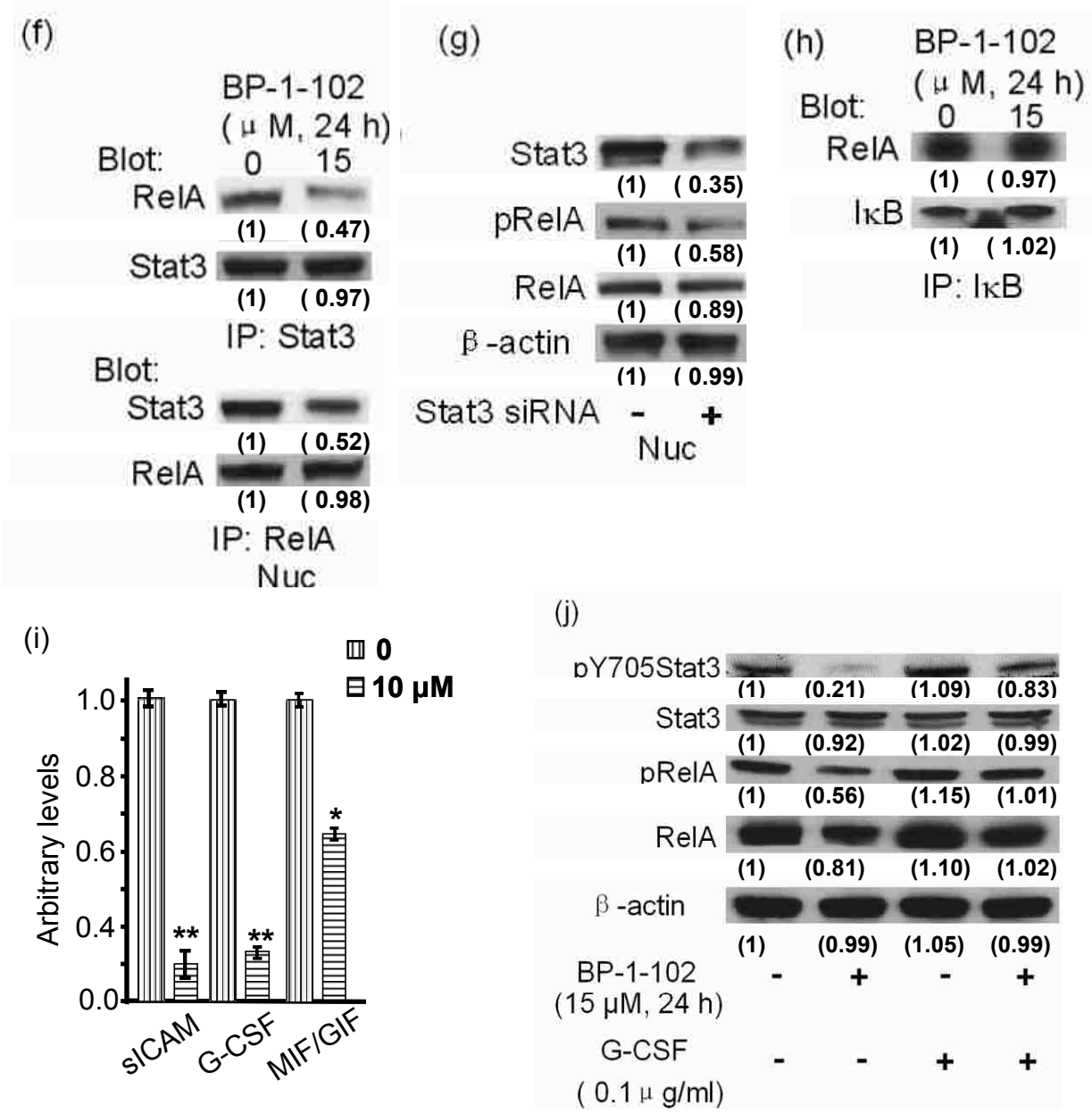

Figure 14. Effect of BP-1-102 or Stat3 siRNA on the induction or expression of FAK, paxillin, E-Cadherin, KLF8, EPSTI1, and NFκB and the production of sICAM, G-CSF and MIF/GIF by human tumor cells.

(a) Immunoblotting analysis of whole-cell lysates prepared from the human breast cancer (MDA-MB-231) cells treated with 0-15 μM BP-1-102 for 24 h and probing for FAK, phospho-FAK,

paxillin, phospho-paxillin, E-cadherin, and β-actin;

(b) (i) and (ii) immunoblotting analysis of whole-cell lysates prepared from the human breast cancer (MDA-MB-231) cells (i) untreated or treated with 15 μM BP-1-102 for 24 h or (ii) transfected with control (-) or Stat3 siRNA (+) and probing for KLF8, EPSTI1, and β-actin, or (iii) normalized luciferase reporter activity in cytosolic extracts of equal total protein prepared from normal NIH3T3 fibroblasts transiently co-transfected with the KLF8 promoter-driven luciferase reporter, pLucKLF8 and v-Src expression vector and untreated or treated with 10 μM BP-1-102 for 16 h;

(c and d) Boyden Chamber (c) migration and (d) invasion assays of doxycycline-induced (I) or un-induced (U) MDA-MB-231-K8ikd cells and the effects of 10 μM BP-1-102- treatment for 16 h on the (i) migration/invasion rates, (ii) represented as relative inhibition derived from bars 2 versus 3 or 5 versus 6 in (i) and normalized to the U condition;

(e-h), immunoblotting analysis of (e) whole-cell (WC), nuclear (Nuc), or cytosolic (Cyto) lysates of MDA-MB-231 cells treated or untreated with BP-1-102 and probing for pY705Stat3, Stat3, pRelA, RelA, β-actin or HDAC1, or (f) immune-complexes of Stat3 (upper panel) and RelA (lower panel) prepared from MDA-MB-231 cells treated or untreated with BP-1-102 and probing for RelA and Stat3, or (g) whole-cell lysates of MDA-MB-231 cells transfected with control (-) or Stat3 siRNA (+) and probing for Stat3, pRelA, RelA, or β-actin, or (h) IκB immune-complex prepared from MDA-MB-231 cells treated with or without BP-1-102 and probing for RelA or IκB; (i) cytokine

analysis of conditioned medium from cultures of MDA-MB-231 cells untreated or treated with 10 μM BP-1-102 for 48 h for the levels of G-CSF, sICAM, and MIF/GIF represented as plots; and (j) immunoblotting analysis of whole-cell lysates of MDA-MB-231 cells stimulated with G-CSF in the presence or absence of BP-1-102 and probing for pY705Stat3, Stat3, pRelA, RelA, and β-actin. Positions of proteins in gel are shown. Data are representative of 3-4 independent determinations. Values are the mean and S.D. of 2-3 independent determinations each performed in triplicates. MDA-MB-231-K8ikd, the human breast cancer cells expressing inducible KLF8 shRNA. *p - <0.05, **p - <0.01, and ***p - <0.005.

Fig. 15

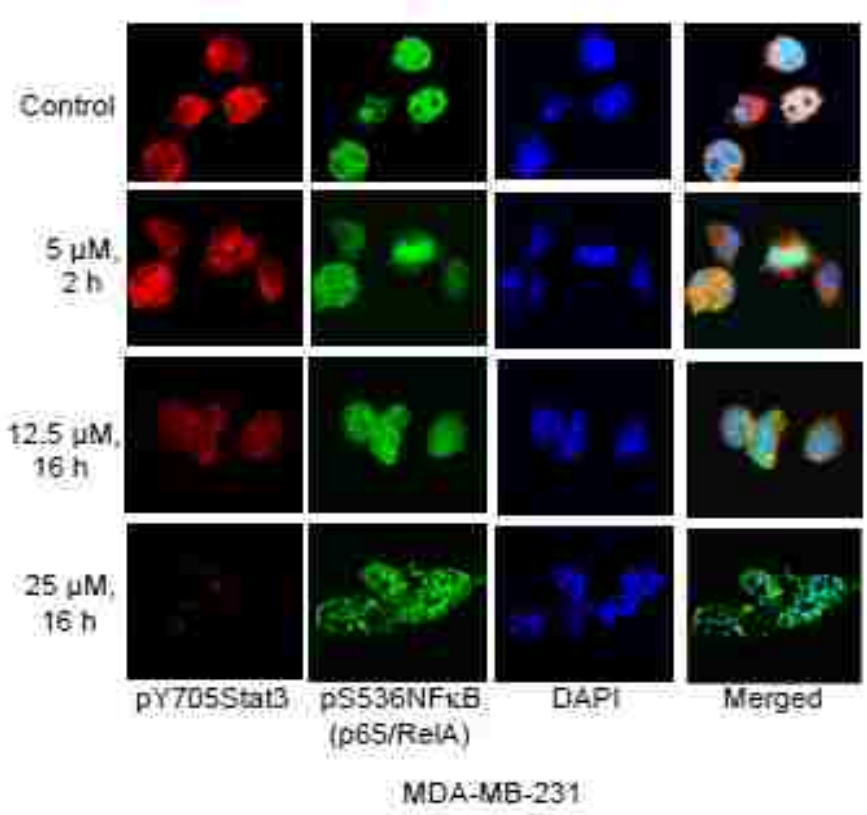

Figure 15. Effect of BP-1-102 on the colocalization of Stat3 with NFκB/p65RelA and on Stat3 nuclear localization.

Immunofluorescence imaging/confocal microscopy of Stat3 colocalization with p65RelA in MDA-MB-231 cells growing in culture and treated with or without 5-25 μM BP-1-102 for 2 or 16 h, fixed and stained with (i) anti-Stat3 antibody and secondary AlexaFluor546 antibody (red) or (ii) anti-p65RelA and secondary AlexaFluor488 antibody (green), or DAPI nuclear staining (blue). Images were captured using Leica TCS SP5 laser-scanning confocal microscope. Data are representative of 3 independent studies.

BP-1-102 inhibits growth of human breast and non-small cell lung tumor xenografts and modulates Stat3 activity, Stat3 target genes, and soluble factors in vivo

Consistent with Stat3's importance in tumor growth and progression and the antitumor cell effects of BP-1-102 *in vitro*, BP-1-102 inhibited growth of mouse xenografts of human breast (MDA-MB-231) and non-small cell lung (A549) tumors that harbor aberrantly-active Stat3 when administered via intravenous (tail vein injection, 1 or 3 mg/kg, every 2 or 3 days for 15 days) (Fig. 16a and c) or oral gavage (3 mg/kg, 100 μL, every day) (Fig. 16b). No significant changes in body weights (Fig. 17) or obvious signs of toxicity, such as loss of appetite and decreased activity or lethargy were observed.

These findings indicate that BP-1-102 is orally bioavailable. The apparent stronger anti-tumor response to oral gavage is likely due to the daily dosing. Analysis of tumor tissue lysates for Stat3 activation by EMSA shows strongly decreased Stat3 activity in BP-1-102-treated tumors (T1, and T2) compared to non-treated control (Con) (Fig. 16d, upper panel). Furthermore, consistent with the in vitro data, immunoblotting analysis of lysates from residual tumor tissues showed strong suppression of pY705Stat3, together with suppression of c-Myc, Cyclin D1, Bcl-xL, Survivin, and VEGF expression that occurred in a dose-dependent manner (Fig. 16, lower panel), and the reduction in pFAK, pPaxillin, KLF8, and EPSTI1 levels, with the up-regulation of E-cadherin, compared to control (Con) tumors (Fig. 16e). To further explore the molecular basis of the BP-1-102-induced antitumor effects and the role of aberrantly-active Stat3 in the tumor microenvironment, we probed RelA induction and cytokine levels in tumor tissue lysates. Consistent with the *in vitro* data (Fig. 14e-g and i), immunoblotting analysis showed substantially diminished pRelA induction (Fig. 16f), while cytokine analysis showed suppressed sICAM-1, MIF/GIF, serpin peptidase inhibitor, clade E (nexin, plasminogen activator inhibitor type 1), member 1 (Serpine1), and the interleukin 1 receptor antagonist (IL- 1RA) levels (Fig. 16g) in residual tumor tissues in response to treatment with BP-1-102, and undetectable G-CSF. Therefore, BP-1-102 induces a strong antitumor effect that is largely due to the effect on aberrantly-active Stat3 and its functions.

BP-1-102 is detectable at micromolar concentrations in plasma and in micro-gram amounts in tumor tissues

Among the limiting factors in the development of any of the reported Stat3 inhibitors are pharmacokinetic issues. *In vivo* pharmacokinetic profiling of plasma samples from a cohort of three mice collected at 15, 30, 60, 90, 180, and 360 min post i.v. treatment (3 mg/kg) with a single dose showed BP-1-102 levels in upwards of 35 μM at 15 min post dosing, which rapidly declines by 30 min to a steady 5-10 μM level for up to 6 h (Fig. 18(a)), while plasma samples post oral dosing at 3 mg/kg showed peak BP-1-102 levels of about 30 μM at 30 min, which steadily declined to 5-10 μM over a 6-h period (Fig. 18(b)). These data show blood levels of BP- 1-102 can exceed the IC_{50} values intended to inhibit Stat3 activation for a prolonged time period and that orally-delivered BP-1-102 is absorbed reasonably well. Furthermore, BP-1-102 was detectable at 55 or 32 μg/g tumor tissue, respectively, for i.v. or oral delivery of 3 mg/kg, fifteen minutes after the last dosing, and at 25 or 15 μg/g tumor tissue, respectively, for i.v. or oral delivery of 3 mg/kg, twenty-four hours after the last dosing (Fig. 18). Data together suggest that BP-1-102 accumulates in tumor tissues at levels sufficient to inhibit aberrantly-active Stat3 and its functions and inhibit tumor growth.

Fig. 16

(a) i. v.

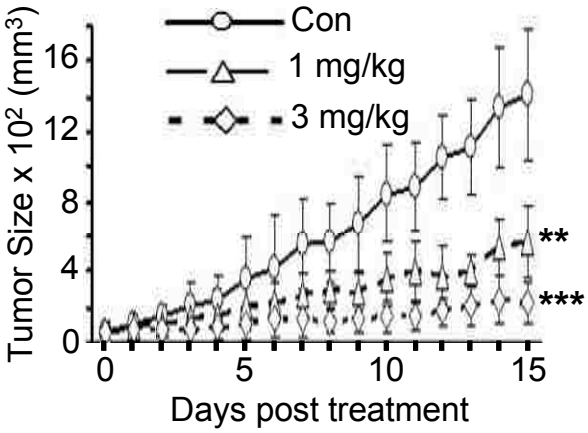

(b) Oral gavage

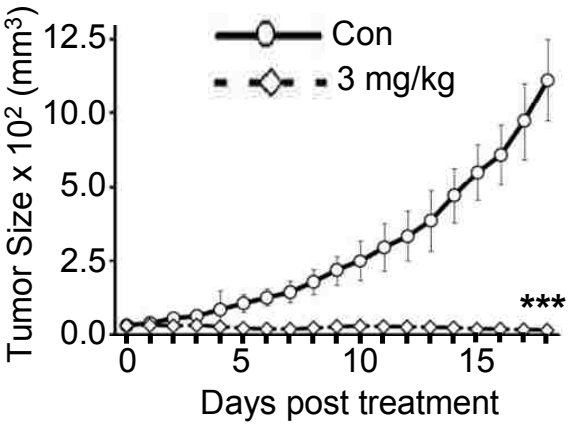

(c) i.v.

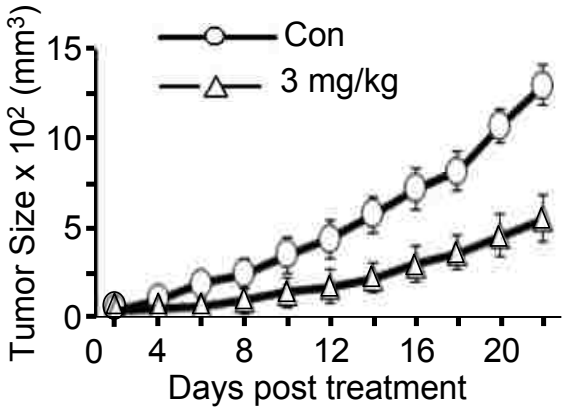

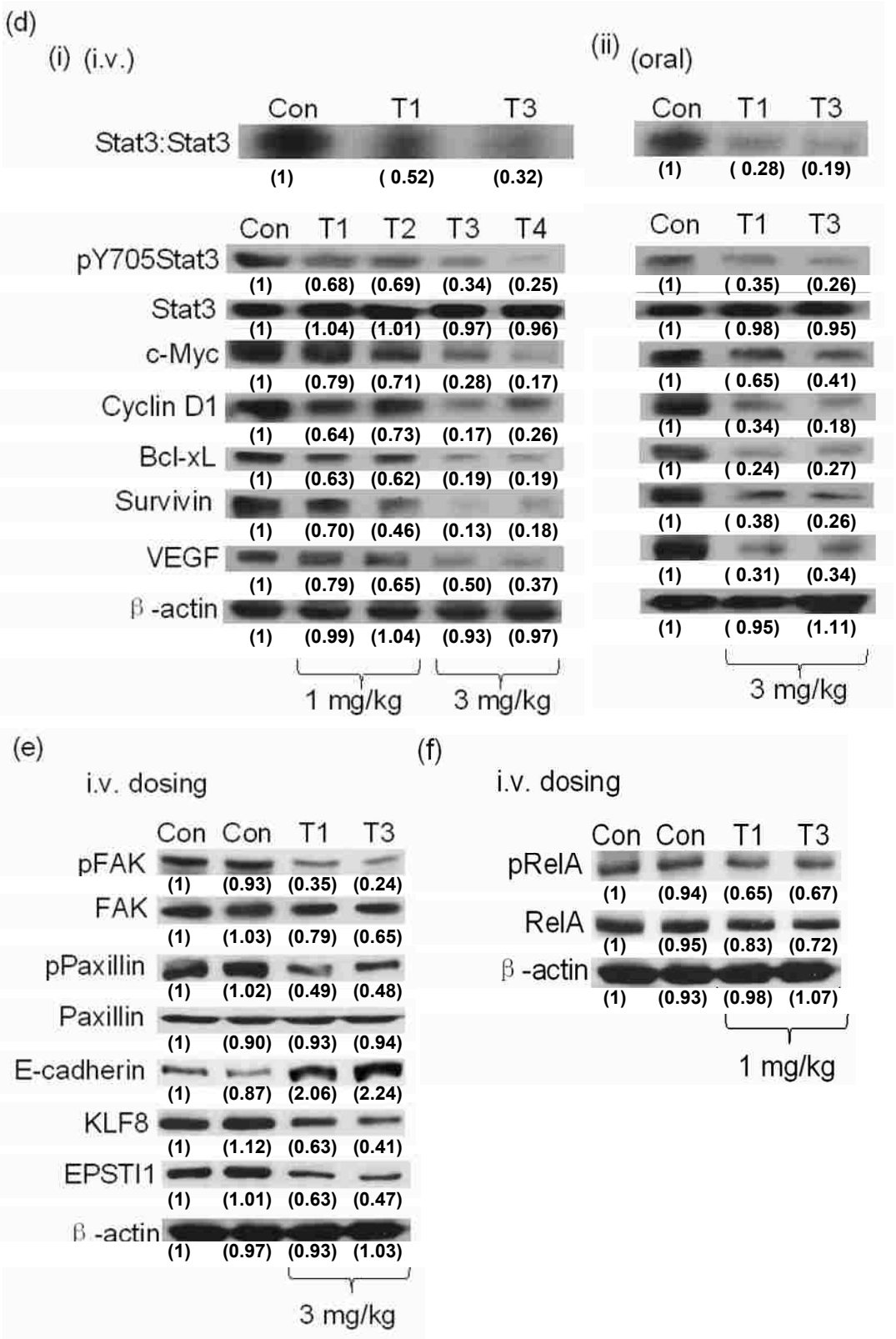
(d)
(i) (i.v.)
Con T1 T3
Stat3:Stat3
(1) (0.52) (0.32)
Con T1 T2 T3 T4
pY705Stat3
(1) (0.68) (0.69) (0.34) (0.25)
Stat3
(1) (1.04) (1.01) (0.97) (0.96)
c-Myc
(1) (0.79) (0.71) (0.28) (0.17)
Cyclin D1
(1) (0.64) (0.73) (0.17) (0.26)
Bcl-xL
(1) (0.63) (0.62) (0.19) (0.19)
Survivin
(1) (0.70) (0.46) (0.13) (0.18)
VEGF
(1) (0.79) (0.65) (0.50) (0.37)
β -actin
(1) (0.99) (1.04) (0.93) (0.97)
1 mg/kg
3 mg/kg
(ii) (oral)
Con T1 T3
(1) (0.28) (0.19)
Con T1 T3
(1) (0.35) (0.26)
(1) (0.98) (0.95)
(1) (0.65) (0.41)
(1) (0.34) (0.18)
(1) (0.24) (0.27)
(1) (0.38) (0.26)
(1) (0.31) (0.34)
(1) (0.95) (1.11)
3 mg/kg
(e)
i.v. dosing
Con Con T1 T3
pFAK
(1) (0.93) (0.35) (0.24)
FAK
(1) (1.03) (0.79) (0.65)
pPaxillin
(1) (1.02) (0.49) (0.48)
Paxillin
(1) (0.90) (0.93) (0.94)
E-cadherin
(1) (0.87) (2.06) (2.24)
KLF8
(1) (1.12) (0.63) (0.41)
EPSTI1
(1) (1.01) (0.63) (0.47)
β -actin
(1) (0.97) (0.93) (1.03)
3 mg/kg
(f)
i.v. dosing
Con Con T1 T3
pRelA
(1) (0.94) (0.65) (0.67)
RelA
(1) (0.95) (0.83) (0.72)
β -actin
(1) (0.93) (0.98) (1.07)
1 mg/kg

(g)

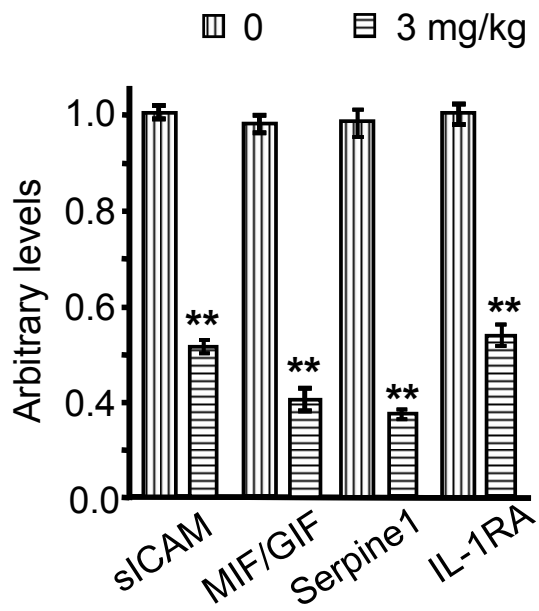

Figure 16. Growth of human breast and non-small cell lung tumor xenografts and the antitumor effects and the *in vivo* pharmacokinetic properties of BP-1-102.

a, b, and c: Mice bearing human breast (MDA-MB-231) (a, b) or non-small cell lung (c) tumors were administered BP-1-102 via i.v., 1 or 3 mg/kg or vehicle (0.05% DMSO in PBS) (a and c) or oral gavage, 3mg/kg or vehicle (0.05% DMSO) (b) every 2 or 3 days. Tumor sizes, measured every 2 or 3 days were converted to tumor volumes and plotted against days of treatment;

d, e, and f: tumor lysates prepared from control (Con) human breast tumor xenografts or from residual tumor (T1-T4) tissues from mice treated with BP-1-102 via i.v. (i) or oral gavage (ii) were subjected to (d) Stat3 DNA-binding activity/EMSA analysis (upper panel) or immunoblotting analysis probing for pY705Stat3, Stat3, c-Myc, Cyclin D1, Bcl-xL, Survivin, VEGF or β-actin (lower panel), or (e and f) immunoblotting analysis probing for (e) pFAK, FAK, pPaxillin, Paxillin,

E-cadherin KLF8, EPSTI1, and β-actin or (f) pRelA, RelA, and β-actin; (g) cytokine profiling of tumor tissue lysates from control (0) or BP-1-102-treated mice (3 mg/kg, i.v.) and represented as the plots shown in this figure;

Fig. 17

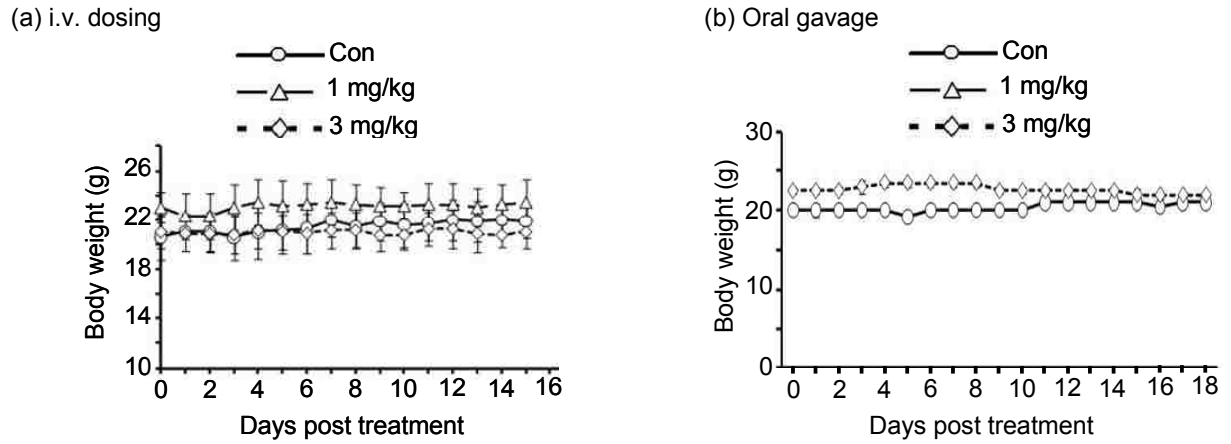

Figure 17. Graphical representation of the weights of tumor-bearing mice and the effect of treatments with BP-1-102.

Mice bearing human breast (MDA-MB-231) and treated with BP-1-102 via (a) i.v., 1 or 3 mg/kg or vehicle (0.1% DMSO in PBS) or (b) oral gavage 1 or 3 mg/kg or vehicle (0.1% DMSO) every 2 or 3 days. Mice were weighed every day or every 2 days and weights plotted against days of treatment. Values are the mean and S.D. from replicates of 7-10 tumor-bearing mice in each group.

Fig. 18

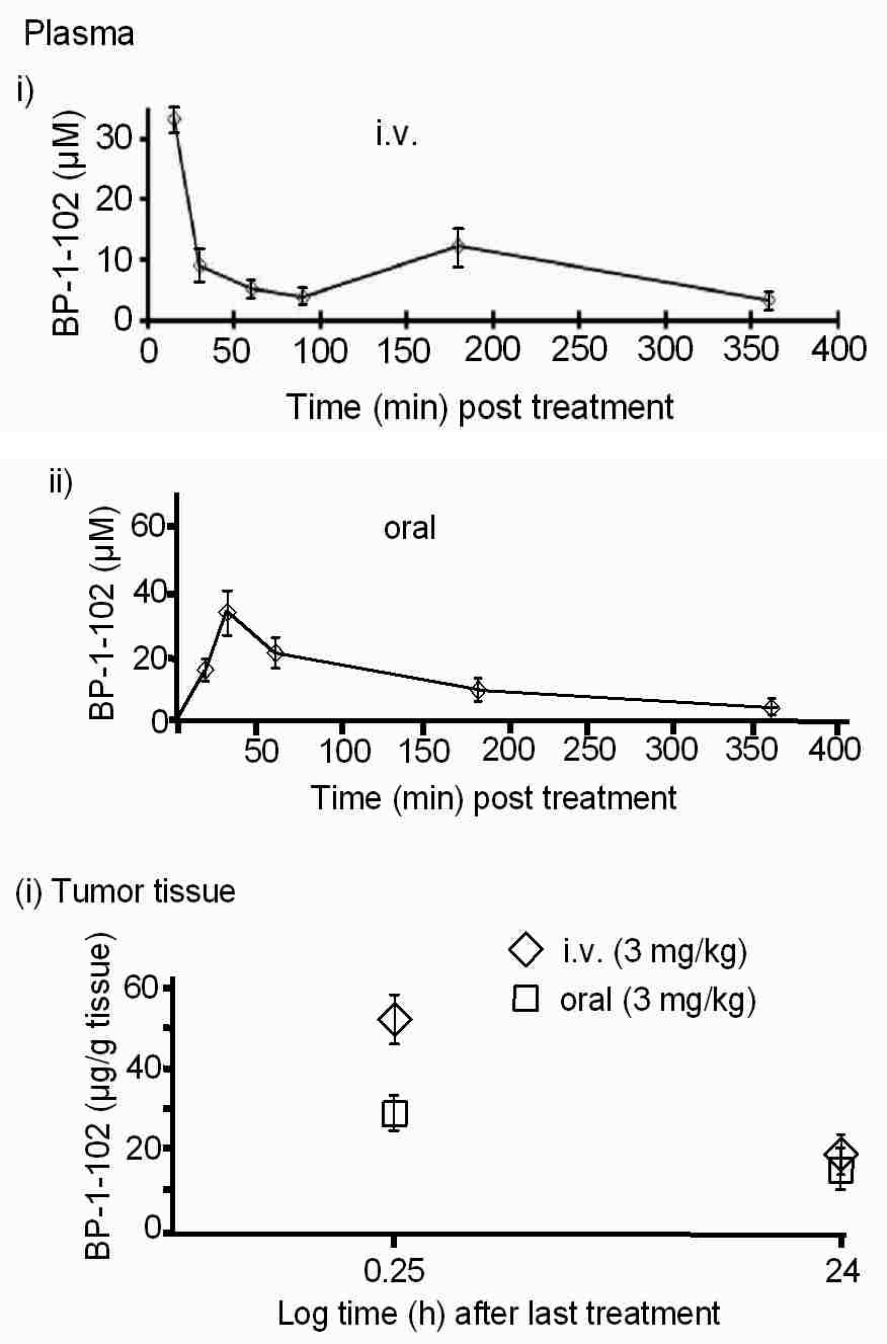

Figure 18. The in vivo pharmacokinetic properties of BP-1-102.

Graphical representations of the pharmacokinetic analysis of BP-1-102 in plasma samples

collected from mice 15 -360 min post single dosing of 3 mg/kg via (a) i.v. or (b) oral gavage; or (a) tumor tissues extracted 15 min or 24 hours after the last dosing with 3 mg/kg, i.v. or oral gavage. Data are representative of 7-10 independent determinations. Values are the mean and S.D. from replicates of 7-10 tumor-bearing mice in each group or of 3-5 independent determinations. *p - <0.05, **p - <0.01, and ***p - <0.005.

Discussion

Several of the inhibitors of Stat3 activity reported [7, 12, 30, 72, 73, 87] have efficacy and other pharmacological liabilities that have limited their clinical development. BP-1-102 is a Stat3:Stat3 dimerization disruptor with optimized structural features that promote enhanced inhibitory activity and an improved solubility. Conferred by the more polar pentafluorobenzene unit, the enhanced solubility facilitates oral bio-availability that in turn ensures higher anti-tumor efficacy against Stat3-dependent human tumors.

The Stat3:Stat3 dimerization is promoted by the pTyr: SH2 domain interaction [35], and the dimer presents an interface broadly composed of three, solvent-accessible sub-pockets. By contrast to the existing Stat3 dimerization inhibitors that access only two, BP-1-102 binds to all three subpockets (Fig. 2b). The unique pentafluorobenzene-dependent hydrogen bonds in the third sub-pocked and the

additional interactions with the charged Lys side chain are key factors in the increased activity. The binding to the Stat3 SH2 domain disrupts the SH2 domain interactions with pTyr peptide motifs and hence, disrupts pre-existing Stat3:Stat3 dimers, and blocks *de novo* Stat3 phosphorylation at the level of the receptor and dimer formation (Fig. 19A). The reduced nuclear phospho-Stat3 is due to the impact on nuclear translocation of the inhibitory effect on Stat3 activation (Fig. 19A) and the Stat3 nuclear exit that follows dimer disruption in the nucleus [7].

The antitumor cell effects on several human tumor lines and the *in vivo* antitumor efficacy in response to BP-1-102-mediated inhibition of constitutively-active Stat3 are consistent with Stat3's key role in promoting tumorigenesis [8, 9, 56], in part via dysregulation of gene expression [53, 56, 64] that leads to uncontrolled growth, survival and angiogenesis. While Stat3 also promotes tumor metastasis, except for the induction of matrix metalloproteinases [13, 22], the molecular basis of Stat3-induced tumor cell motility, migration and invasiveness has remained largely undefined. The BP-1-102-mediated suppression of FAK and paxillin induction and the downregulation of the expression of KLF8 and the epithelial-stromal interaction protein, EPSTI1, concomitant with its mediated up-regulation of the epithelial marker, E-cadherin altogether suggests aberrantly-active Stat3 regulates these proteins. In addition to its regulation by FAK [81, 88],

our data suggests KLF8 is directly induced by activated Stat3. It is also noteworthy that both KLF8 and EPSTI1 promote epithelial-mesenchymal transition and tumor invasiveness and the two proteins are upregulated in invasive and metastatic tumors, as is aberrantly-active Stat3 [82, 83, 89, and 90]. By modulating these events, Stat3 would repress epithelial cell assembly and cadherin-based cell-cell adhesions, while promoting a dynamic regulation of cell-matrix adhesions, and hence drive tumor migration and invasiveness. By inhibiting aberrantly-active Stat3, BP-1-102 attenuates these processes (Fig. 19B).

The tumor maintains a strong interplay with the microenvironment for malignant progression. A significant factor in this is the aberrantly-active Stat3's regulation of key inflammatory cytokines/chemokines in a manner that suppresses the functions of immune and inflammatory cells and thereby promotes tumor immune tolerance [70, 84]. The outcome of Stat3 regulation on soluble factors and the biological effects appear to be context and cell-type dependent. In melanoma and other tumor models, constitutively-active Stat3 suppressed IL-6, RANTES and IP-10, but induced VEGF and IL-10 production that inhibit dendritic cell maturation [70]. Moreover, in supporting the tumor phenotype, a number of these factors, including IL-6, VEGF and NFκB provide a positive feedback response by further promoting Stat3 activation or engaging in

cross-talk that perpetuates Stat3's pro-tumorigenic functions [71, 85], and vice-versa, such as aberrantly-active Stat3 in turn upregulating NFκB signaling, in part through protein complex formation that promotes NFκB nuclear retention [86]. Our study supports earlier reports showing that aberrantly-active Stat3 promotes sICAM expression in progressive tumors, including breast [91] and implicating sICAM expression in tumor angiogenesis and immune suppression [92]. The present data further identifies a novel mechanism by which constitutively-active Stat3 regulates the tumor microenvironment through the induction of G-CSF, MIF/GIF, Serpine1 and IL-1RA production by breast cancer cells, and that G-CSF in turn potentiates Stat3 and NFκB activation (Fig. 19B). The upregulation of these factors have significance to the tumor phenotype, as MIF is overexpressed in breast cancer [93] and potentially contributes to breast cancer progression [94], while Serpine1 expression correlated with advanced clear cell renal cell carcinoma and promoted tumor angiogenesis and aggressiveness [95]. Furthermore, IL-1RA antagonized the antitumor cell effects of IL-1 in prostate cancer cells *in vitro* [96], and enhanced the proliferation [97] and growth of hepatic and glioblastoma cells [98], while sIL-1RA mRNA expression correlated with lymph node and hepatic metastases in gastric carcinoma patients [99]. Constitutively-active Stat3 regulation of these events is susceptible to the BP-1-102 activities.

Herein is presented a novel high-affinity Stat3 inhibitor, BP-1-102, which induces antitumor responses in xenografts of human breast and lung tumors that harbor aberrantly-active Stat3. The oral bioavailability of BP-1-102 represents a substantial advancement in the discovery of small-molecule Stat3 inhibitors as novel anticancer agents.

Fig. 19

a)

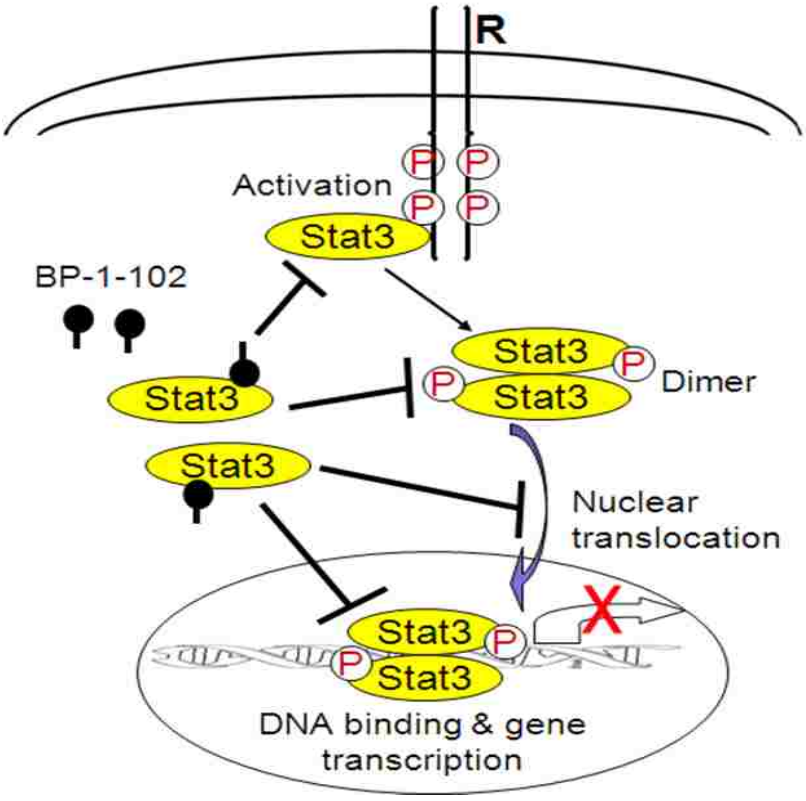

b)

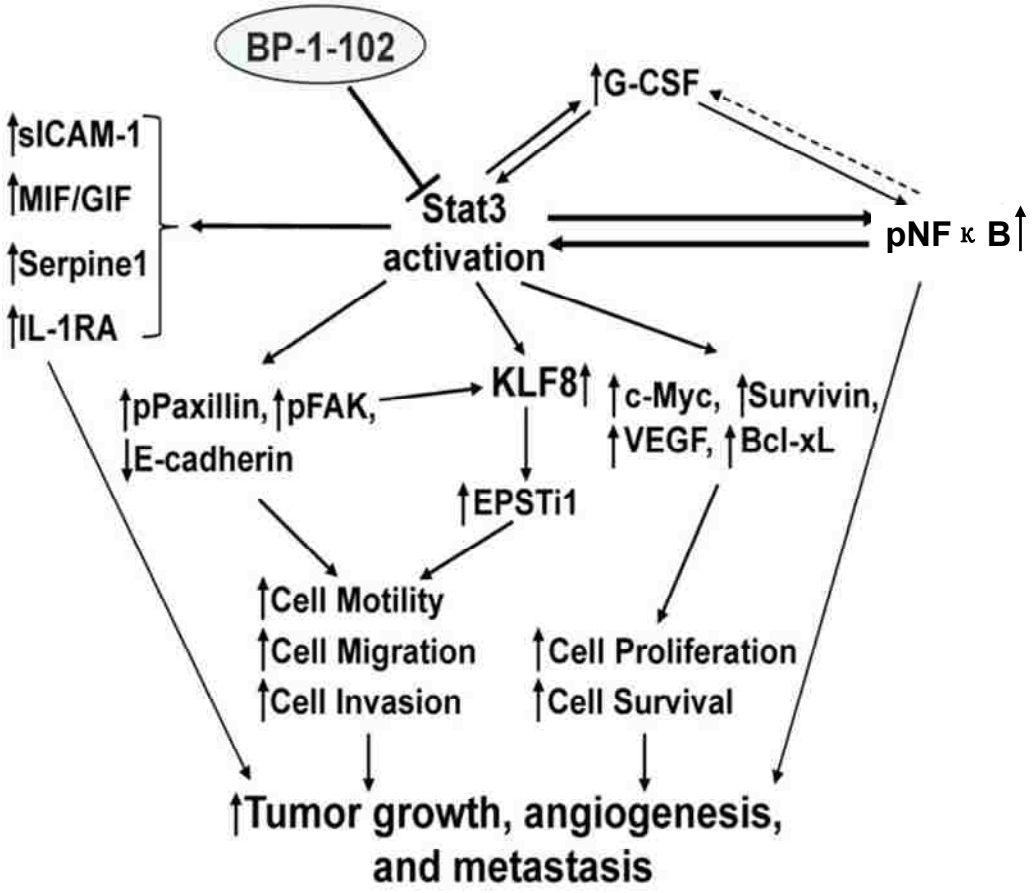

Figure 19. Model for BP-1-102-mediated inhibition of Stat3 activation and transcriptional activity and the consequent effects on Stat3-dependent events, tumor processes, and tumor growth.

(a) BP-1-102 interacts with the Stat3 SH2 domain, thereby disrupts pre-existing Stat3:Stat3 dimers, prevents *de novo* activation of Stat3 by blocking the association with phospho (P)- Tyr peptide motifs of receptor (R), and blocks Stat3 nuclear translocation and transcriptional function;

(b) BP-1-102 attenuates aberrant Stat3 activation, and consequently suppresses nuclear

Stat3-NFκB crosstalk and nuclear pNFκB levels, and blocks Stat3-mediated phospho-paxillin and phospho-FAK induction, E-cadherin repression, and KLF8, EPSTI1, sICAM, G-CSF, MIF/GIF, Serpine1, and IL-1RA expression, and the Stat3-dependent induction of c-Myc, Cyclin D1, Survivin, VEGF, Bcl-xL genes. The modulation of these events by BP-1- 102 through effect on Stat3 activity leads to inhibition of tumor cell growth, survival, motility, migration, invasion, and tumor angiogenesis, and block of tumor growth and metastasis *in vivo*.

SUMMARY AND GENERAL CONCLUSION

Several lines of evidence have established a critical role for abnormal Stat3 activity in malignant transformation and tumor progression. In that context, the targeting of aberrant Stat3 signaling provides a novel strategy for treating the wide variety of human tumors that harbor abnormal Stat3 activity. The knowledge of the Stat3 structure and the mode of activation of Stats gained in recent years have allowed the initiation of small-molecule discovery programs aimed at identifying potent and specific inhibitors of Stat functions. These discovery programs have benefited from computational modeling, which has paved the way to study *in silico* molecular events of which structural information is available and to facilitate the rational design of compounds.

In the present context, several studies testing the proof-of-concept show that the inhibition of Stat3 activation or disruption of dimerization induces cancer cell death and tumor regression [7-12]. Leading agents from those earlier studies have been explored in the rational design of optimized molecules, in conjunction with molecular modeling of their binding to the Stat3 SH2 domain [12, 30]. One of those leads, S3I-201 [12] had previously been shown to exert antitumor effects against human breast cancer xenografts via mechanisms that involve the inhibition of aberrant Stat3 activity. By computational and structural analyses of the interaction between Stat3 and the lead

dimerization disruptor, S3I-201, we derived key structural information for lead optimization and a rational synthetic program that furnished exciting new analogs and designed a diverse set of analogs. Computational analysis shows the lead agent can be structurally modified to enhance binding to the Stat3 SH2 domain surface, and this became the basis for the derivation of analogs with additional structural appendages.

The first generation analog, S3I-201.1066 harbors a cyclohexyl benzyl moiety, which facilitate additional hydrophobic interactions with the Stat3 SH2 domain. Our data shows that S3I-201.1066 possesses improved potency and selectivity compared to the lead agent, S3I-201; it directly interacts with Stat3 or the SH2 domain, with an affinity (K_D) of 2.74 μM, disrupts Stat3:pTyr-peptide interactions, with an IC_{50} of 23 μM, and shows improved Stat3-inhibitory potency and selectivity in vitro, with intracellular Stat3-inhibitory activity that is enhanced 2–3-fold compared to the lead, S3I-201. From computational modeling, we surmise that the improved activity could in part be due to the enhanced interactions with the Stat3 protein, possibly by the (para-cyclohexyl) benzyl moiety that extends from the scaffold amide nitrogen and makes important contacts with the hydrophobic residues Trp623, Ile659, Val637 and Phe716 within the unexplored pocket. Furthermore, the effect of S3I-201.1066 on Stat3 oncogenic function is shown by the significant antitumor in mouse models of human breast cancer following in vivo

administration, which correlates with the inhibition of constitutively active Stat3 and the suppression of known Stat3-regulated genes.

Although these studies identified a more potent Stat3 inhibitor, a novel small-molecule, pharmacokinetic properties were not optimum. Indeed, although several dimerization-disrupting small-molecule Stat3 inhibitors have been reported, in some cases with cellular activities and evidence of *in vivo* efficacy [7, 12, 30, 72, 74], thus far none has reached the clinic for several reasons, including the suitability of the scaffolds and pharmacokinetic issues. The leading dimerization-disrupting agent, S3I-201.1066 [75] was subjected to computer-aided lead optimization. The Stat3:Stat3 dimerization is promoted by the pTyr: SH2 domain interaction [35], and the dimer presents an interface broadly composed of three, solvent-accessible sub-pockets. Computational modeling revealed all the reported Stat3 dimerization inhibitors, including S3I-201 and S3I-201.1066 only accessed two out of the three sub-pockets. Furthermore, S3I-201.1066, while more active due to the cyclohexyl benzyl group, and this group also introduced additional hydrophobicity that made the molecule less soluble. Our studies show that BP-1-102, with the pentafluorobenzene moiety can access all three sub-pockets. Also, the unique pentafluorebenzene-dependent hydrogen bonds in the third sub-pocket and the additional interactions with the charged Lys side chain are key factors in the increased

activity. The more polar pentafluorobenzene unit also confers enhanced solubility that in turn facilitates oral bio-availability and hence, ensures higher anti-tumor efficacy against Stat3-dependent human tumors.

Significantly, our studies also identify novel mechanisms, beyond the well-described de-regulation of gene expression, by which aberrantly-active Stat3 promotes tumor progression. Although Stat3 is reported to induce tumor cell motility, migration, invasion, and tumor metastasis, except for the induction of matrix metalloproteinases, the molecular mechanisms are unknown. We present the first evidence that aberrantly-active Stat3 mediates the repression of E-cadherin, the induction of focal adhesion kinase and paxillin, the transcriptional up-regulation of Krüppel-like factor 8, the expression of stromal interaction protein, EPSTI1, and the production of the soluble factors, GCSF, sICAM, MIF/GIF, and Serpine1, and IL-1RA *in vitro* and *in vivo*. These key events would alter cell-cell interaction and promote matrix dynamics essential to tumor metastasis. We then show that BP-1-102 suppresses these Stat3-dependent events and blocks nuclear Stat3-NFκB crosstalk.

Finally, the oral bioavailability of BP-1-102 represents a substantial advancement in the discovery of small-molecule Stat3 inhibitors as novel anticancer agents.

APPENDIX: MAIN PUBLICATIONS

Main Publications Contributed To This Dissertation

1. **Xiaolei Zhang**, Peibin Yue, Brent D.G. Page, Tianshu Li, Wei Zhao, Jihe Zhao, Patrick T. Gunning, and James Turkson An orally-bioavailable small-molecule Stat3 inhibitor regresses human breast and lung cancer xenografts and reveals novel Stat3 functions. *Submitted to Proc Natl Acad Sci*

2. Zhang X, Yue P, Fletcher S, Zhao W, Gunning PT, Turkson J. A novel small-molecule disrupts Stat3 SH2 domain-phosphotyrosine interactions and Stat3-dependent tumor processes. *Biochem Pharmacol. 2010 May 15;79(10):1398-409.*

3. Fletcher S, Page BD, **Zhang X**, Yue P, Li ZH, Sharmeen S, Singh J, Zhao W, Schimmer AD, Trudel S, Turkson J, Gunning PT. Antagonism of the Stat3-Stat3 Protein Dimer with Salicylic Acid Based Small Molecules. *Chem Med Chem*. 2011 May 25. doi: 10.1002/cmdc.201100194.

Other Co-Author Publications

4. Peibin Yue, **Xiaolei Zhang,** David Paladion, James Turkson. Hyperactive EGF receptor and Stat3 signaling promote enhanced colony-forming ability motility and migration of Cisplatin-resistant ovarian cancer cells. *Oncogene (accepted).*

5. Fletcher S, Singh J, **Zhang X,** Yue P, Page BD, Sharmeen S, Shahani VM, Zhao W, Schimmer AD, Turkson J, Gunning PT. Disruption of transcriptionally active Stat3 dimers with non-phosphorylated, salicylic acid-based small molecules: potent in vitro and tumor cell activities. *Chem biochem. 2009 Aug 17;10(12):1959-64*.

6. Vijay M. Shahani, Peibin Yue, Sina Haftchenary, Wei Zhao, Julie L. Lukkarila, **Xiaolei Zhang,** Daniel Ball, Christina Nona, Patrick T. Gunning, and James Turkson. Identification of Purine-Scaffold Small-Molecule Inhibitors of Stat3 Activation by QSAR Studies *ACS Med. Chem. Lett., 2011 Jan 13;2(1):79-84*.**78.** Shahani VM, Yue P, Fletcher S, Sharmeen S, Sukhai MA, Luu DP, **Zhang X**, Sun H, Zhao W, Schimmer AD, Turkson J, Gunning PT. Design, synthesis, and in vitro characterization of novel hybrid

peptidomimetic inhibitors of STAT3 protein. *Bioorg Med Chem. 2011 Mar 1;19(5):1823-38*

7. Drewry JA, Fletcher S, Yue P, Marushchak D, Zhao W, Sharmeen S, **Zhang X**, Schimmer AD, Gradinaru C, Turkson J, Gunning PT. Coordination complex SH2 domain proteomimetics: an alternative approach to disrupting oncogenic protein-protein interactions. *Chem Commun (Camb). 2010 Feb 14;46(6):892-4.*

Co-Author Manuscript Submitted

9. Mitra, Rajendra; Doshi, Mona; **Zhang, Xiaolei**; Tyus, Jessica; Bengtsson, Niclas; Fletcher, Steven; Page, Brent; Turkson, James; Gesquiere, Andre; Gunning, Patrick; Walter, Glenn; Santra, Swadeshmukul. Targeted Cellular-Shuttle" – an activatable multimodal/multifunctional nanoprobe for direct imaging of intercellular drug delivery. *submitted to JACS (Journal of American Chemical Society)*

Poster & Presentations

1. Xiaolei Zhang, Peibin Yue, Brent D.G. Page, Steven Fletcher, Wei Zhao, Patrick T. Gunning, James Turskon. A novel orally-bioavailable salicylic acid-based small molecular Stat3 inhibitor suppress growth of human breast tumor xenografts. *AACR 102nd Annual meeting 2011, Orlando, USA*

2*.* Peibin Yue, **Xiaolei Zhang,** James Turkson. Enhanced colony-forming ability, and motility and migratory properties of Cisplatin-resistant ovarian cancer cells. *AACR 102nd Annual meeting 2011, Orlando, USA*

3. Astha Malhotra, **Xiaolei Zhang**, Padmavathy Tallury, James Turkson and

Swadeshmukul Santra Buffer-stable fluorescent chitosan-PGA hybrid nanoparticles for biomedical applications. *ACS 240th National Meeting, Boston, USA & Particles 2010, Orlando, USA*

REFERENCES

[1] Darnell, J. E., Jr. STATs and gene regulation, *Science* 1997: 277, 1630–1635.

[2] Peter J. Murray . The JAK-STAT Signaling Pathway:Input and Output Integration *The Journal of Immunology*, 2007:178: 2623–2629

[3] Darnell, J. E. Validating Stat3 in cancer therapy, *Nat. Med.* 2005:11, 595–596.

[4] Bowman, T., Garcia, R., Turkson, J., and Jove, R. (2000) STATs in oncogenesis, *Oncogene 19*, 2474–2488.

[5] Thorsten Berg. Signal Transducers and activator of transcription as targets for small organic molecules *ChemBioChem* 2008: 9: 2039-2044

[6] James Turkson. Stat proteins as novel targets for cancer drug discovery. *Expert Opin. Ther. Targets* 2004:8(5) 409-422.

[7] Khandaker A. Z. Siddiquee, Gunning PT, Glenn M, Katt WP, Zhang S, Schrock C, Sebti SM, Jove R, Hamilton AD, Turkson J. An Oxazole-Based Small-Molecule Stat3 Inhibitor Modulates Stat3 Stability and Processing and Induces Anti-tumor Cell Effects, *ACS Chem Biol* 2007; 2:787– 98.

[8] Turkson, J., Ryan D, Kim JS, Zhang Y, Chen Z, Haura E, Laudano A, Sebti S, Hamilton AD, Jove R. Phosphotyrosyl peptides block Stat3-mediated DNA- binding activity, gene regulation and cell transformation, *J. Biol. Chem.* 2001: 276, 45443–45455.

[9] Turkson J, Kim JS, Zhang S, Yuan J, Huang M, Glenn M, Haura E, Sebti S, Hamilton AD, Jove R. Novel peptidomimetic inhibitors of signal transducer and activator of transcription 3 dimerization and biological activity, *Mol. Cancer Ther.* 2004: 3, 261–269.

[10] Turkson, J., Zhang, S., Palmer J, Kay H, Stanko J, Mora LB, Sebti S, Yu H, Jove R. Inhibition of constitutive signal transducer and activator of transcription 3 activation by novel platinum complexes with potent anti-tumor activity, *Mol. Cancer Ther.*2004: 3,1533–1542.

[11] Turkson, J., Zhang, S., Mora, L. B., Burns, A., Sebti, S., and Jove, R. A novel platinum compound inhibits constitutive Stat3 signaling and induces cell cycle arrest and apoptosis of malignant cells, *J. Biol. Chem.*2005: 280, 32979–32988.

[12] Siddiquee, K, Zhang S, Guida WC, Blaskovich MA, Greedy B, Lawrence HR, Yip ML, Jove R, McLaughlin MM, Lawrence NJ, Sebti SM, Turkson J. Selective chemical probe inhibitor of Stat3, identified through structure-based virtual screening, induces antitumor activity, *Proc. Natl. Acad. Sci. U.S.A. 2007:104*, 7391–7396.

[13] Peibin Yue, James Turkson. Targetiing STAT3 in Cancer: how successful are we? *Expert Opin Investig Drugs*. 2009 Jan;18(1):45-56.

[14] Bromberg J. Signal transducers and activators of transcription as regulators of growth, apoptosis and breast development. *Breast Cancer Res* 2000;2:86–90.

[15] Darnell Jr JE. Transcription factors as targets for cancer therapy. *Nat Rev Cancer* 2002;2:740–9.

[16] Schröder M, Kroeger K, Volk HD, Eidne KA, Grütz G. Pre-association of nonactivated STAT3 molecules demonstrated in living cells using bioluminescence resonance energy transfer: a new model of STAT activation? *J Leukoc Biol* 2004;75:792–7.

[17] Sehgal PB. Paradigm shifts in the cell biology of STAT signaling. Semin Cell Dev Biol 2008;19:329–40.

[18] Bromberg J, Darnell Jr JE. The role of STATs in transcriptional control and their impact on cellular function. *Oncogene* 2000: 19:2468–73.

[19] Hirano T, Ishihara K, Hibi M. Roles of STAT3 in mediating the cell growth, differentiation and survival signals relayed through the IL-6 family of cytokine receptors. *Oncogene*. 2000,15;19(21):2548-56.

[20] Turkson J, Jove R. STAT proteins: novel molecular targets for cancer drug discovery. *Oncogene* 2000;19:6613–26.

[21] Buettner R, Mora LB, Jove R. Activated STAT signaling in human tumors provides novel molecular targets for therapeutic intervention. *Clin Cancer Res* 2002; 8:945–54.

[22] Yu H, Jove R. The STATs of cancer-new molecular targets come of age. Nat Rev

Cancer 2004;4:97–105.

[23] Smalley KS, Herlyn M. Targeting intracellular signaling pathways as a novel strategy in melanoma therapeutics. *Ann N Y Acad Sci.* 2005;1059:16-25.

[24] Lee H, Pal SK, Reckamp K, Figlin RA, Yu H. STAT3: a target to enhance antitumor immune response. *Curr Top Microbiol Immunol.* 2011;344:41-59.

[25] Kortylewski M, Yu H. Stat3 as a potential target for cancer immunotherapy. *J Immunother* 2007;30:131–9.

[26] Kortylewski M, Yu H. Role of Stat3 in suppressing anti-tumor immunity. *Curr Opin Immunol* 2008;20:228–33.

[27] Shuai K, Horvath CM, Huang LH, Qureshi SA, Cowburn D, Darnell Jr JE. Interferon activation of the transcription factor Stat91 involves dimerization through SH2-phosphotyrosyl peptide interactions. *Cel*l 1994;76:821–8.

[28] Costantino L, Barlocco D. STAT 3 as a target for cancer drug discovery. *Curr Med Chem.* 2008;15(9):834-43.

[29] Germain D, Frank DA. Targeting the cytoplasmic and nuclear functions of signal transducers and activators of transcription 3 for cancer therapy. *Clin Cancer Res.* 2007 Oct 1;13(19):5665-9.

[30] Song H, Wang R, Wang S, Lin J. A low-molecular-weight compound discovered through virtual database screening inhibits Stat3 function in breast cancer cells. *Proc*

Natl Acad Sci U S A 2005;102:4700–5.

[31] Coleman DRI, Ren Z, Mandal PK, Cameron AG, Dyer GA, Muranjan S, Campbell M, Chen X, McMurray JS. Investigation of the binding determinants of phosphopeptides targeted to the Src Homology 2 domain of the signal transducer and activator of transcription.3. Development of a high-affinity peptide inhibitor. *J Med Chem* 2005;48:6661–70.

[32] Ren Z, Cabell LA, Schaefer TS, McMurray JS. Identification of a high-affinity phosphopeptide inhibitor of stat3. *Bioorg Med Chem Lett* 2003;13:633–6.

[33] Schust J, Berg T. A high-throughput fluorescence polarization assay for signal transducer and activator of transcription 3. *Anal Biochem* 2004;330: 114–8.

[34] Gunning PT, Glenn MP, Siddiquee KA, Katt WP, Masson E, Sebti SM, Turkson J, Hamilton AD. Targeting protein–protein interactions: suppression of Stat3 dimerization with rationally designed small-molecule, nonpeptidic SH2 domain binders. *Chembiochem* 2008;9:2800–3.

[35] Fletcher S, Turkson J, Gunning PT. Molecular approaches towards the inhibition of the signal transducer and activator of transcription 3 (Stat3) protein. *ChemMedChem* 2008;3:1159–68.

[36] Becker S, Groner B, Muller CW. Three-dimensional structure of the Stat3beta homodimer bound to DNA. *Nature* 1998;394:145–51.

[37] Johnson PJ, Coussens PM, Danko AV, Shalloway D. Overexpressed pp60c-src can induce focus formation without complete transformation of NIH 3T3 cells. *Mol Cell Biol* 1985;5:1073–83.

[38] Yu CL, Meyer DJ, Campbell GS, Larner AC, Carter-Su C, Schwartz J, Jove R. Enhanced DNA-binding activity of a Stat3-related protein in cells transformed by the Src oncoprotein. *Science* 1995;269:81–3.

[39] Garcia R, Bowman TL, Niu G, Yu H,Minton S, Muro-Cacho CA, Cox CE, Falcone R, Fairclough R, Parsons S, Laudano A, Gazit A, Levitzki A, Kraker A, Jove R. Constitutive activation of Stat3 by the Src and JAK tyrosine kinases participates in growth regulation of human breast carcinoma cells. *Oncogene* 2001;20:2499–513.

[40] Ouyang H, Mou LJ, Luk C, Liu N, Karaskova J, Squire J, Tsao MS. Immortal human pancreatic duct epithelial cell lines with near normal genotype and phenotype. *Am J Pathol* 2000;157:1623–31.

[41] Maritano D, Sugrue ML, Tininini S, Dewilde S, Strobl B, Fu X, Murray Tait V, Chiarle R, Poli V. The STAT3 isoforms alpha and beta have unique and specific functions. *Nat Immunol* 2004;5:401–9.

[42] Turkson J, Bowman T, Adnane J, Zhang Y, Djeu JY, Sekharam M, Frank DA, Holzman LB, Wu J, Sebti R, Jove R. Requirement for Ras/Rac1-mediated p38 and c-Jun N-terminal kinase signaling in Stat3 transcriptional activity induced by the Src

oncoprotein. *Mol Cell Bio*l 1999;19:7519–28.

[43] Turkson J, Bowman T, Garcia R, Caldenhoven E, De Groot RP, Jove R. Stat3 activation by Src induces specific gene regulation and is required for cell transformation. *Mol Cell Biol* 1998;18:2545–52.

[44] Wagner M, Kleeff J, Friess H, Buchler MW, Korc M. Enhanced expression of the type II transforming growth factor-beta receptor is associated with decreased survival in human pancreatic cancer. *Pancreas* 1999;19:370–6.

[45] Gouilleux F, Moritz D, Humar M, Moriggl R, Berchtold S, Groner B. Prolactin and interleukin-2 receptors in T lymphocytes signal through a MGF-STAT5- like transcription factor. *Endocrinology* 1995;136:5700–8.

[46] Seidel HM, Milocco LH, Lamb P, Darnell Jr JE, Stein RB, Rosen J. Spacing of palindromic half sites as a determinant of selective STAT (signal transducers and activators of transcription) DNA binding and transcriptional activity. *Proc Natl Acad Sci U S A* 1995;92:3041–5.

[47] Aggarwal BB, Sethi G, Ahn KS, Sandur SK, Pandey MK, Kunnumakkara AB, Sung B, Ichikawa H. Targeting signal-transducer-and-activator-of-transcription-3 for prevention and therapy of cancer: modern target but ancient solution. *Ann N Y Acad Sci.* 2006, 1091:151-69.

[48] Zhang Y, Turkson J, Carter-Su C, Smithgall T, Levitzki A, Kraker A, Krolewski JJ,

Medveczky P, Jove R. Activation of Stat3 in v-Src transformed fibroblasts requires cooperation of Jak1 kinase activity. *J Biol Chem* 2000;275:24935–44.

[49] Zhao S, Venkatasubbarao K, Lazor JW, Sperry J, Jin C, Cao L, Freeman JW. Inhibition of STAT3Tyr705 phosphorylation by Smad4 suppresses transforming growth factor b–mediated invasion and metastasis in pancreatic cancer cells. *Cancer Res* 2008;68:4221–8.

[50] Jones G, Willett P, Glen RC, Leach AR, Taylor R. Development and validation of a genetic algorithm for flexible docking. *J Mol Biol* 1997;267:727–48.

[51] Fletcher S, Jardeephi S, Zhang X, Yue P, Page BD, Sharmeen S, Shahani VM, Zhao W, Schimmer AD, Turkson J, Gunning PT. Disruption of transcriptionally active Stat3 dimers with non-phosphorylated. Salicylic acidbased small molecules: potent in vitro and tumour cell activities. *ChemBio-Chem* 2009;10:1959–64.

[52] Siddiquee KAZ. STAT3 as a target for inducing apoptosis in solid and hematological tumors. *Cell Res* 2008;18:254–67.

[53] Xie TX, Wei D, Liu M, Gao AC, Ali-Osman F, Sawaya R, Huang S. Stat3 activation regulates the expression of matrix metalloproteinase-2 and tumor invasion and metastasis. *Oncogene* 2004;23:3550–60.

[54] Huang C, Cao J, Huang KJ, Zhang F, Jiang T, Zhu L, Qiu ZJ. Inhibition of STAT3 activity with AG490 decreases the invasion of human pancreatic cancer cells in vitro.

Cancer Sci 2006;97:1417–23.

[55] Bhasin D, Cisek K, Pandharkar T, Regan N, Li C, Pandit B, Lin J, Li PK. Design, synthesis, and studies of small molecule STAT3 inhibitors. *Bioorg Med Chem Lett* 2008;18:391–5.

[56] Catlett-Falcone R, Landowski TH, Oshiro MM, Turkson J, Levitzki A, Savino R, Ciliberto G, Moscinski L, Fernández-Luna JL, Nuñez G, Dalton WS, Jove R. Constitutive activation of Stat3 signaling confers resistance to apoptosis in human U266 myeloma cells. *Immunity* 1999;10:105–15.

[57] Mora LB, Buettner R, Seigne J, Diaz J, Ahmad N, Garcia R, Bowman T, Falcone R, Fairclough R, Cantor A, Muro-Cacho C, Livingston S, Karras J, Pow-Sang J, Jove R.. Constitutive activation of Stat3 in human prostate tumors and cell lines: direct inhibition of Stat3 signaling induces apoptosis of prostate cancer cells. *Cancer Res* 2002;62:6659–66.

[58] Niu G,Wright KL, Huang M, Song L, Haura E, Turkson J, Zhang S, Wang T, Sinibaldi D, Coppola D, Heller R, Ellis LM, Karras J, Bromberg J, Pardoll D, Jove R, Yu H. Constitutive Stat3 activity up-regulates VEGF expression and tumor angiogenesis. *Oncogene* 2002;21:2000–8.

[59] Wei D, Le X, Zheng L, Wang L, Frey JA, Gao AC, Peng Z, Huang S, Xiong HQ, Abbruzzese JL, Xie K. Stat3 activation regulates the expression of vascular

endothelial growth factor and human pancreatic cancer angiogenesis and metastasis. *Oncogene* 2003;22:319–29.

[60] Fuh B, Sobo M, Cen L, Josiah D, Hutzen B, Cisek K, Bhasin D, Regan N, Lin L, Chan C, Caldas H, DeAngelis S, Li C, Li PK, Lin J. LLL-3 inhibits STAT3 activity, suppresses glioblastoma cell growth and prolongs survival in amouse glioblastoma model. *Br J Cancer* 2009;100:106–12.

[61] Blaskovich MA, Sun J, Cantor A, Turkson J, Jove R, Sebti SM. Discovery of JSI-124 (cucurbitacin I), a selective Janus kinase/signal transducer and activator of transcription 3 signaling pathway inhibitor with potent antitumor activity against human and murine cancer cells in mice. *Cancer Res* 2003;63:1270–9.

[62] Sun J, Blaskovich MA, Jove R, Livingston SK, Coppola D, Sebti SM. Cucurbitacin Q: a selective STAT3 activation inhibitor with potent antitumor activity. *Oncogene* 2005;24:3236–45.

[63] Real PJ, Sierra A, De Juan A, Segovia JC, Lopez-Vega JM, Fernandez-Luna JL. Resistance to chemotherapy via Stat3-dependent overexpression of Bcl-2 in metastatic breast cancer cells. *Oncogene* 2002;21:7611–8.

[64] Gritsko T, Williams A, Turkson J, Kaneko S, Bowman T, Huang M, Nam S, Eweis I, Diaz N, Sullivan D, Yoder S, Enkemann S, Eschrich S, Lee JH, Beam CA, Cheng J, Minton S, Muro-Cacho CA, Jove R. Persistent activation of stat3 signaling induces

survivin gene expression and confers resistance to apoptosis in human breast cancer cells. *Clin Cancer Res* 2006;12:11–9.

[65] Frank DA. STAT3 as a central mediator of neoplastic cellular transformation. *Cancer Lett.* 2007, 28;251(2):199-210

[66] Aggarwal BB, Shishodia S. Molecular targets of dietary agents for prevention and therapy of cancer. *Biochem Pharmacol.* 2006,14;71(10):1397-421.

[67] Yang, J. Chatterjee-Kishore M, Staugaitis SM, Nguyen H, Schlessinger K, Levy DE, Stark GR. Novel Roles of Unphosphorylated STAT3 in Oncogenesis and Transcriptional Regulation. *Cancer Res.* 2005:65, 939-947

[68] Inghirami G, Chiarle R, Simmons WJ, Piva R, Schlessinger K, Levy DE. New and old functions of STAT3: a pivotal target for individualized treatment of cancer. *Cell Cycle.* 2005 ;4(9):1131-3.

[69] Gough, D.J. Corlett A, Schlessinger K, Wegrzyn J, Larner AC, Levy DE. Mitochondrial STAT3 Supports Ras-Dependent Oncogenic Transformation. *Science* 2009:324, 1713 - 1716 .

[70] Wang, T, Niu G, Kortylewski M, Burdelya L, Shain K, Zhang S, Bhattacharya R, Gabrilovich D, Heller R, Coppola D, Dalton W, Jove R, Pardoll D, Yu H. Regulation of the innate and adaptive immune responses by Stat-3 signaling in tumor cells. *Nat Med* 2004:10, 48-54 .

[71] Grivennikov, S.I. & Karin, M. Dangerous liaisons: STAT3 and NF-kB collaboration and crosstalk in cancer. *Cytokine & Growth Factor Reviews* 2010:21, 11-19

[72] Gunning, PT, Katt WP, Glenn M, Siddiquee K, Kim JS, Jove R, Sebti SM, Turkson J, Hamilton AD. Isoform selective inhibition of STAT1 or STAT3 homo-dimerization via peptidomimetic probes: structural recognition of STAT SH2 domains. *Bioorg Med Chem Lett* 2007:17, 1875-1878.

[73] Chen, J, Bai L, Bernard D, Nikolovska-Coleska Z, Gomez C, Zhang J, Yi H, Wang S. Structure-Based Design of Conformationally Constrained, Cell-Permeable STAT3 Inhibitors. *ACS Med Chem Lett* 2010:1, 85-89.

[74] Lin, L, Hutzen B, Zuo M, Ball S, Deangelis S, Foust E, Pandit B, Ihnat MA, Shenoy SS, Kulp S, Li PK, Li C, Fuchs J, Lin J. Novel STAT3 phosphorylation inhibitors exhibit potent growth-suppressive activity in pancreatic and breast cancer cells. *Cancer Res* 2010: 70, 2445-2454

[75] Zhang, X. Yue P, Fletcher S, Zhao W, Gunning PT, Turkson J. A novel small-molecule disrupts Stat3 SH2 domain- phosphotyrosine interactions and Stat3-dependent tumor processes. *Biochem Pharmacol* 2010:79, 1398-1409.

[76] Fletcher, S, Page BD, Zhang X, Yue P, Li ZH, Sharmeen S, Singh J, Zhao W, Schimmer AD, Trudel S, Turkson J, Gunning PT. Antagonism of the Stat3-Stat3 Protein Dimer with Salicylic Acid Based Small Molecules. *ChemMedChem.* doi:

10.1002/cmdc.201100194. [Epub ahead of print] (2011).

[77] Page BD, Ball DP, Gunning PT. Signal transducer and activator of transcription 3 inhibitors: a patent review. *Expert Opin Ther Pat.* 2011 Jan;21(1):65-83

[78] Razgulin, A.V. & Mecozzi, S. Binding properties of aromatic carbon-bound fluorine. *J. Med. Chem.* 2006: 49, 7902-7906.

[79] Silver, D.L., Naora, H., Liu, J., Cheng, W. & Montell, D.J. Activated signal transducer and activator of transcription (STAT) 3: localization in focal adhesions and function in ovarian cancer cell motility. . *Cancer Res.* 2004:64, 3550-3558.

[80] Maa, M.C. et al. EPS8 Facilitates Cellular Growth and Motility of Colon Cancer Cells by Increasing the Expression and Activity of Focal Adhesion Kinase. *J Biol Chem*. 2007:282, 19399-19409.

[81] Zhao, J, Bian ZC, Yee K, Chen BP, Chien S, Guan JL. Identification of Transcription Factor KLF8 as a Downstream Target of Focal Adhesion Kinase in Its Regulation of Cyclin D1 and Cell Cycle Progression. *Mol. Cell* 2003:11, 1503-1515 .

[82] Wang, X, Zheng M, Liu G, Xia W, McKeown-Longo PJ, Hung MC, Zhao J. Kruppel-like factor 8 induces epithelial to mesenchymal transition and epithelial cell invasion. *Cancer Res* 2007:67, 7184-7193.

[83] Wang, X, Lu H, Urvalek AM, Li T, Yu L, Lamar J, DiPersio CM, Feustel PJ, Zhao J. KLF8 promotes human breast cancer cell invasion and metastasis by transcriptional

activation of MMP9. *Oncogene* 2011: 30, 1901-1911.

[84] De Neergaard M, Kim J, Villadsen R, Fridriksdottir AJ, Rank F, Timmermans-Wielenga V, Langerød A, Børresen-Dale AL, Petersen OW, Rønnov-Jessen L. Epithelial-stromal interaction 1 (EPSTI1) substitutes for peritumoral fibroblasts in the tumor microenvironment. *Am J Pathol.* 2010:176, 1229-1240.

[85] Yu, H., Pardoll, D. & Jove, R. STATs in cancer inflammation and immunity: a leading role for STAT3. *Nat Rev Cancer* 2009:9, 798-809.

[86] Lee H, Herrmann A, Deng JH, Kujawski M, Niu G, Li Z, Forman S, Jove R, Pardoll DM, Yu H. Persistently activated Stat3 maintains constitutive NF-kappaB activity in tumors. *Cancer Cell* 2009 :15, 283-293.

[87] Kenji Matsuno, Yoshiaki Masuda, Yutaka Uehara, Hiroshi Sato, Ayumu Muroya, Osamu Takahashi, Takane Yokotagawa, Toshio Furuya, Tadashi Okawara, Masami Otsuka, Naohisa Ogo, Tadashi Ashizawa, Chie Oshita, Sachiko Tai, Hidee Ishii, Yasuto Akiyama, and Akira Asai. Identification of a New Series of STAT3 Inhibitors by Virtual Screening. *ACS Med Chem Lett* 2010:1, 371-375 .

[88] Wang, X., Urvalek, A.M., Liu, J. & Zhao, J. Activation of KLF8 transcription by focal adhesion kinase in human ovarian epithelial and cancer cells. *J Biol Chem* 2008:283, 13934- 13942.

[89] Nielsen, H.L., Rønnov-Jessen, L., Villadsen, R. & Petersen, O.W. Identification of EPSTI1, a Novel Gene Induced by Epithelial–Stromal Interaction in Human Breast Cancer. *Genomics* 2002: 79, 703-710.

[90] Li JC, Yang XR, Sun HX, Xu Y, Zhou J, Qiu SJ, Ke AW, Cui YH, Wang ZJ, Wang WM, Liu KD, Fan J. Up-regulation of Krüppel-Like Factor 8 Promotes Tumor Invasion and Indicates Poor Prognosis for Hepatocellular Carcinoma. *Gastroenterology* 2010:139, 2146-2157.

[91] Kim DH, Cho IH, Kim HS, Jung JE, Kim JE, Lee KH, Park T, Yang YM, Seong SY, Ye SK, Chung MH. Anti-inflammatory effects of 8-hydroxydeoxyguanosine in LPS-induced microglia activation: suppression of STAT3-mediated intercellular adhesion molecule-1 expression. *Exp Mol Med.* 2006:38, 417-427

[92] Gho YS, Kim PN, Li HC, Elkin M, Kleinman HK. Stimulation of Tumor Growth by Human Soluble Intercellular Adhesion Molecule-1. *Cancer Res* 2001 :61, 4253-4257.

[93] Jesneck JL, Mukherjee S, Yurkovetsky Z, Clyde M, Marks JR, Lokshin AE, Lo JY. Do serum biomarkers really measure breast cancer? *BMC Cancer. 2009:*9, 164

[94] Abe, R., Peng, T., Sailors, J., Bucala, R, Metz, C.N. Regulation of the CTL response by macrophage migration inhibitory factor. *J. Immunol. 2001:*166, 747-753

[95] Zubac, D.P., Wentzel-Larsen, T., Seidal, T., Bostad, L. Type 1 plasminogen

activator inhibitor (PAI-1) in clear cell renal cell carcinoma (CCRCC) and its impact on angiogenesis, progression and patient survival after radical nephrectomy. *BMC Urol. 2010:*10, 20

[96] Hsieh, T.C., Chiao, J.W. Growth modulation of human prostatic cancer cells by interleukin-1 and interleukin-1 receptor antagonist. *Cancer Lett. 1995:*95, 119-123.

[97] Yamada, Y., Karasaki, H., Matsushima, K., Lee, G.H., Ogawa, K. Expression of an IL-1 receptor antagonist during mouse hepatocarcinogenesis demonstrated by differential display analysis. *Lab Invest.* 1999:79, 1059-1067

[98] Oelmann E, Kraemer A, Serve H, Reufi B, Oberberg D, Patt S, Herbst H, Stein H, Thiel E, Berdel WE. Autocrine interleukin-1 receptor antagonist can support malignant growth of glioblastoma by blocking growth-inhibiting autocrine loop of interleukin-1. *Int J Cancer.* 1997:71, 1066-1076.

[99] Iizuka N, Hazama S, Hirose K, Abe T, Tokuda N, Fukumoto T, Tangoku A, Oka M. Interleukin-1 receptor antagonist mRNA expression and the progression of gastric carcinoma. *Cancer Lett*. 1999:142, 179-184.

[100] Zhao W, Jaganathan S, Turkson J. A cell-permeable Stat3 SH2 domain mimetic inhibits Stat3 activation and induces antitumor cell effects in vitro. *J Biol Chem.* 2010: 285, 35855-35865.